TITLE: Understanding the mechanism of host deacetylases SIRT1 and SIRT3 in the modulation of *Salmonella* pathogenesis

INTRODUCTION

Sirtuins are NAD+-dependent deacetylases that are present in all forms of life. *Saccharomyces cerevisiae* serve as the founder for the discovery of Sir2. Sirtuins comprises of a conserved core catalytic domain that removes acetyl moiety from the lysine residues of proteins in presence of NAD+ as cofactor (1) giving rise to 2'O-acetyl-ADP-ribose and free nicotinamide as products (2). Free nicotinamide acts as a non-competitive inhibitor of sirtuins (3). They possess variable N terminal and C terminal domain that confer different subcellular localization, substrate specificity and functions (4). Mammals have seven sirtuins which act on different substrates like histones and transcriptional factors like p53, FOXO, PGC1α, UCP2, liver X-receptor and others. Thus, they are responsible for regulating various biological functions such as cell survival, apoptosis, oxidative stress, metabolism and inflammation (5, 6). SIRT1,6 and 7 have nuclear localization, SIRT2 is cytoplasmic and SIRT 3,4 and 5 comprise the mitochondrial SIRTs. SIRT1 is the most characterized of all the SIRTs and possess strong homology with the yeast Sir2 protein. In addition to their deacetylase activity, they possess ADP ribosylation (SIRT1, SIRT4, and SIRT6), desuccinylation and demalonylation (SIRT5), delipoylation (SIRT4), and demyristoylation and depalmitoylation (SIRT6) enzymatic activities (7).

SIRT1 mediated alteration in gene expression interlinks metabolism and inflammation. SIRT1 gets activated in response to acute immune response and help in its resolution. It deacetylates RelA/p65 component of NF-κB thereby mediating its proteasomal degradation (8). On the other hand, it activates RelB component of NF-κB pathway. RelB causes heterochromatinization of pro-inflammatory genes like TNF-α and IL-β (9) and causes activation of the fatty acid oxidation genes. With the gradual progression toward the adaptive phase of the immune response, SIRT1 activates Peroxisome proliferator-activated receptor γ (PPARγ) coactivator-1α (PGC-1α) mediating a metabolic switch from glycolysis toward fatty

acid oxidation. SIRT1 mediated RelB activation in turn activates SIRT3 causing the promotion of mitochondrial bioenergetics (10).PGC-1α, a major player in mitochondrial biogenesis, activates SIRT3 (11) which in turn cause activation of PGC-1α, thereby fuelling a positive feedback loop. PGC-1α associates with nuclear respiratory factors 1 and 2 (NRF1, 2), causing activation of TFAM. TFAM promotes activation of the nuclear gene encoding the five complex subunits of the mitochondrial electron transport chain (ETC) (12). SIRT3 accounts for the major mitochondrial deacetylase orchestrating several metabolic processes such as fatty acid oxidation, promotion of the TCA cycle, inhibition of ROS production (13).

Salmonella enterica serovar Typhimurium is a facultative intracellular Gram-negative pathogen with peritrichous flagella(14), causing gastroenteritis in humans and typhoid-like disease in mice (15). *Salmonella* gains entry inside the body through the orofecal route along with the ingestion of contaminated food and water. *Salmonella* resist the low acidic pH of the stomach by utilizing the acid tolerance response (ATR) genes and finally reach the lumen of the small intestine(16). In the intestinal tract, it uses specialised microfold (M) cells for macro-pinocytic entry. The pathogen gain entry into the non-phagocytic epithelial cells via its *Salmonella* Pathogenicity Island-1 (SPI-1) effectors to breach the intestinal barrier (17). Once, traversing through the mucosal lining of the gut epithelium, it reaches the lamina propria (17). Apart from M cells, the dendritic cells can also sample the bacteria from the lumen to the lamina propria. In the lamina propria, it encounters various host immune cells like neutrophils, macrophages, dendritic cells and so on. Macrophages, dendritic cells and neutrophils are responsible for successful dissemination throughout the body through the reticulo-endothelial system (RES) to the secondary organs such as Mesenteric Lymph Node (MLN), liver spleen and so on(17).]. Inside the macrophages, they harbour within the *Salmonella* containing vacuoles (SCV) by virtue of its SPI-2 effectors.

Macrophages, serving as an intracellular niche for *Salmonella,* exhibit several continua of polarization states. At the two extreme ends of the spectrum lie the classically polarized M1 macrophages and alternatively activated M2 macrophages. M1 macrophages comprise the proinflammatory antimicrobial state producing IL-1β, IL-6, TNF-α, IL-12, and IFN-γ cytokines with enhanced expression of CD80, CD86 surface markers. Whereas the anti-inflammatory M2 macrophages promote bacterial persistence by producing anti-inflammatory cytokines like IL-10, TGF-β and show increased expression of Arg-1, CD206 surface markers (18, 19). To sustain the continuous production of proinflammatory cytokines M1 macrophages rely on glycolysis for their energy requirements. On the other hand, M2 macrophages are fuelled by enhanced oxidative phosphorylation (OXPHOS) and fatty acid oxidation (FAO) (20). It has been previously reported that sirtuins mediated attuning of metabolism impact polarization of macrophages *in vivo*. SIRT1 has the ability to promote the polarization of M2 macrophages and inhibit inflammation in macrophages of adipose tissue (21-23) .SIRT3 suppresses ROS by deacetylating and activating MnSOD (24).

Several bacteria are known to subvert the host immune system toward an immunosuppressive state. At the initial phases of infection bacteria exerts an acute inflammatory response by initiating M1 polarization which confers resistance to intracellular growth. Pathogens like *Salmonella* or *Mycobacterium* have evolved mechanisms to counteract the M1 state of the host macrophage. *Salmonella* Typhimurium uses its SPI-2 effectors to inhibit the recruitment of NADPH oxidase to the *Salmonella* Containing Vacuoles (SCV), thereby preventing oxidative burst mediated microbicidal activity (25, 26). *Salmonella* Typhimurium also prevents iNOS association to SCV using its specialized SPI-2 machinery (27). Similarly, *Mycobacterium bovis* bacillus Calmette-Gue´rin prevents NOS2 recruitment to phagosomes (26). *Salmonella* Dublin cause inhibition of the production of pro-inflammatory cytokine like IL-18 and IL-12p70 (28). Moreover, *Mycobacteria* inhibits NF-κB signalling and IFN-γ mediated downstream pathways

via direct interaction of ESAT-6 with TLR2 (29). Furthermore, *Yersinia enterocolitica* elicits a M2 response by inducing Arginase-1 expression and TGFβ1 and IL-4 production (30). *Yersinia* TTSS effector LcrV induces a M2 phenotype supposedly by IL-10 production (31).

Instances of the contribution of Sirtuins in several infection scenario are reported in the literature. In RSV infected dendritic cells, SIRT1 was shown to regulate mitochondrial function and RSV induced innate cytokine production leading to the tuning of adaptive immune responses (32). SIRT1 deletion in dendritic cells enhanced inflammatory response in *Listeria monocytogenes* challenged mice (33). The role of SIRT1 in ameliorating the *Mycobacterium tuberculosis* infection through anti-inflammatory responses via inhibition of TAK1 activation was also reported (34).SIRT3 is shown to play a vital role in promoting antimycobacterial resistance in the host by reducing excessive inflammation during infection. It also regulated mitochondrial damage and oxidative stress and resulted in the activation of antibacterial autophagy via SIRT3-PPARA-TFEB signalling (35).

Since SIRT1 and SIRT3 are the major modulators of the immuno-metabolic paradigm, we intend to decipher the role of SIRT1 and SIRT3 in influencing host and *Salmonella* metabolism. This study highlights the role of SIRT1 and SIRT3 in intracellular pathogen survival by promoting *Salmonella* glycolysis and concomitantly driving host metabolism towards fatty acid oxidation. Additionally, *Salmonella* trigger an immunosuppressive M2 environment conducive to its intravacuolar proliferation by modulating SIRT1 and SIRT3 levels. Here, we have shown that SIRT1 and SIRT3 knockdown cause decreased M2 surface marker expression such as CD206 along with increased production of pro-inflammatory cytokines and ROS generation, together amounting to attenuated bacterial intracellular proliferation within the infected macrophages. Moreover, SIRT1 mediated p65 NF-κB deacetylation played a vital role in immune function regulation within the *Salmonella* infected macrophages with increased interaction of SIRT1 with p65 NF-κB. SIRT1 knockdown or inhibition resulted in

hyperacetylation of p65 NF-κB thereby leading to enhanced pro-inflammatory response in *S.* Typhimurium infected macrophages. Further, SIRT1 and SIRT3 knockdown or inhibition skewed the *Salmonella*-induced host metabolic shift by regulating acetylation status of HIF-1α and PDHA. This caused increased host glycolysis and reduced fatty acid oxidation. However, the *Salmonella* shows the opposing metabolic profile with increased fatty acid oxidation and reduced glycolysis upon SIRT1 or SIRT3 inhibition. In the contrary to the macrophages, in *in vivo* mice-model of infection, SIRT1 and SIRT3 inhibition resulted in increased pathogen loads in organs and triggered enhanced bacterial dissemination, together leading to increased susceptibility of the mice to *S.* Typhimurium infection owing to increased ROS and IL-6 production.

Mitochondria are considered to play a central role in bacterial infections. Numerous microbial pathogens modulate mitochondrial functions and dynamics to evade host immune responses. On the other hand, the elicited host immune responses are dependent on the overall mitochondrial bioenergetics and their function (36). Thus, mitochondrial health is a crucial determinant for the outcome of several bacterial infections.

Pathogens like *Listeria monocytogenes* induce mitochondrial fragmentation upon infection via its listeriolysin O protein (37). Similarly, *Helicobacter pylori* utilize its VacA effector protein to induce mitochondrial network fragmentation(38). DRP-1- (Dynamin-related protein 1) dependent mitochondrial fragmentation is reported in both *Shigella flexneri* (39) and *Legionella pneumophila* infections(40). On the other hand, *Chlamydia trachomatis* infection promotes mitochondrial elongation in the early phases of infection. Elongated mitochondria contribute to enhanced ATP production, promoting the intracellular proliferation of *C. trachomatis*(41, 42).

Mitochondria, being attributed as the cell's powerhouse, perform critical functions like governing the regulation of the TCA cycle, oxidative phosphorylation and ATP production. Several bacteria reprogram host metabolism to facilitate their intracellular survival. *Mycobacterium tuberculosis(43)*, *Brucella abortus(44)*, and *Chlamydia trachomatis(45)* infections leads to reduced TCA cycle, increased aerobic glycolysis, and augmented lactate production.

Sirtuin 3 (SIRT 3) is a mitochondrial NAD+ dependent Class III deacetylase that governs important host mitochondrial functions like mitochondrial bioenergetics, metabolism, and energy homeostasis(46, 47). It regulates vital enzymatic processes involved in oxidative phosphorylation and fatty acid oxidation in mitochondria(48, 49). It performs a crucial role in ameliorating oxidative stress by inducing activation of SOD2 (superoxide dismutase 2), CAT (catalase) that reduces ROS levels(50). SIRT1, on the other hand, also plays a major role in mitochondrial function in various tissues(51, 52), and its effect on mitochondrial biogenesis is mediated by PGC1α(53). SIRT1 catalyzes the deacetylation of PGC1α, leading to its activation(54). The activated PGC1α co-ordinates mitochondrial biogenesis by acting as a master regulator. It induces the expression of the nuclear respiratory factors (NRF1 and NRF-2) and transcription factor A of the mitochondria (TFAM), which mediates the transcription of the nuclear and mitochondrial genome respectively(55). Recent findings by Kim *et al*., highlighted the role of SIRT3 in anti-mycobacterial host defenses by limiting ROS production and preserving mitochondrial function via autophagy(35). Furthermore, SIRT3 downregulation leads to the reprogramming of mitochondrial metabolism and cell-death in *Mycobacterium tuberculosis* infected macrophages(56). However, the role of SIRT1 or SIRT3 in the modulation of mitochondrial function and dynamics pertaining to *Salmonella* infection is largely unexplored.

In this study, we have further explored the role of host deacetylases SIRT1 and SIRT3 in the modulation of mitochondrial bioenergetics and dynamics. We show that inhibition of SIRT3 either by shRNA mediated knockdown or by the application of specific catalytic inhibitors leads to increased mitochondrial dysfunction in the *Salmonella* infected macrophages. We have shown that inhibition of SIRT3 function leads to increased mitochondrial superoxide production in the infected macrophages. The increased mitochondrial ROS generation in the infected macrophages coincides with mitochondrial membrane hyperpolarization, increased proton leakage and respiration rate, and decreased ATP production and ETC function. The Seahorse ECF mitostress test profile suggested an overall increase in respiratory parameters such as basal respiration, non-mitochondrial respiration, proton leakage and ATP-linked respiration along with an increase in the Extracellular Acidification Rate (ECAR) upon treatment with either SIRT1 or SIRT3 inhibitor. Here, we show that loss or inhibition of SIRT1 or SIRT3 trigger increased the macrophage cytosol acidification, consequently leading to a loss in intra-bacterial acidification; together resulting in decreased SPI-2 gene expression. Alongside the decline in mitochondrial bioenergetics, the *S.* Typhimurium infected macrophages depict alteration in mitochondrial dynamics with increased mitochondrial fission and mitophagy alongside decreased mitochondrial fusion dynamics. Together, our results suggest the role of SIRT1 and SIRT3 in preserving the mitochondrial bioenergetics and dynamics in *S.* Typhimurium infection scenario, thereby influencing the bacterial intracellular niche.

Aims and Objectives of the current study

Thus, we intend to elucidate the role of two Sirtuins, SIRT1 and SIRT3, in the modulation of *Salmonella* pathogenesis. Therefore, we investigated the following key questions:

1. **To investigate the role of SIRT1 and SIRT3 in mediating immuno-metabolic shift along the course of *Salmonella* infection**
2. **To understand the role of SIRT1 and SIRT3 on the modulation of mitochondrial dynamics and mitochondrial bioenergetics upon *Salmonella* infection**

MATERIALS AND METHODS

Bacterial Strains, and culture conditions

Salmonella enterica serovar Typhimurium (STM) wildtype strain ATCC 14028S or ATCC 14028S constitutively expressing green fluorescent protein (eGFP) or mCherry (RFP) through pFPV plasmid were used. 4% paraformaldehyde fixed STM (PFA) was used as the killed fixed bacteria control. The above-mentioned live bacterial strain was grown overnight in LB broth in 37 ^{0}C at 160 rpm shaking condition in presence or absence of appropriate antibiotic (Ampiciilin-50µg/ml) (Table-1) after revival of the bacterial strains from glycerol stock (stored at -80 ^{0}C).

Table: List of strains and plasmids used in this study

Strains/Plasmids	**Characteristics**	**Source**
Salmonella enterica serovar Typhimurium ATCC strain 14028S (STM)	Wild Type (WT)	Gifted by Prof. M. Hensel
pFPV:GFP	Amp^{R}	Laboratory Stock
pFPV:mCherry	Amp^{R}	Laboratory Stock
pLKO.2 : shRNA	Amp^{R}	Gifted by Prof. Subba Rao Gangi Setty
STM Δ *invC*	Kan^{R}	Laboratory Stock
STM Δ *ssaV*	Chl^{R}	Laboratory Stock

STM Δ *steE*	Kan^R	Laboratory Stock
STM Δ OmpR	KanR	Laboratory Stock
pBAD-pHuji	AmpR	Addgene#61555
mito-BFP	KanR	Addgene#49151
STM-pBAD-pHuji	AmpR	Laboratory Stock
Mito-EGFP-mCherry	KanR	Gifted by Prof. Subba Rao Gangi Setty

Cell Culture

RAW 264.7 murine macrophages were cultured in DMEM (Lonza) containing 10% FBS (Gibco) at 37 ^{0}C in a humified incubator with 5% CO_2. Prior to each experiment, cells were seeded into 24 well or 6 well plate as per requirement at a confluency of 60%.

For macrophage polarization experiments, the seeded macrophages were subjected to 100ng/ml LPS + 20ng/ml IFN-γ treatment for M1 polarization and 20ng/ml IL-4 treatment for M2 polarization for 24 hrs. Following this, the cell supernatant were collected for validation of polarization status by ELISA and were further subjected to infection protocol.

Peritoneal macrophages were collected in PBS from the peritoneal cavity of C57BL/6 mice aseptically post thioglycolate treatment using 20G needle and 5ml syringe. Following centrifugation, cell pellet was resuspended in RPMI-1640 (Lonza) containing 10% heat-inactivated FBS (Gibco), 100 U/ml penicillin and 100 µg/ml streptomycin and seeded into 6 well- plates. 6hr prior to infection, antibiotic containing media was replaced with Penicillin-Streptomycin free RPMI-1640 (Lonza) containing 10% heat-inactivated FBS (Gibco).

Transfection

shRNA mediated knockdown was carried out by PEI mediated transfection protocol. Plasmid harbouring shRNA in pLKO.2 vector backbone specific to SIRT1 and SIRT3 were used for transfection. Plasmid harbouring scrambled sequence of shRNA, served as a control, was also used for transfection. Plasmid DNA was used at a concentration of 500ng and 1µg per well of

a 24-well plate and 6-well plate respectively. Plasmid and PEI were added in 1:2 ratio in serum free DMEM media and incubated for 20 mins at room temperature. Post incubation, the DNA: PEI cocktail was added to the seeded RAW 264.7 macrophages. After 6-8hrs of incubation, serum-free media was replaced with complete media containing 10% FBS. Post 48hr of transfection, transfected cells were either harvested for knockdown confirmation studies or subjected to infection with STM.

Table: List of shRNA used for knockdown

Sirtuins	**Construct ID**	**TRC ID**	**Sequence (5'---3')**
SIRT1	C4	TRCN0000218734	GTACCGGCATGAAGTGCCTCAGATATTACTCGAGTAATATCTGAGGCACTTCATGTTTTTTG
SIRT1	C12	TRCN0000018979	CCGGGCAAAGCCTTTCTGAATCTATCTCGAGATAGATTCAGAAAGGCTTTGCTTTTT
SIRT3	E8	TRCN0000038889	CCGGCCCAACGTCACTCACTACTTTCTCGAGAAAGTAGTGAGTGACGTTGGGTTTTTG
SIRT3	E12	TRCN0000038893	CCGGCCACCTGCACAGTCTGCCAAACTCGAGTTTGGCAGACTGTGCAGGTGGTTTTTG

Infection Protocol

Macrophages were infected with stationary-phase bacterial culture with MOI of 10. For synchronization of the infection, tissue culture plates were subjected to centrifugation at 600rpm for 5 min and incubated at 37 ^{0}C humified incubator with 5% CO_2 for 25 min. Cells were washed with PBS and were treated with DMEM (Lonza) + 10% FBS (Gibco) containing 100 μg/ml gentamicin for 1 hr. Subsequently, the gentamicin concentration was reduced to 25 μg/ml and maintained until the cells were harvested. For the inhibitor treatment studies, along with 25 μg/ml containing complete media 1μM of SIRT1 (EX-527) inhibitor or SIRT3 (3TYP) or 10mM of N-Acetyl Cysteine (NAC) were added to the cells.

Immunofluorescence confocal microscopic studies

At the specified time points post infection with GFP tagged STM, the macrophage cells were fixed with 3.5% paraformaldehyde for 15 min. Primary antibody staining was performed with specific primary antibody in the presence of a permeabilizing agent, 0.01% saponin (Sigma) dissolved in 2.5% BSA containing PBS at 4°C for overnight or for 6hr at room temperature (RT). Following this, cells were washed with PBS stained with appropriate secondary antibody tagged with fluorochrome for 1 hr at RT. This was followed by DAPI staining and mounting of the coverslip onto a clean glass slide using the mounting media containing the anti-fade agent. The coverslip sides were sealed with a transparent nail paint. All immunofluorescence images were obtained using Zeiss LSM 710 or Zeiss LSM 880 and were analyzed using ZEN black 2012 software.

For mitophagy flux and mitochondrial dynamics determination, RAW264.7 macrophages were transfected with mitoGFP-mCherry plasmid. After 24 hrs, RAW264.7 macrophages were infected with *S.* Typhimurium (MOI of 10) and treated with SIRT1 (EX-527) and SIRT3 (3TYP) at 1μM concentration. At designated time points post-infection, cells were fixed, and intracellular *Salmonella* were stained with anti-*Salmonella* antibody. Immunofluorescence

images were obtained and analyzed as mentioned earlier. Quantification of mitochondrial tubular length was performed using ImageJ software.

Quantitative Real Time PCR

Total RNA was isolated at specific time points post infection by using TRIzol (Takara) as per manufacturer's protocol. Quantification of RNA was performed in Nano Drop (Thermo-Fischer scientific). Quality of isolated RNA was detected by performing 2% agarose gel electrophoresis. 2 µg of RNA was subjected to DNaseI (Thermo Fischer Scientific) treatment at 37°C for 1 hr followed by addition of 0.5M EDTA (final concentration 5mM) and heat inactivation at 65°C for 10 mins. The mRNA was reverse transcribed to cDNA using oligo $(dT)_{18}$ primer, buffer, dNTPs and reverse transcriptase (Takara) as per manufacturer's protocol. The expression profile of target gene was evaluated using specific primers (Table-3) by using SYBR green RT-PCR master mix (Takara) in BioRad Real time PCR instrument. β-actin was used as an internal control for mammalian genes and for bacterial genes 16S rRNA was used. All the reaction was setup in 384 well plate with two replicates for each sample.

Intracellular proliferation or gentamicin protection assay

Infection protocol was followed as described earlier. Post 2hr and 16hr post-infection, cells were lysed in 0.1% triton-X-100. Lysed cells were serially diluted and plated on *Salmonella-Shigella* (SS) agar to obtain colony-forming units (CFU). Fold proliferation was calculated as CFU at 16hr divided by CFU at 2hr.

Fold Proliferation= [CFU at 16h]/[CFU at 2h]

Western Blotting

Post appropriate time points of infection, the cells were washed in PBS and subsequently harvested in PBS. The cell pellets were obtained after centrifugation at 300g for 7 minutes at

4ºC. Cells were lysed in 1X RIPA (10X-0.5M NaCl, 0.5M EDTA pH-8.0, 1M Tris, NP-40, 10% sodium deoxycholate, 10% SDS) buffer containing 10% protease inhibitor cocktail (Roche) for 30 min on ice. Total protein was estimated using Bradford (Bio-Rad) method of protein estimation. Protein samples were subjected to 12 % SDS polyacrylamide gel electrophoresis and then were transferred onto 0.45µm PVDF membrane (18V, 2 hrs). The membrane was blocked using 5% skim milk in TBST (Tris Buffered Saline containing 0.1% Tween-20) for 1hr at RT and subsequently probed with appropriate primary antibody (Table-4) for overnight at 4°C. Following wash in TBST, blot was probed with specific HRP conjugated secondary antibody for 1hr at RT. The membrane was developed using ECL (Advansta) and images were captured using ChemiDoc GE healthcare. All densitometric analysis was performed using ImageJ software.

Immunoprecipitation

For co-immunoprecipitation, cells were washed with PBS and were lysed in native lysis buffer containing 1% Nonidet P-40, 20 mM Tris (pH 8), 2 mM EDTA, 150 mM NaCl and protease inhibitors mixture (Roche Diagnostics) for 30 min at 4°C. Cell debris was removed by centrifugation at 10,000 rpm for 10 min and the supernatant was treated with the specific antibody against the protein to be precipitated. Antibody-lysate complexes were immunoprecipitated using Protein A/G- linked magnetic beads (MagGenome) according to the manufacturer's protocol. Beads were extensively washed with washing buffer and denatured at 95 ºC for 10 min. Denatured precipitates were subjected to SDS-PAGE (12% gel) followed by transfer to 0.45 µ PVDF membrane. The membrane was blocked using 5% skimmed milk in TBST (Tris Buffered Saline containing 0.1% Tween-20) for 1h at room temperature and eventually probed for the target primary antibodies or Anti-acetylated Lysine (Ac-K) primary antibody overnight at 4°C. The blot was probed with a specific HRP-conjugated secondary

antibody for 1hr at RT after rigorous washing in TTBS. ECL (BioRad) was used for detection and images were captured using ChemiDoc GE healthcare.

ELISA

Estimation of cytokines in cell-free supernatant or in mice serum was performed according to the manufacturer's instructions. Briefly, 96-well ELISA plates (BD Bioscience) were coated overnight with capture antibody at 4°C. Following day, plates were washed with 0.1% Tween-20 containing PBS and blocked with 10% FBS for 1 h. Following blocking, wells were washed and incubated with 100 µL of test samples for 2 h at room temperature. Subsequently, plates were washed and incubated with detection antibody and enzyme reagent for 1 h at room temperature (BD Bioscience). TMB (Sigma) was used as a substrate and reactions were stopped with 2 N H_2SO_4. Absorbance was measured at 450 nm wavelength in Tecan Plate reader and the concentration of cytokines were interpolated from a standard curve.

Flow cytometry

After specific time points post infection, cells were washed and harvested in PBS. Following centrifugation, cell pellet was resuspended in FACS buffer comprised of 1% BSA in PBS. Blocking was performed with Fc blocker (purified Anti-mouse CD16/CD32, eBioscience) dissolved in FACS blocking buffer for 30 min on ice. Following a washing step with PBS, antibody staining was performed with PE-conjugated CD86 antibody or APC-conjugated CD206 (Thermo Scientific) for 45 min on ice. After washing in PBS, the cell pellet was resuspended in 1% PFA in PBS. Subsequently, PFA was removed, and cells were resuspended in FACS buffer and reading was taken in BD FACSVerse instrument. For flow cytometry studies, the harvested liver or spleen were homogenized into single cell suspension post RBC lysis (RBC lysis Buffer, Sigma). The homogenized cell suspension was washed and resuspended in FACS buffer containing the PE-conjugated Rat anti-mouse F4/80 antibody (BD

Horizon, Cat-565411). Following staining protocol, the cells were washed in PBS and the cells were resuspended in FACS buffer and the FACS protocol was performed in BD FACSVerse.

For DCFDA staining, one hour before the indicated time point of infection, cells were incubated with 10µM DCFDA containing DMEM media at 37°C humidified incubator with 5% $CO_2$for 45 min. Post incubation, cells were washed and harvested in PBS. Readings were measured in BD FACSVerse instrument.

At specific timepoints post-infection, the cell growth media was removed, and cells were washed with PBS. TMRM (Thermoscientific, cat no. T668) staining solution at 100nM concentration was added to the cells and incubated for 30 mins at 37°C. After washing in PBS, cells were harvested for flow cytometry with 488 nm laser excitation and a 570 ±10 nm emission filter. For MitoSox Red staining, 5µM of MitoSox Red (Invitrogen, cat no.M36008) was used. Cells treated with 10µM of antimycin served as a positive control for mitochondrial ROS production (57, 58). Post 10-30 mins incubation at 37°C, protected from light, cells were analyzed via flow cytometry. For BCECF-AM staining, cells were stained with 10µM of BCECF-AM (Invitrogen, cat no.B1150) in 1X PBS. Two hours prior to the specific timepoints, cells were treated with 50µg/ml chloroquine in 25µg/ml gentamicin- containing DMEM media (59). This chloroquine treated cells served as a control for increased intracellular pH(60). After incubation for 10-30 mins at 37°C, protected from light, cells were washed before analyzing via flow cytometry (BD FACSVerse) using 405nm and 488nm excitation and 535nm emission channel. The median fluorescence intensity (MFI) of the macrophage population at 488 nm and 405 nm was estimated using BD FACSuite software. The 488/ 405 ratio was determined to estimate the acidification level of cytosol. A standard curve of known pH versus the 488nm/405nm ratio was obtained by exposing the macrophages at different pH buffered solution in presence of 10µM valinomycin and 10µM nigericin. The obtained standard curve was used to interpolate the unknown pH of the test samples.

All analysis was done using BD FACSuite software.

Phenol Red-Hydrogen Peroxidase Assay

Post 48hr of transfection, cells were infected with STM culture at an MOI of 10. Cells were incubated with Phenol Red solution containing hydrogen peroxidase enzyme (8.5U/ml). At the designated time points post-infection, the supernatant was collected, and the absorbance was taken at 610 nm in Tecan Plate reader. The exogenously produced H_2O_2 was quantified using a standard curve of known concentration of H_2O_2.

Gene expression studies by nanoString nCounter technology

Total RNA was isolated at specific time points post infection by using TRIzol (Takara) as per manufacturer's protocol. Quantification of RNA was performed in Nano Drop (Thermo-Fischer scientific) and Qubit Bioanalyzer (Agilent 2100 Bioanalyzer). Quality of isolated RNA was detected by performing 2% agarose gel electrophoresis. Post quality check, samples were subjected to nanoString nCounter technology (theraCUES). This technology allows multi-plex, spatially resolved RNA expression quantification with appropriate probes designed against the target gene.

Lactate Estimation Assay

Cell-supernatant was harvested at the specific time-points post-infection and lactate content of the sample was estimated using the Lactate Assay Kit (Sigma, Catalog Number-MAK064) as per manufacturer's protocol. Briefly, 50µl of the sample was added to each 96 well-plate and each of the well 50µl of the master reaction mix containing 46µl of lactate assay buffer, 2µl of lactate enzyme mix, and 2µl of lactate probe was added. After the addition of the master reaction mix to the sample, they were mixed by horizontal shaker or via pipetting. The plate was incubated for 30 minutes in dark at room temperature. Post incubation, absorbance was

measured at 570nm. The lactate content of the sample was estimated from the lactate standard curve ranging from 0-10 nmole/µl.

Fatty Acid Oxidation Assay

At 16h post-infection, cell pellets were harvested and stored at-80ºC. The fatty acid oxidation assay protocol was followed as per manufacturer's instructions (AssayGenie Fatty Acid Oxidation (FAO) Assay Kit, Catalogue Code-BR00001). Briefly, cell pellets were lysed using 1X Cell lysis buffer (provided in the kit) and the cell supernatant were obtained post centrifugation of the cell lysate in a cold microfuge at 14,000rpm for 5min. The protein content of the cell supernatants was estimated using Bradford (Bio-Rad) method. 20µl of the protein sample was added to each 96-well plate in duplicate on ice. Each sample was treated with 50µl of control solution and 50µl of reaction solution by swiftly adding one 50µl of control solution to one set of wells and 50µl of reaction solution to the other set of wells. The contents were gently mixed for 10s. The plate is covered and incubated in a 37ºC incubator for 30-60 min (without CO_2). After incubation cherry red colour appears in the wells. The O.D. is measured at 492nm using a plate reader at 30 min,60 min or 120 min. The control well reading was subtracted from the reaction well reading for each sample for each time point. The subtracted reading is used for enzyme activity calculation by considering the incubation time.

SOD2 Assay

Cell culture supernatant collected at 16h post-infection was analyzed using Mouse Superoxide dismutase [Mn], mitochondrial ELISA kit (SOD2) (ABclonal, Catalog Number-RK04590) following the manufacturer's instructions. Briefly, 50µl of standards or the test samples were added to each well and incubation was carried for 1 h at 37ºC followed by three washes with wash buffer. 100µl of the working Streptavidin-HRP solution was added and incubated for 30 minutes at 37ºC. After five washes, 90µL of TMB substrate solution was added per well and

incubated for 15-20 minutes at 37ºC under darkness. 50 µL of stop solution was added to each well and the optical density was measured within 5 minutes at 450nm with correction wavelengths set at 570nm or 630nm. The concentration of the samples was extrapolated from the standard curve.

ATP Estimation Assay

Cells harvested at required timepoints post-infection were estimated for ATP content using ATP Colorimetric Assay Kit (Sigma, MAK190) following the manufacturer's protocol. In duplicates,50µL samples were added per 95-well plate. A master mix containing 44µL of ATP assay buffer, 2µL of ATP probe, 2µL of ATP converter and 2µL of Developer Mix was added. After mixing, the plate was incubated for 30 minutes in dark at RT. Post-incubation, absorbance was measured at 570nm and ATP content was estimated from the ATP standard curve ranging from 0-10 nmole/µl. A treatment of 10µM oligomycin, an ATP synthase inhibitor, was provided to the cells as negative control (61, 62).

Seahorse OCR Measurement

Mitochondrial oxidative phosphorylation was assessed by measuring the oxygen consumption rate (OCR) using a modified mitostress test(63) on a XF Extracellular Flux Analyzer (Agilent Technologies) at 6hr post-infection following SIRT1/SIRT3 inhibitor treatment. 8-well XF sensor cartridge containing 200 µl/well of XF calibrate solution was preincubated overnight at 37 °C in a CO2-free incubator. 10-fold concentrated compound of oligomycin (Complex V inhibitor), and a combination of rotenone (Complex I inhibitor) and antimycin A (Complex III inhibitor) were loaded into a sensor cartridge to achieve final concentrations of 1.5 µM, and 2 µM, respectively. After a 30-min calibration of the XF sensor with the preincubated sensor cartridge, the cell plate was loaded into the analyzer, and OCR was analyzed under basal conditions. Sequential injection of complex inhibitors was used to assess oxygen utilization for

ATP generation and net mitochondrial oxygen consumption. Data were analyzed using WAVE software (Agilent Technologies).

2.2.16. Animal Experiment

For all experiments, 6–8 weeks old C57BL/6 or *gp91phox*-/- mice were used. For organ burden analysis, 6 weeks old C57BL/6 or *gp91phox*-/- mice were infected with 10^7 CFU bacteria via oral gavaging. For bacterial enumeration via flow cytometry, mice were infected with 10^7 GFP-expressing bacteria orally. Infected mice were intraperitoneally injected on every other day with either 1 mg/kg body weight of SIRT1 inhibitor EX-527 (Sigma-Aldrich) [32], or SIRT3 inhibitor 3TYP (Selleck Chemical) [33] or SIRT1 activator SRT1720 (Calbiochem, Sigma-Aldrich) [34] or treated with vehicle alone. 5 days post infection, mice were sacrificed, and bacterial organ load was estimated by plating the tissue homogenates on SS agar plates. For calculating percentage survival, 6 weeks old C57BL/6 mice were infected with 10^8 bacteria orally and monitored till fatality. For flow cytometry studies, the harvested liver or spleen were homogenized into single cell suspension and were subjected to flow cytometry. The animal experiments were carried out in accordance with the approved guidelines of the institutional animal ethics committee at the Indian Institute of Science, Bangalore, India (Registration No: 48/1999/CPCSEA). All procedures involving the use of animals were performed according to the Institutional Animal Ethics Committee (IAEC)-approved protocol.

2.2.17. *In vivo* knockdown

For in vivo knockdown adeno-associated virus serotype 6 (AAV6) was used. AAV6 viruses were produced in HEK293T cells. Briefly, HEK293T cells were transfected with AAV plasmid encoding shRNAs targeting SIRT1, SIRT3 and scramble control under U6 promoter together with helper plasmid using PEI Max 40000 (Polysciences USA). Next day transfection medium was removed, and fresh culture medium was added. Forty-eight hours later, medium was

collected, and fresh culture medium was added and incubated for next forty-eight hours. Again, culture medium was collected, and cells were harvested by trypsinization. Collected medium containing secreted AAV viral particles was incubated with 40% PEG 8000 overnight. Precipitated viral particles were then collected by centrifugation and re-suspended in PBS. Cells containing AAV viral particles were then lysed with citrate buffer and incubated with 40% PEG 8000 and processed similarly to medium for viral particle precipitation. Precipitated viral particles were then cleaned with chloroform and loaded on iodixanol gradient for further cleaning using ultracentrifugation. Cleaned viral particles were collected from the forty percent gradient and loaded on Amicon 100K cut-off columns. Purified AAV particles were then titrated by real-time PCR. For infection of AAV6, the mice were intravenously injected with a volume of 200 µl containing approximately 10^{12} viral particles harbouring the respective scrambled or shRNA constructs. The mice were infected at 7^{th} day after injection of the virus with 10^6 cfu units of *S.* Typhimurium orally. Fifth day post-infection, mice were euthanized, and dissected out for organ harvesting and blood collection. The knockdown was validated by performing western blotting and qPCR of the harvested liver tissue (Fig. S9).

2.2.18. Haematoxylin and Eosin Staining

6-8 weeks old C57BL/6 mice were infected with 10^7 bacteria orally. Infected mice were intraperitoneally injected every alternate with either 1 mg/kg body weight of SIRT1 inhibitor EX-527, or SIRT3 inhibitor 3TYP or SIRT1 activator SRT1720 or treated with vehicle alone. 5 days post infection, mice were euthanized, and liver were collected and fixed using 3.5% paraformaldehyde. The fixed liver was then dehydrated using a gradually increasing concentration of ethanol and embedded in paraffin. 5µm sections were collected on coated plates. Sections were further rehydrated and then stained with hematoxylin and eosin. Images were collected in a Leica microscope.

Cell Death Estimation Assay

Cell death estimation assay was performed using Propidium iodide (PI) solution (BD Pharmingen, Cat No.-556463) following manufacturer's protocol by subjecting the cells subjected to PI staining (at concentration of 50µg/ml in PBS (pH 7.4) at the desired time-point post-infection. The samples were analyzed using flow cytometry as described earlier.

Intra-phagosomal pH measurement

To measure SCV pH of macrophages, a previously reported protocol (64) was followed. Overnight grown stationary phase cultures of STM WT was labelled with 20 µM pH rhodo red succinimidyl ester (Molecular Probes, Invitrogen) at 37ºC for 1h. Bacteria were washed with 0.1 M sodium bicarbonate buffer (pH= 8.4) before and after labelling. RAW264.7 cells were infected with these labelled bacteria at MOI 10. At 6- and 16 h post-infection, macrophages were washed and resuspended in PBS for flow cytometric analysis (CytoFLEX by Beckman Coulter Life Sciences) using 560 nm excitation and 585 nm emission filter. To generate a standard curve of known pH, macrophages were infected with pH rhodo-red-labelled bacteria and subjected to different pH-buffered solution ranging from pH 5.0 to 8.0 in presence of valinomycin (10µM) and nigericin (10µM). Post-equilibration for 1h, macrophages were harvested and subjected to flow cytometric analysis. The percentage pH rhodo-red-positive population was plotted as a function of pH to obtain a standard curve, which was used to obtain the SCV pH.

Intracellular bacterial pH Measurement

STM WT and STM Δ*ompR* strains, transformed with a pH sensitive plasmid pBAD-pHUji (Plasmid#61555)(65), were equilibrated at different pH range (5.0 to 9.0) using a buffered solution with 40µM sodium benzoate. Flow cytometric analysis of the fluorescence intensity ratios produced a standard curve. The above-mentioned strains were used to infect the

macrophages (knockdown macrophages or inhibitor treated). 16hr post- infection, the cells were harvested for flow cytometric analysis to obtain fluorescence ratios. The standard curve was used to interpolate ratios measured to obtain intracellular bacterial pH within infected macrophages.

2.2.19. Statistical analysis

Data were analyzed and plotted using the GraphPad Prism 8 software (San Diego, CA). Statistical significance was determined by Student's t-test or Two-way ANOVA and Bonferroni post-t-test to obtain p values. Adjusted p-values below 0.05 are considered statistically significant (****$p<0.0001$,***$p < 0.001$, ** $p<0.01$, *$p<0.05$). The results are expressed as mean ± SD or SEM of three independent experiments.

RESULTS

Salmonella modulates SIRT1 and SIRT3 expression along its course of infection in macrophages

Upon infection of RAW 264.7 murine macrophages with wildtype *Salmonella* Typhimurium strain 14028S, we observed an increased expression level of *SIRT 1* and *SIRT3* at initial and middle phases of infection, precisely at 2hr and 6hr post infection through qPCR (Fig.1, A and B). The *SIRT1* expression level declined at later phases of infection. On the other hand, the *SIRT3* transcript levels remained elevated at all time points with respect to uninfected control with a marked increment at 16hr time point post-infection which subsided at 20hr post-infection. We even monitored the expression profile of *SIRT1* and *SIRT3* in primary macrophages like peritoneal macrophages of C57BL/6 mice and observed a similar trend of elevated expression at initial (2hr), middle (6hr), and late (16hr) time points post-infection (Fig.1, C and D). In Confocal Laser Scanning Microscopy (CSLM) studies, we observed a similar increase in SIRT1 and SIRT3 expression at 6hr post infection within the infected

macrophages RAW264.7 macrophages. (Fig.1, E-H). Subsequently, to ascertain whether indeed *Salmonella* could modulate SIRT1 or SIRT3 expression levels, we evaluated the *SIRT1* and *SIRT3* mRNA and SIRT1 and SIRT3 protein expression profile within RAW264.7 macrophages upon infection with wildtype *S*. Typhimurium and SPI-1 (Δ*invC*) (InvC- protein export apparatus) or SPI-2 (Δ*ssaV* and Δ*steE*) (SsaV- Structural component of SPI-2 needle apparatus, SteE- SPI-2 effector protein involved in driving M2 polarization) mutants of *S*. Typhimurium. Our results depict the ability of wildtype *S*. Typhimurium to induce the expression of both SIRT1 and SIRT3 within the infected RAW264.7 macrophages. However, infection with either SPI-1 or SPI-2 mutant abrogates the induction of *SIRT1* whereas only SPI-2 mutants (Δ*ssaV* and Δ*steE*) and not SPI-1 mutant infection caused reduction in *SIRT3* transcript level expression in the infected macrophages, implicating the role of SPI-1 and SPI-2 genes in triggering SIRT1 and SIRT3 in the infected macrophages (Fig. 1, I-J). Thus, an increase in expression profile both at transcript and protein levels indicates their role in *Salmonella* pathogenesis.

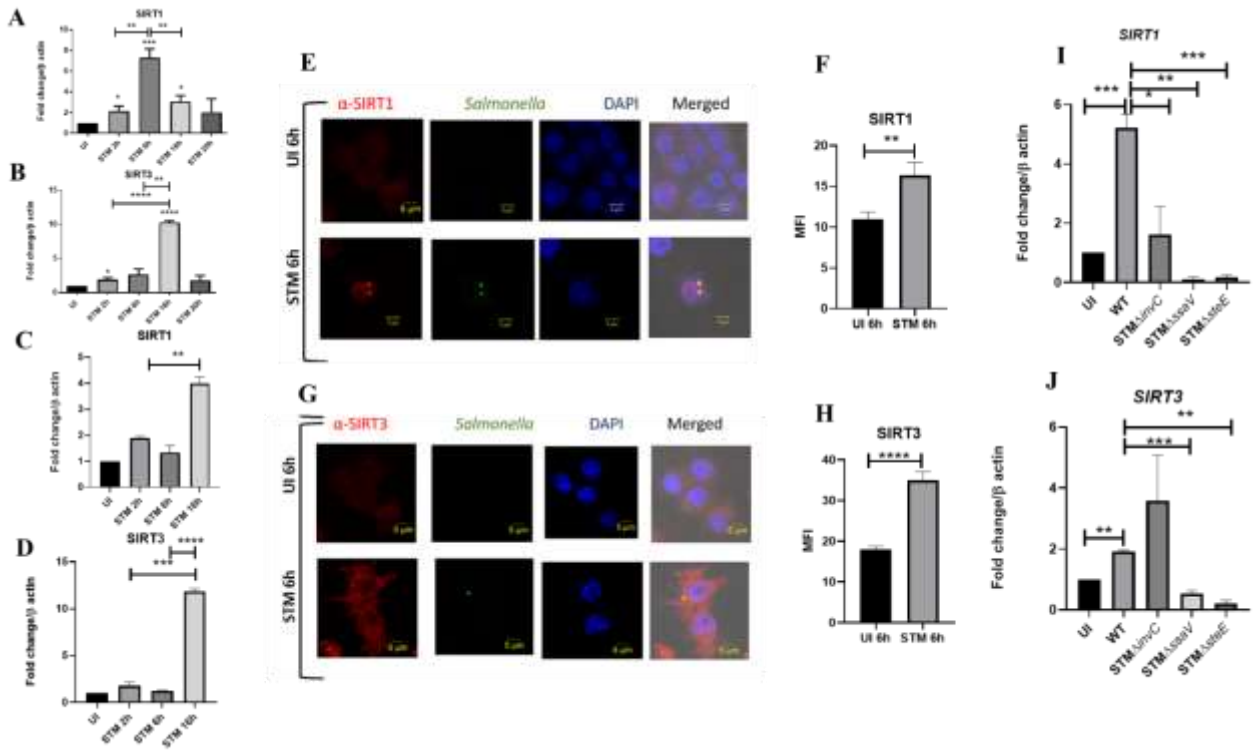

Fig.1- *Salmonella* modulates the expression of SIRT1 and SIRT3 along its course of infection

A-B. Expression studies of *SIRT1* and *SIRT3* through qPCR in RAW 264.7 macrophages. Data is representative of N=4, n=2. Unpaired two tailed Student's t test was performed to obtain the p values. (****p<0.0001,***p < 0.001, ** p<0.01, *p<0.05)

C-D-Expression studies of *SIRT1* and *SIRT3* through qPCR in peritoneal macrophages derived from C57BL/6. Data is representative of N=3, n=2. . Unpaired two tailed Student's t test was performed to obtain the p values. (****p<0.0001,***p < 0.001, ** p<0.01, *p<0.05)

E. Representative confocal images of RAW264.7 macrophages exhibiting SIRT1 expression upon *S.* Typhimurium infection at indicated time points post infection. Data is representative of N=3, n=80 (microscopic field).

F. Quantitative representation of the expression profile as depicted in the confocal images (E) in terms of Mean Fluorescence Intensity (MFI). Unpaired two tailed Student's t test was performed to obtain the p values. (****p<0.0001,***p < 0.001, ** p<0.01)

G. Representative confocal images of RAW264.7 macrophages exhibiting SIRT3 expression upon *S.* Typhimurium infection at indicated time points post infection. Data is representative of N=3, n=80 (microscopic field).

H. Quantitative representation of the expression profile as depicted in the confocal images (G) in terms of Mean Fluorescence Intensity (MFI). Unpaired two tailed Student's t test was performed to obtain the p values. (****p<0.0001, *** p < 0.001, ** p<0.01)

I. qPCR mediated expression of *SIRT1* in RAW264.7 macrophages upon infection with wildtype *S.* Typhimurium or SPI-1 (Δ*invC*)or SPI-2 (Δ*ssaV* and Δ*steE*) *m*utants of *S.* Typhimurium. Data is representative of N=3,n=3. Unpaired two tailed Student's t test was performed to obtain the p values. (****p<0.0001,***p < 0.001, ** p<0.01)

J. qPCR mediated expression of *SIRT3* in RAW264.7 macrophages upon infection with wildtype *S.* Typhimurium or SPI-1 (Δ*invC*) or SPI-2 (Δ*ssaV* and Δ*steE*) *m*utants of *S.* Typhimurium. Data is representative of N=3, n=3. Unpaired two tailed Student's t test was performed to obtain the p values. (****p<0.0001,***p < 0.001, ** p<0.01)

SIRT1 and SIRT3 play crucial role in intracellular bacterial proliferation in infected murine macrophages

As our previous *SIRT1* and *SIRT3* expression data in the polarized macrophages, hinted at the role of SIRT1 and SIRT3 in driving polarization of macrophages in the infected macrophages. To evaluate the role of SIRT 1 and SIRT3 in the intracellular proliferation of the bacteria within

murine macrophages, we have undertaken knockdown of SIRT1 and SIRT3 in RAW 264.7 (F macrophages through PEI-mediated transfection of shRNA plasmids directed against SIRT1 and SIRT3. Post 48hr of transfection, the transfected cells were infected with MOI=10 of wildtype *S*. Typhimurium and a gentamicin protection assay was performed. Intracellular proliferation of the bacteria was quantified by plating the cell lysate at 2hr and 16hr post-infection. *Salmonella* exhibits compromised intracellular survival in SIRT1 and SIRT3 knock-down RAW264.7 macrophages in comparison to the un-transfected and scrambled controls (Fig.2, A). Further, we have assessed the intracellular proliferation in peritoneal macrophages isolated from thioglycolate-treated adult C57BL/6 mice post SIRT1 (EX-527) and SIRT3 (3TYP) inhibitor treatment. SIRT1 or SIRT3 inhibitor-treated macrophages exhibited attenuated intracellular replication in comparison to the untreated peritoneal macrophages (Fig,2, B). Together, our results depict the role of SIRT1 and SIRT3 in controlling the intracellular proliferation of *S*. Typhimurium.

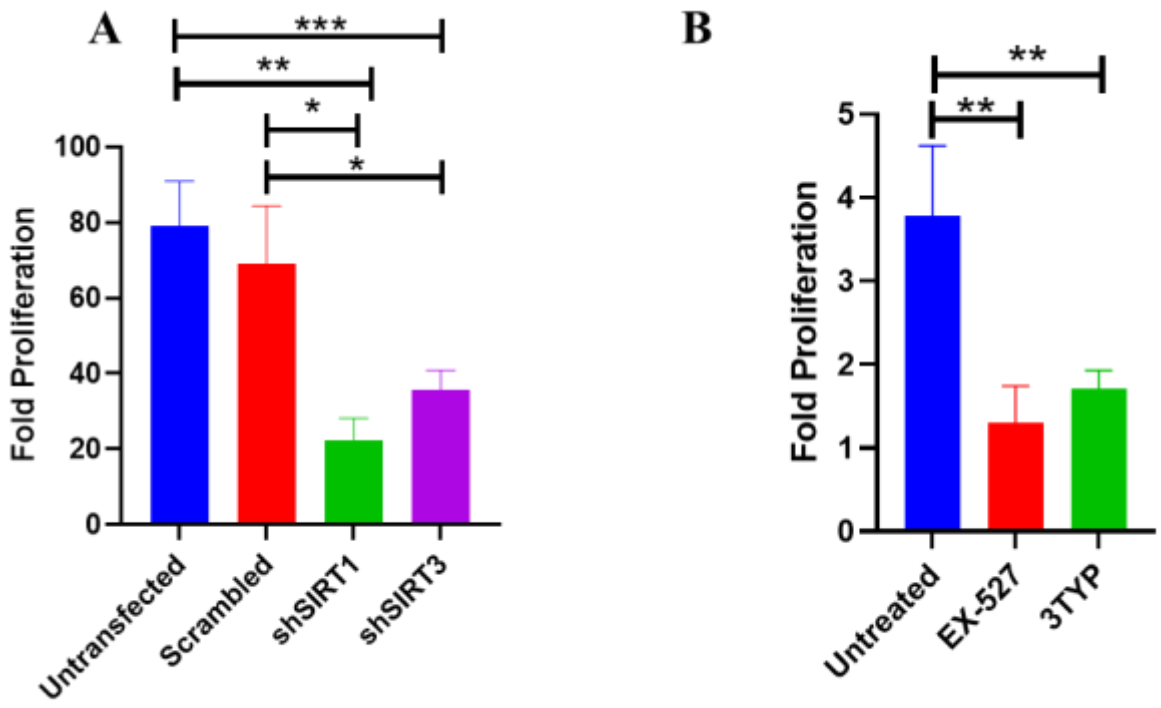

Fig. 2. Effect of SIRT1 and SIRT3 knockdown in intracellular bacterial proliferation within RAW 264.7 and primary murine macrophages.

A. Fold Proliferation of *Salmonella* Typhimurium within RAW 264.7 macrophages in transfected and un-transfected conditions. Data is representative of N=3, n=3. Unpaired two tailed Student's t test was performed to obtain the p values. (** $p<0.01$, * $p<0.05$)

B. Fold Proliferation of *Salmonella* Typhimurium within infected peritoneal macrophages isolated from adult male C57BL/6 mice upon SIRT1 (EX-527) or SIRT3 (3TYP) inhibitor treatment at the concentration 1µM. Data is representative of N=3, n=3. Unpaired two tailed Student's t test was performed to obtain the p values. (** $p<0.01$, * $p<0.05$)

SIRT1 and SIRT3 inhibition contribute to skewed inflammatory host responses upon *Salmonella* infection

Several reports indicate the role of SIRT1 and SIRT3 in modulation of host immune responses pertaining to infection scenario(33, 35). Therefore, we intend to check whether SIRT1 or SIRT3 regulate immune functions in *Salmonella* infected macrophages**.**

Immune functions are an important determinant of macrophage polarization. Since SIRT1 and SIRT3 played an immune-modulatory role in *Salmonella* infection, we investigated whether *Salmonella* infection is associated with a shift in macrophage polarization status. To assess the ability of the pathogen to alter the polarization state of the macrophage, we have undertaken gene expression profiling of various M1 and M2 markers using nanoString nCounter technology along the course of *Salmonella* Typhimurium infection at the indicated time points in RAW 264.7 macrophages. A gradual shift from pro-inflammatory M1 toward the anti-inflammatory M2 state was observed with the progression of *Salmonella* infection. Along the course of infection, there was a reduction in the expression of M1 markers like *NOS2*, *CD40*,*CD86*, *TNF-α*, *Nfkb2*,*IL-6* and a corresponding increase in the expression of the M2 markers such as *Arg-1*, *CCL-17*, *CD 206*, *IL4ra* with an exception of *Tgf-β* (Fig.3, A).In order to validate the polarization potency of the pathogen, FACS was performed using a pro-inflammatory M1 surface marker, CD86 tagged with PE. The data suggests a distinct decrease in CD86 positive population in the infected sets in comparison to the uninfected and the fixed dead bacteria control along the course of *S.* Typhimurium infection (Fig.3, B). Thus, the live pathogen has a propensity to skew the polarization state of the macrophage toward an anti-inflammatory M2 state to subvert the initial acute inflammatory response mounted by the host immune system.

To assess the role of SIRT1 and SIRT3 in macrophage polarization, we determined anti-inflammatory CD206 surface marker profiling of the infected macrophages through flow cytometry. Knockdown of SIRT1 or SIRT3 in infected RAW 264.7 macrophages resulted in a reduction in anti-inflammatory CD206 surface marker expression at 16hr post-infection (Fig.

3, C). Moreover, SIRT1 or SIRT3 knockdown led to enhanced intracellular ROS generation within the infected macrophages in comparison to the scrambled or the untransfected control (Fig.S5). Further, the Haematoxylin and Eosin staining of the *S.* Typhimurium infected mice liver tissue sections depicted exacerbated signs of inflammation in the SIRT1 (EX-527) or SIRT3 (3TYP) inhibitor-treated cohorts in comparison to the untreated controls with multiple necrotic foci and increased influx of inflammatory cell inflates. Moreover, these acute inflammatory signs of the liver sections get ameliorated in the SIRT1 (SRT1720) activator-treated infected cohort (Fig.8, T-U) (Data described later). Together, these data suggest the role of SIRT1 and SIRT3 in the modulation of host inflammatory response. Previous literature reports have shown that SIRT1 physically interacts with p65 subunit of NF-κB and inhibits transcription by deacetylating p65 at lysine 310(66). Moreover, SIRT1-mediated deacetylation of the p65 subunit of the master regulator of the inflammatory response, NF-κB, results in the reduction of the inflammatory responses mediated by this transcription factor (67). To evaluate the immune regulatory mechanism of SIRT1 in the *S.* Typhimurium (STM) infection scenario, we undertook SIRT1 immunoprecipitation in the infected RAW264.7 macrophages at 16h post-infection alongside the uninfected macrophages and probed for NF-κB p65 interaction. We observed an increased interaction of SIRT1 with NF-κB p65 in the infected macrophages in comparison to the uninfected control (Fig.4, A). Further, the knockdown of SIRT1 resulted in increased acetylation status of the NF-κB p65 upon infection in comparison to the scrambled, infected control (Fig.4, B, C). To understand whether the enzymatic domain of SIRT1 possess any role in mediating this interaction, we carried out NF-κB p65 immunoprecipitation in infected RAW264.7 macrophages in presence or absence of SIRT1 catalytic chemical inhibitor, EX-527(1μM) treatment at 16h post-infection. We observed an increased interaction of NF-κB p65 with SIRT1 in the infected untreated macrophages when compared to the untreated uninfected control (Fig.4, D). However, the interaction of NF-κB p65 with SIRT1 gets

abrogated under the EX-527 inhibitor treatment in the infected macrophages thereby implying the function of the catalytic domain in mediating the interaction (Fig.4, D). Moreover, an increased acetylation status of NF-κB p65 was observed in the EX-527 treated infected macrophages in comparison to the untreated infected macrophages (Fig. 4 E).

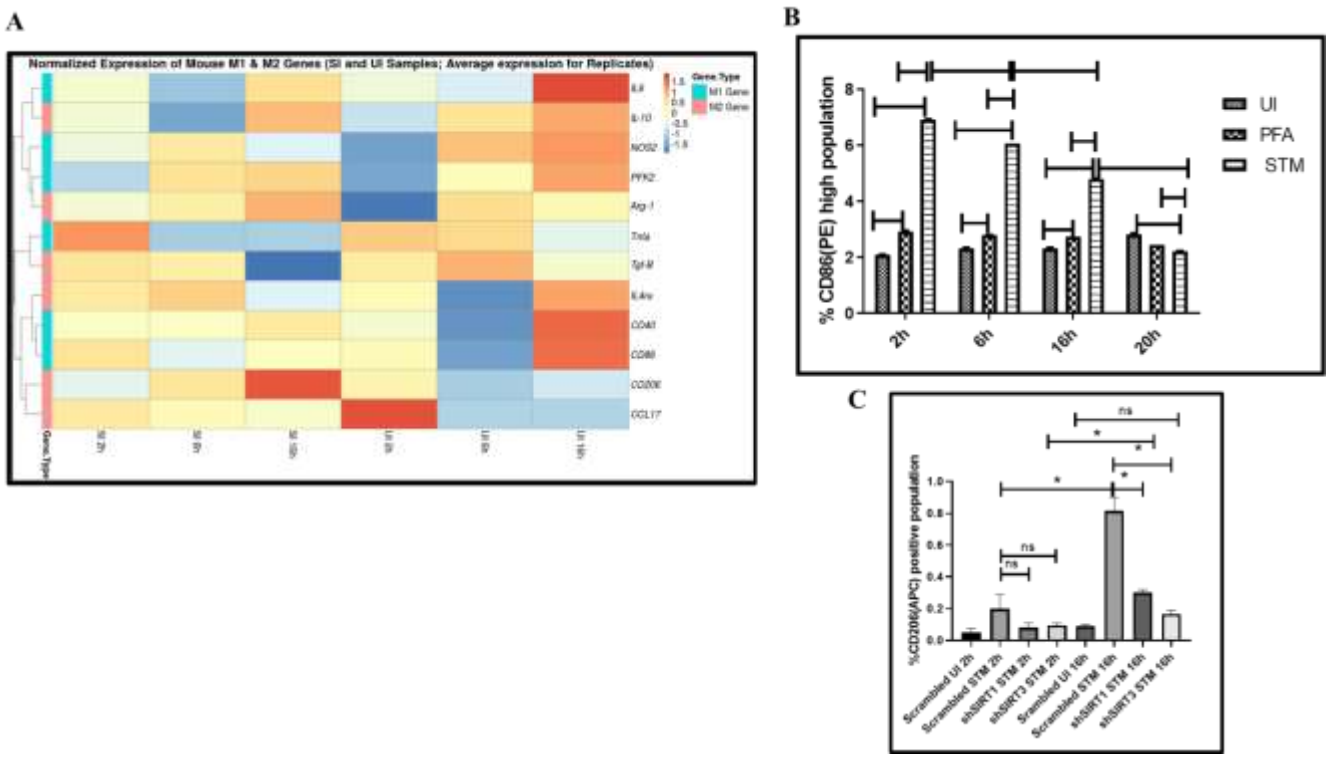

Fig.3- *Salmonella* Typhimurium skews the polarization state of the macrophage toward an immunosuppressive M2 state along the course of infection

A. nanoString gene expression profiling data of *S.* Typhimurium infected RAW 264.7 macrophages versus uninfected control data sets at 2hr, 6hr and 16hr time points of infection. Data is representative of N=2,n=2.

B. Quantitative representation of flow cytometric analysis of alteration in M1 CD86 positive population in *S.* Typhimurium (STM) infected samples in comparison to uninfected (UI) and Paraformaldehyde Fixed (PFA) bacteria at the indicated time post-infection. Data is

representative of N=2, n=3. Two-way ANOVA and Bonferroni post-t-test was used to obtain p values. (*** $p < 0.001$)

C. Quantitative representation of flow cytometric analysis of M2 surface marker CD206 in *S.* Typhimurium (STM) infected SIRT1 or SIRT3 knockdown RAW264.7 macrophages in comparison to the scrambled control at the indicated time post-infection. UI-Uninfected sample. Data is representative of N=3, n=3. Two-way ANOVA and Bonferroni post-t-test was used to obtain p values. (*** $p < 0.001$)

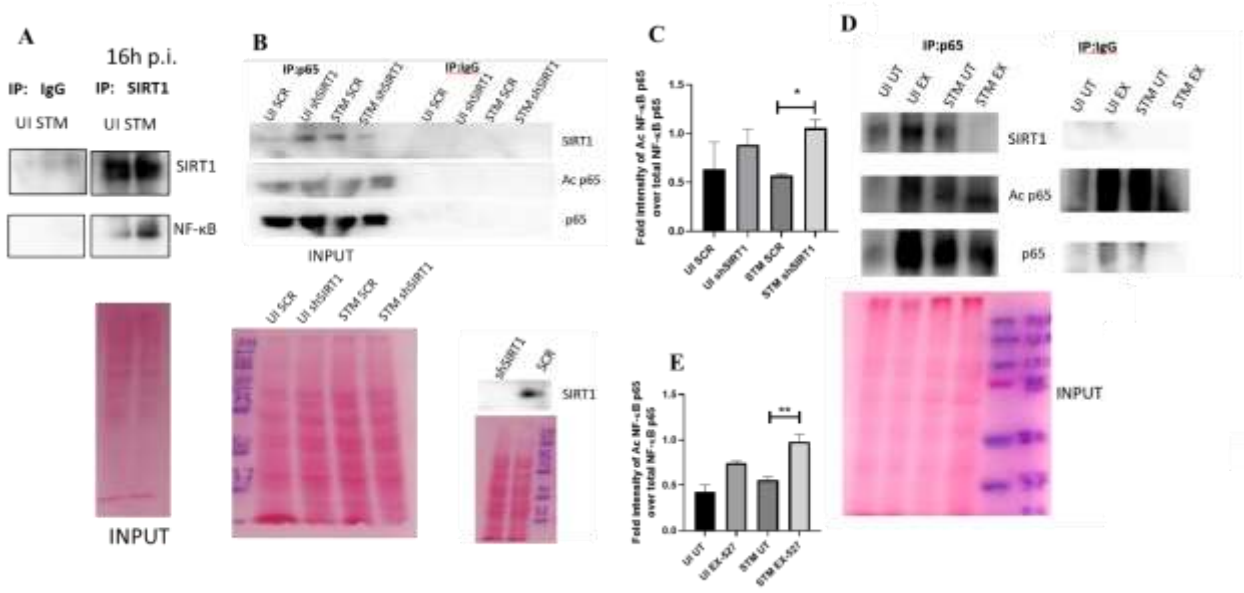

Fig.4- SIRT1 mediates modulation of immune functions via deacetylation of p65 subunit of NF-κB in *S.*Typhimurium infected macrophages.

A. Immunoblot depicting p65 NF-κB interaction with SIRT1 post immunoprecipitation of SIRT1 in uninfected (UI) or *S.* Typhimurium (STM) infected RAW264.7 macrophages at 16hr post-infection. Data is representative of N=3, n=1

B. An immunoblot depicting p65 NF-κB interaction with SIRT1 as well as the p65 NF-κB acetylation status post immunoprecipitation of p65 (IP: p65) or with control IgG (IP: IgG) in

uninfected (UI) or *S.* Typhimurium (STM) infected RAW264.7 macrophages upon knockdown with SIRT1 shRNA or scrambled control.

C. Densitometric plot depicting the band intensities of Acetylated p65 over total p65 in blot B.

D. An immunoblot depicting p65 NF-κB interaction with SIRT1 as well as the p65 NF-κB acetylation status post immunoprecipitation of p65 (IP: p65) or with control IgG (IP: IgG) in uninfected (UI) or *S.* Typhimurium (STM) infected RAW264.7 macrophages upon SIRT1 inhibitor (EX-527, 1μM) treatment at 16hr post-infection. UT- Untreated.

E. Densitometric plot depicting the band intensities of Acetylated p65 subunit of NF-κ B over total p65 NF-κB in blot D.

SIRT1 and SIRT3 play crucial role in mediating metabolic switch in infected macrophages

Macrophage polarization is not only governed by immunological changes but is also contributed by metabolic reprogramming(23, 68, 69)**.** Since previous data suggested progression of *Salmonella* infection with the shift in polarization state of the macrophage, we decided to investigate alteration of the metabolic state of the macrophages as macrophage polarization is governed by immune-metabolic shift. In pursuit of fulfilling such requirement, we performed gene expression studies of various metabolic genes through nanoString nCounter technology in *S.* Typhimurium infected RAW 264.7 macrophages. Analysis of the gene profile revealed upregulation of genes involved in fatty acid oxidization and tricarboxylic acid cycle and corresponding downregulation of genes involved in glycolysis (Fig.5, A). To validate the findings, we carried out qRTPCR to quantitatively measure the expression of a fatty acid oxidation gene, *PPARδ* in infected RAW 264.7 macrophages. We found that mRNA level was elevated to 2-fold at 2hr and 6hr post-infection. At the late phase of infection, 16hr post infection around 6-fold upregulation in mRNA transcript was noted (Fig.5, B). Lactate

estimation assay of *S.* Typhimurium infected RAW264.7 macrophages at the initial time point of 2hr and at the late time point of 16hr post infection revealed decline in lactate (glycolysis end product) production at 16hr in comparison to 2hr post-infection timepoint (Fig. 5C). Together, these results suggest the capability of the pathogen to drive a shift in the metabolic status of the infected macrophages toward fatty acid oxidation. Next, we evaluated the function of SIRT1 and SIRT3 in influencing the metabolic switch in the infected macrophages through qRT PCR with several host fatty acid oxidizing genes (*Acox*, *Hadha, Pdha*, *and AcadL)* and glycolytic gene (*PfkL*) in SIRT1 and SIRT3 knockdown macrophages (Fig. S7, A) and via lactate production assay (Fig. 5, D-E). Lactate estimation assay in SIRT1 and SIRT3 knockdown condition revealed enhanced lactate production at 16hr post infection in comparison to the scrambled control which further authenticates the increased host glycolysis upon SIRT1 and SIRT3 knockdown scenario (Fig. 5, D-E). Moreover, SIRT1 and SIRT3 knockdown or catalytic inhibition in peritoneal macrophages resulted in increased protein expression of host glycolytic genes such as Phosphoglycerate kinase (Pgk), Phosphofructokinase (Pfk) with concomitant reduction in protein expression of TCA cycle gene like Pyruvate dehydrogenase (Pdha1) and fatty acid oxidation genes such as Hadha and Acox1 (Fig.5, F). Fatty acid oxidation assay in the RAW264.7 macrophages under SIRT1 or SIRT3 knockdown condition or inhibition treatment revealed significant decrease in fatty acid β oxidation activity of the infected macrophages in comparison to the scrambled or the untreated control (Fig.5, G). To investigate whether the host metabolic switch toward increased fatty acid oxidation is being driven by the pathogen, we performed fatty acid β oxidation activity assay under wildtype *S*. Typhimurium (STM WT), SPI-1 (Δ*invC*) or SPI-2 (Δ*ssaV* and Δ*steE*) mutants of *S*. Typhimurium infection condition. We found that the wildtype bacteria with its intact SPI-2 effector secretion apparatus could promote increased host fatty acid β

oxidation. In the contrary, the SPI-2 (Δ*ssaV* and Δ*steE*) mutants of *S.* Typhimurium failed to drive host metabolic shift towards increased fatty acid oxidation (Fig. 5, H).

Collectively, these data suggest the role of SIRT1 and SIRT3 in mediating the *Salmonella* induced host metabolic shift in the infected macrophages.

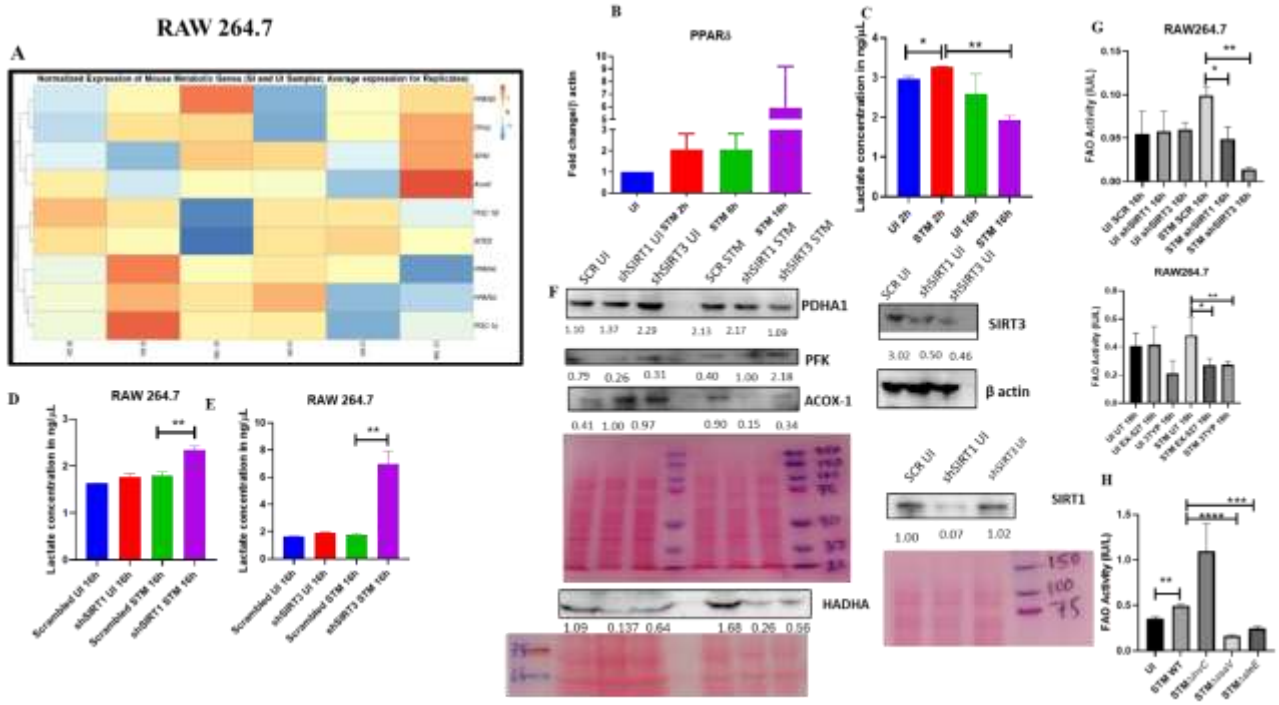

Fig.5- *Salmonella* Typhimurium drives the metabolism of the infected macrophage toward fatty acid oxidation

A. Metabolic gene expression data of *S.* Typhimurium infected RAW 264.7 macrophages at 2hr, 6hr and 16hr time points of infection through nanoString. Data is representative of N=2, n=1.

B. *PPARδ* qPCR expression data in *S.* Typhimurium infected RAW 264.7 macrophages at the indicated time points of infection. Data is representative of N=3, n=2.

C. Lactate estimation assay of *S.*Typhimurium infected RAW264.7 macrophages at the initial time point of 2hr and at the late time point of 16hr post infection. Data is representative of N=3, n=3. Unpaired two-tailed Student's t test was performed to obtain the p values. (** $p<0.01$, * $p<0.05$)

D-E-Lactate estimation assay of *S.*Typhimurium infected RAW264.7 macrophages upon SIRT1 (D) or SIRT3 (E) knockdown condition at16h post-infection. Data is representative of N=3 , n=3. Unpaired two-tailed Student's t test was performed to obtain the p values.

F. Immunoblotting of host glycolytic (PGK), TCA cycle (PDHA1) and fatty acid oxidation (HADHA, ACOX-1) proteins under SIRT1 and SIRT3 knockdown condition of *S.* Typhimurium infected RAW264.7 macrophages at 16h post-infection.

G. Fatty Acid Oxidation (FAO) Assay of uninfected (UI) and infected (STM) RAW264.7 macrophages under SIRT1 or SIRT3 knockdown or inhibitor treatment. N=2, n=2. (** $p<0.01$, * $p<0.05$)

H. Fatty Acid Oxidation (FAO) Assay of uninfected (UI) and infected RAW264.7 macrophages under infection with wildtype *S.* Typhimurium (STM WT), SPI-1 (Δ*invC*)or SPI-2 (Δ*ssaV* and Δ*steE*) *m*utants of *S.* Typhimurium. Data is representative of N=2,n=2. (** $p<0.01$, * $p<0.05$)

SIRT1 and SIRT3 concomitantly influence *Salmonella* metabolism

Our previous data indicated a shift in host metabolism toward increased fatty acid oxidation along the course of *Salmonella* Typhimurium infection in murine RAW 264.7 macrophages. This observation led us to investigate the influence of host metabolic shift on the metabolic status of the pathogen present inside the infected macrophages(70). We were intrigued whether increased glucose availability within the fatty-acid oxidizing macrophages is utilized by the

bacteria. Thus, we undertook simultaneous gene expression studies of various *Salmonella* genes involved in their pathogenesis and metabolism through nanoString nCounter technology in *S.* Typhimurium infected RAW 264.7 macrophages. The nanoString gene profile revealed enhanced expression of genes involved in *Salmonella* glycolysis and glucose uptake such as *pfkA* and *ptsG*, respectively (Fig.6, A). This finding indicates the ability of the pathogen to drive the metabolic state of the host toward fatty acid oxidation with corresponding increased glucose utilization by the bacteria favoring their survival inside the host. qRT PCR results with several bacterial fatty acid oxidizing genes (*fadA, fadB,fadL,aceA, aceB*) and glycolytic genes (*ptsG*) in knockdown condition of SIRT1 and SIRT3 in RAW 264.7 macrophages further validated the nanoString gene expression profiles (Fig.6, B). In scrambled control, *Salmonella* infection progresses with increased *Salmonella* glycolysis and reduced bacterial fatty acid oxidation. However, knockdown of SIRT1 and SIRT3 abrogate this bacterial metabolic shift by reducing its glycolysis and by exhibiting enhanced fatty acid oxidation thereby attenuating pathogen intracellular survival. Similar observations were obtained from the qPCR data in the infected mice liver and spleen samples with increased transcript level expression of bacterial fatty acid oxidation genes and decreased expression of bacterial glycolytic genes upon SIRT1 or SIRT3 inhibitor treatment (Fig. 6 C, D). Therefore, SIRT1 and SIRT3 driven host metabolic switch potentially influence the metabolic profile of the intracellular pathogen.

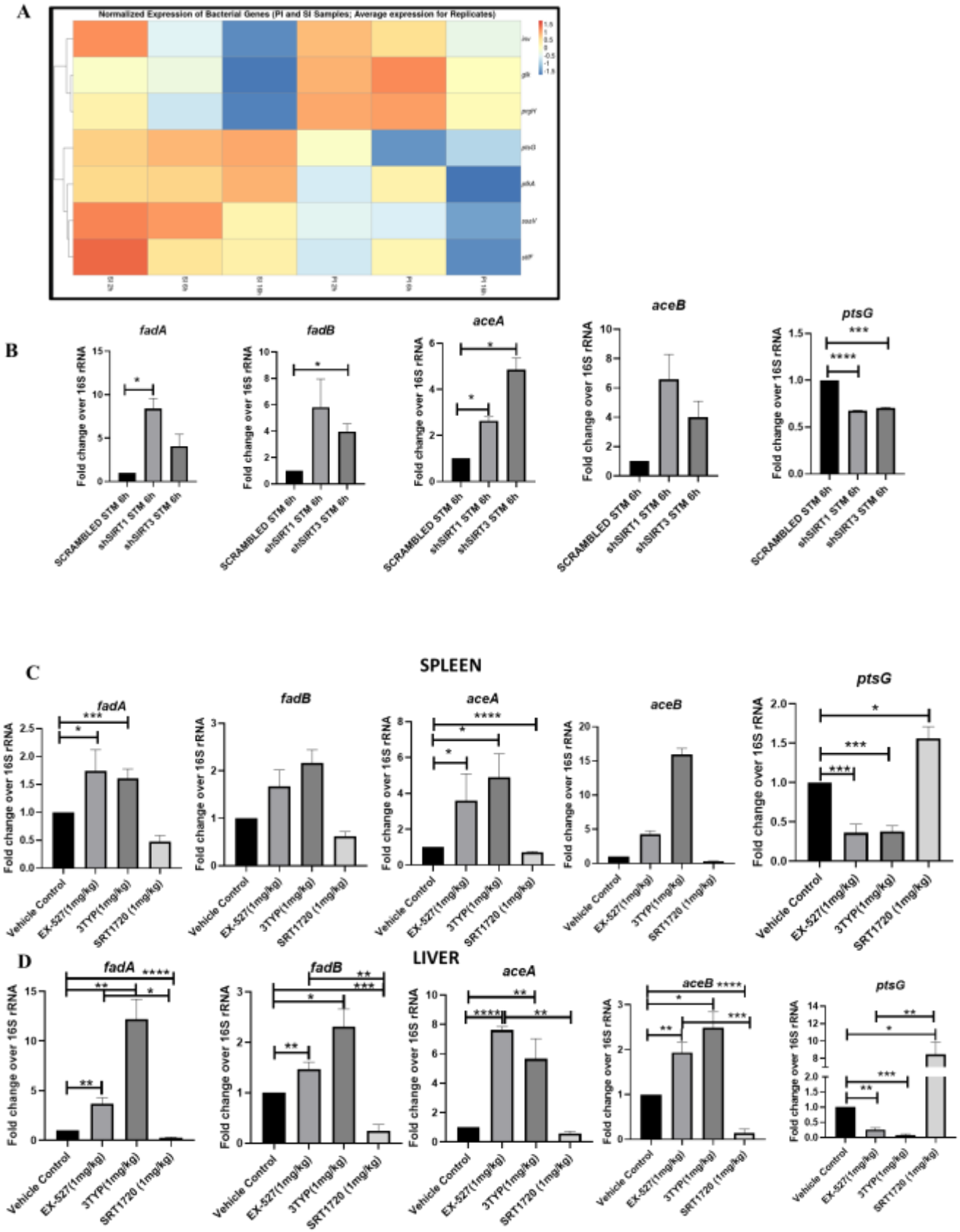
A
Normalized Expression of Bacterial Genes (PI and SI Samples; Average expression for Replicates)
B
fadA
fadB
aceA
aceB
ptsG
Fold change over 16S rRNA
SCRAMBLED STM 6h
shSIRT1 STM 6h
shSIRT3 STM 6h
C
SPLEEN
Vehicle Control
EX-527(1mg/kg)
3TYP(1mg/kg)
SRT1720 (1mg/kg)
D
LIVER

Fig.6- *Salmonella* Typhimurium infection proceeds with increased glycolysis and glucose uptake inside the infected RAW 264.7 macrophages

A. *Salmonella* gene expression profiling data of *S.* Typhimurium infected RAW 264.7 macrophages at 2hr, 6hr and 16hr time points of infection through nanoString. SI- *S.* Typhimurium infected, PI- PFA fixed *S.* Typhimurium infected. SPI-1 genes- *Inv, PrgH* , SPI-2 genes- *ssaV,stfF, glk*- glucokinase, *pfkA*-phosphofrucktose kinase A, *ptsG*-Phosphophenolpyruvate-dependent sugar phosphotransferase system (PTS). Data is representative of N=2, n=2.

B. qRT PCR gene expression profiling of *Salmonella* metabolic genes within infected RAW264.7 macrophages in knockdown condition of either SIRT1 or SIRT3 at 6hr post infection. Data is representative of N=3, n=3.

C-D. qRT PCR gene expression profiling of *Salmonella* metabolic genes within infected female C57BL/6 mice spleen (C) and liver (D) under SIRT1 or SIRT3 inhibitor treatment harvested at 5^{th} day post infection of *S.*Typhimurium (10^7 cfu units/animal). Unpaired two-tailed Student's t test was performed to obtain the p values. Data is representative of N=3, n=3. (****$p<0.0001$, *** $p < 0.001$, ** $p<0.01$, * $p<0.05$)

Mechanism behind SIRT1 or SIRT3 mediated metabolic switch

As per our previous findings, SIRT1 or SIRT3 inhibition led to increased host glycolysis and decline in fatty oxidation in the infected macrophages. HIF1α is a master regulator of glycolysis in host during stress conditions(71). Previous reports have suggested HIF1α to be a target of deacetylation by SIRT1 at Lys 674 which contribute to metabolic reprogramming in cancer cells. During hypoxia, downregulation of SIRT1 leads to increased acetylation and activation of HIF1α(72). Additionally, in CD4+ T cells, ectopic expression of SIRT1 inhibited IL-9 production and glycolysis by negatively regulating HIF1α(73). To delve into the mechanism

behind SIRT1 mediated modulation of metabolic responses, we assessed the interaction of SIRT1 with HIF-1α in infected RAW264.7 macrophages. The immunoprecipitation studies of SIRT1 showed increased interaction of the SIRT1 with HIF1α in the *S.* Typhimurium infection scenario with respect to the uninfected control (Fig.7, A). Further, we evaluated the acetylation status of HIF1α in the SIRT1 knockdown status of the infected macrophages. We found that SIRT1 knockdown showed increased acetylation of HIF1α in the infected macrophages in comparison to the scrambled infected control at 16hr post-infection (Fig. 7, B,C). Immunoprecipitation studies under SIRT1 (EX-527) inhibitor treatment in RAW264.7 macrophages revealed increased acetylation of HIF1-α along with reduced interaction of HIF-1α with SIRT1, thereby indicating the probable role of the catalytic domain in influencing the interaction (Fig. 7 D-F). Further, to ascertain the role of HIF-1α in mediating the glycolytic switch in the infected macrophages, we estimated the lactate production under SIRT1 and SIRT3 knockdown conditions in the presence or absence of HIF-1α inhibitor (chetomin)[53]. Our results depicted a decline in lactate production upon chetomine treatment including under SIRT1 and SIRT3 knockdown conditions (Fig.7G). Together, our results implicate the role of SIRT1 in governing glycolytic shift in the infected macrophages by deacetylating HIF1α. Upon SIRT1 knockdown or inhibition, HIF1α gets hyperacetylated which causes activation of the downstream glycolytic genes. Alternatively, several key literatures suggest the role of SIRT3 in modulating metabolic programming by deacetylating several proteins involved in fatty acid oxidation, the tricarboxylic acid cycle and oxidative phosphorylation [54][55]. PDHA1 (Pyruvate Dehydrogenase E1 subunit alpha) is a key enzyme linking glycolysis to TCA cycle and oxidative phosphorylation. SIRT3 regulates PDHA1 acetylation by deacetylating PDHA1 at lysine 385 residue, thereby playing a key role in metabolic reprogramming [55]. PDHA1 acetylation coincides with PDH activity and increased PDHA1 phosphorylation [55]. Therefore, we investigated the role of SIRT3 in the modulation of host fatty acid oxidation

upon *S*. Typhimurium infection in RAW264.7 macrophages. To do so, we immunoprecipitated PDHA1 and checked for its interaction with SIRT3 or SIRT1 under the knockdown condition of SIRT3 or upon SIRT3 inhibitor treatment (Fig.7 I-J). We observed an increased interaction of PDHA1 with SIRT3 in the infection scenario in comparison to the uninfected control which gets eventually abolished under the knockdown condition (Fig.7 I-J) and under the chemical inhibitor treatment of SIRT3 (Fig.7, K-L) suggesting the role of the SIRT3 in mediating the interaction with PDHA1. Alongside the decreased interaction of PDHA1 with SIRT3, increased acetylation of PDHA1 was detected upon SIRT3 inhibitor treatment in infected macrophages (Fig.7, K-L).

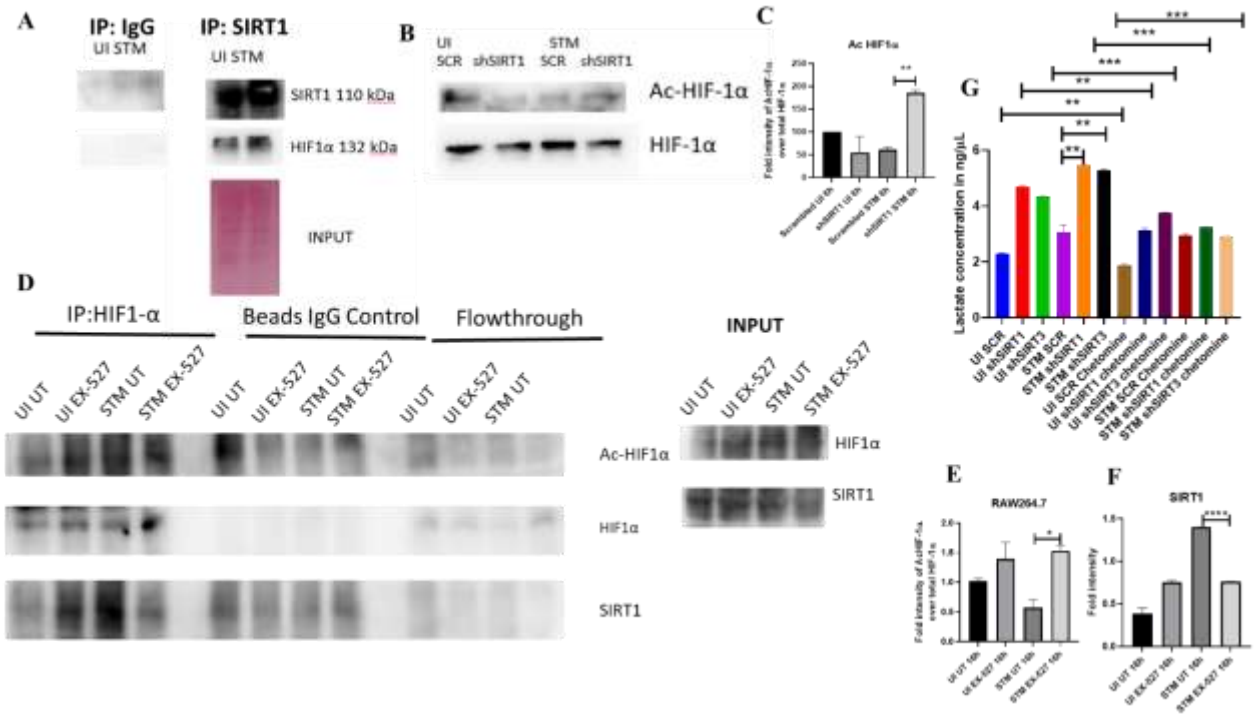

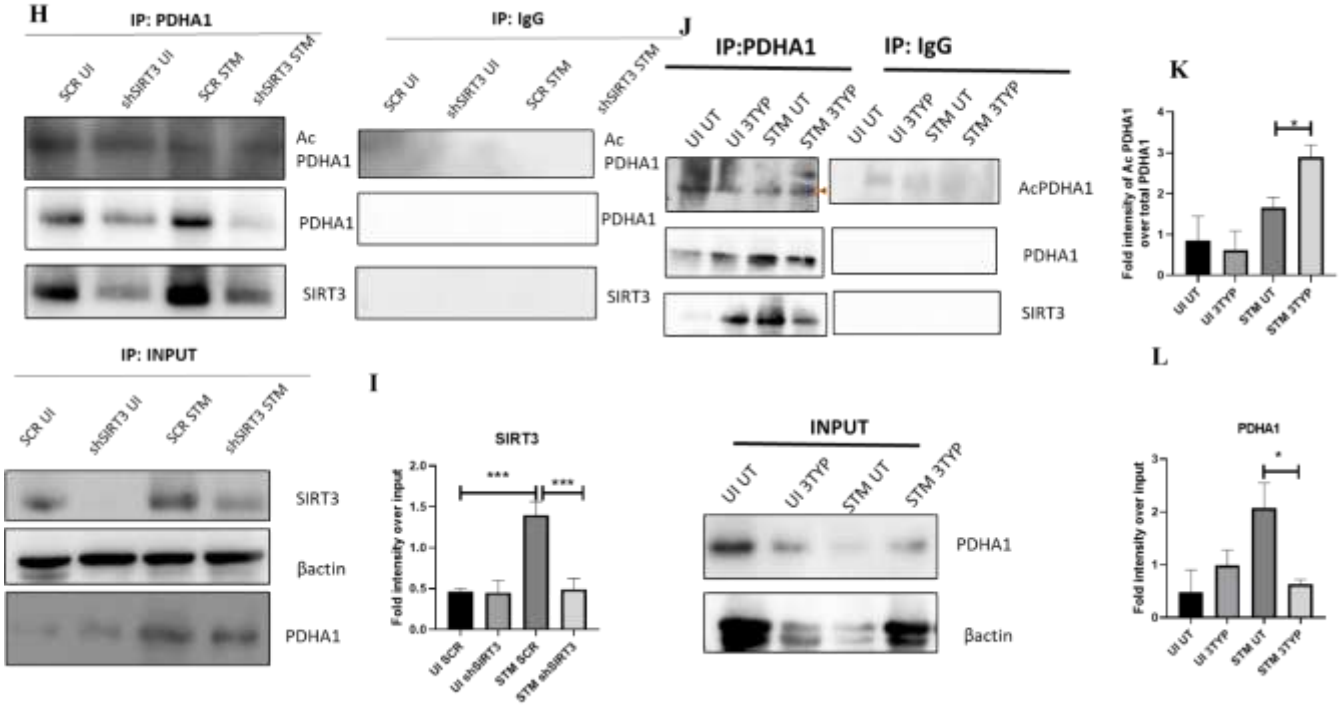

Fig.7- SIRT1 inhibition triggers hyperacetylation of glycolytic master regulator HIF-1α within *S.* Typhimurium infected macrophages while SIRT3 skews metabolism of *S.* Typhimurium-infected macrophages via interaction with PDHA1.

A. An immunoblot depicting HIF-1α interaction with SIRT1 post immunoprecipitation of SIRT1 in uninfected (UI) or *S.* Typhimurium (STM) infected RAW264.7 macrophages at 16hr post-infection. (Derived from same SIRT1 IP blot as in Fig. 4A)

B. Immunoblotting of SIRT1 in SIRT1 knockdown uninfected (UI) or *S.* Typhimurium (STM) infected RAW 264.7 cells at 16hr post-infection to assess the acetylation status of HIF-1α.

C . Densitometric plot depicting the band intensities of Acetylated HIF-1α over total HIF-1α in blot B. Data is representative of N=3.

D. An immunoblot depicting HIF-1α interaction with SIRT1 as well as the HIF-1α acetylation status post immunoprecipitation of HIF-1$^{\alpha}$ (IP:HIF-1α or with control IgG (IP:IgG) in

uninfected (UI) or *S.* Typhimurium (STM) infected RAW264.7 macrophages upon SIRT1 inhibitor (EX-527, 1μM) treatment at 16hr post-infection. UT-untreated.

E. Densitometric plot depicting the band intensities of Acetylated HIF-1α over total HIF-1α in blot D. Data is representative of N=3.

F. Densitometric plot depicting the band intensities of SIRT1 in blot D.

G. Lactate estimation assay of *S.*Typhimurium infected RAW264.7 macrophages upon SIRT1 and SIRT3 knockdown condition in the presence of HIF-1α inhibitor, chetomine (50nM) at16h post-infection. Data is representative of N=3 , n=3. Unpaired two-tailed Student's t test was performed to obtain the p values. (****$p<0.0001$, *** $p < 0.001$, ** $p<0.01$, * $p<0.05$)

H. An immunoblot depicting PDHA1 interaction with SIRT1 or SIRT3 post immunoprecipitation of PDHA1 in uninfected (UI) or *S.* Typhimurium (STM) infected RAW264.7 macrophages in SIRT3 knockdown condition at 16hr post-infection.

I. Densitometric plot depicting the band intensities of SIRT3 interaction over total input in blot. Data is representative of N=3.

J. An immunoblot depicting PDHA1 interaction with SIRT3 post immunoprecipitation of PDHA1 in uninfected (UI) or *S.* Typhimurium (STM) infected RAW264.7 macrophages at 16hr post-infection under SIRT3 inhibitor (3-TYP, 1μM) treatment at 16hr post-infection. UT-untreated.

K. Densitometric plot depicting the band intensities of Acetylated PDHA1 over total PDHA1 in blot I. Data is representative of N=3.

L. Densitometric plot depicting the band intensities of SIRT3 interaction over total input in blot I. Data is representative of N=3.

SIRT1 or SIRT3 inhibition enhances bacterial burden in mice *in vivo*

6-8 weeks old adult male C57BL/6 mice were treated with SIRT1 inhibitor EX-527, SIRT3 inhibitor 3TYP and SIRT1 activator SRT1720 at a dose of 1mg/kg each via intraperitoneal injection (every alternate Day) (Fig. 8A). Following the inhibitor treatment, the mice were orally gavaged with 10^7 CFU of *S.* Typhimurium 14028S for organ burden evaluation or with 10^8 CFU of wildtype *S.* Typhimurium for survival studies. On day 5^{th} post-infection, mice were sacrificed, and the liver, spleen and Mesenteric Lymph Node (MLN) were harvested for enumeration of the organ burden. The SIRT1 inhibitor, EX-527 and SIRT3 inhibitor, 3TYP-treated mice cohorts exhibited increased organ loads in liver, spleen and MLN in comparison to the vehicle control. On the contrary, the SRT1720 treated mice group showed organ burden comparable to that of the vehicle control (Fig. 8, B). Moreover, the SIRT1 and the SIRT3 inhibitor-treated mice cohorts died earlier than the vehicle-treated control mice group or the SIRT1 activator-treated group (Fig. 8, C). Further, the SIRT1 and the SIRT3 inhibitor-treated mice cohorts showed increased splenic length in comparison to the vehicle-treated mice group and the SIRT1 activator-treated mice cohort (Fig. 8, D). The increased organ burden in the EX-527 or 3TYP treated group might be due to increased bacterial dissemination in blood. To assess bacterial dissemination, blood was collected from infected mice post-inhibitor treatment at specific days post-infection retro-orbitally and plated onto *Salmonella Shigella* (SS) agar plates for bacterial enumeration. Indeed, increased bacterial dissemination was observed in the blood of mice treated with SIRT1 inhibitor, EX-527 or SIRT3 inhibitor, 3TYP at day 1-, 2-, 3-,4- post-infection in comparison to the vehicle-treated mice (Fig. 8, E). Further, we wanted to examine whether the increased bacterial dissemination was due to increased ROS production or due to the presence of elevated inflammatory cytokine levels like IL-6 and IL-1β. In the wildtype C57BL/6 mice treated with SIRT3 inhibitor 3TYP showed heightened bacterial burden in blood at 5^{th} day post-infection in comparison to the vehicle control. Nevertheless, the

gp91phox-/- mice group lacking the catalytic subunit of NADPH oxidase did not depict significant variation in the bacterial load among the different mice treatment cohorts (Fig. 8, F). Further, the EX-527 (SIRT1 inhibitor) and the 3TYP (SIRT3 inhibitor) treated mice possessed elevated levels of serum IL-6 (Fig.8G), IL-1β (Fig. S3F) and showed increased intracellular ROS burden in infected liver tissues in comparison to the vehicle-treated control and the SRT1720 (SIRT1 activator) treated mice group (Fig. 8H). The increased mouse serum IL-6 and IL-1β production was in a similar line with the increased IL-6 or IL-1β cytokine generation in EX-527 or 3TYP treated peritoneal macrophages under the infection scenario (Fig. S3, D-E). Moreover, estimation of IL-1β within the infected intestinal ileal sections of the mice revealed increased pro-inflammatory IL-1β generation in the SIRT1 and SIRT3 inhibitor-treated mice groups in comparison to the untreated or the SIRT1-activator treated mice cohorts (Fig. S3G). However, contrary to the *in vitro* studies wherein SIRT1 or SIRT3 knockdown or inhibition resulted in attenuated intracellular proliferation, here in *in vivo* mouse model of infection, we observed increased bacterial organ loads owing to increased bacterial dissemination. To delineate this observation further, we evaluated the bacterial load within splenocytes isolated from control or inhibitor-treated C57BL/6 mice infected with GFP expressing *S.* Typhimurium at 5^{th} day post-infection via flow cytometry. We observed heightened bacterial load in the EX-527 or the 3TYP treated mice cohorts (Fig. 8, I-J). However, when we enumerated the bacterial count within the F4/80+ macrophage population of the infected splenocytes, we noticed decreased bacterial loads in the EX-527 or 3TYP - treated mice group in comparison to the vehicle-treated control group or the SRT-1720 activator-treated group (Fig. 8, K-L). Further, we evaluated additional splenic populations including CD45+, Ly6C+, and CD11c+ populations. Our results show that the CD45+ splenic population depicts increased bacterial loads like that of the total splenic population within the SIRT1 or SIRT3 inhibitor-treated cohorts. However, CD45+ monocytes and Ly6C positive

splenic population exhibit compromised burden within the SIRT1 and SIRT3 inhibitor-treated cohorts. Moreover, CD11c+ population, CD45+ granulocytes, or lymphocytes show comparable organ loads to that of the vehicle control or SIRT1 activator-treated mice group (Fig. 8M-S, Fig. S8). Overall, our data suggest heterogeneous bacterial burden in diverse splenic populations. This opposing phenotype could be attributed to the increased IL-6 and IL-1β cytokine storm and elevated ROS production upon the SIRT1 or SIRT3 inhibitor treatment which in turn resulted in bacterial dissemination *in vivo* and concomitantly restricted the *in vitro* intracellular proliferation within macrophages. To validate this observation, we estimated the ROS levels within the liver and spleen tissues harvested from *S.* Typhimurium infected C57BL/6 mice, treated with specific catalytic inhibitor, activator or vehicle via DCFDA staining using flow cytometry at 5^{th} day post-infection. We detected escalated levels of ROS within both the infected liver and spleen tissues of the EX-527 or 3TYP-treated mice groups in comparison to the vehicle-treated or the SRT1720 treated mice cohorts (Fig. 8, H, S9). Haematoxylin and eosin staining of the liver sections (harvested at 5^{th} day post-infection) revealed increased inflammation with multiple areas of severe acute hepatic necrosis with complete loss of hepatic architecture in the EX-527 and 3-TYP treated liver samples in comparison to the vehicle-treated control and SRT-1720 treated liver samples (Fig. 8, T-U). In line with the inhibitor-treated studies, the increased organ loads, and systemic dissemination driven heightened susceptibility of mice toward *S.* Typhimurium infection were replicated in *in vivo* SIRT1 and SIRT3 adeno-associated virus serotype 6 (AAV6) mediated knockdown mice model which showed elevated IL-6 production in comparison to the scrambled control treated mice cohort (Fig. 8, V-X, Fig. S10). Simultaneously, the haematoxylin-eosin-stained sections of the liver tissues harvested from the shSIRT1 or shSIRT3 mice cohorts depicted increased pathological scoring with multiple necrotic areas and severely damaged liver tissue

architecture in comparison to the scrambled mice control (Fig. 8, Y). Altogether, our results implicate the role of SIRT1 and SIRT3 in controlling *S.* Typhimurium infection *in vivo*.

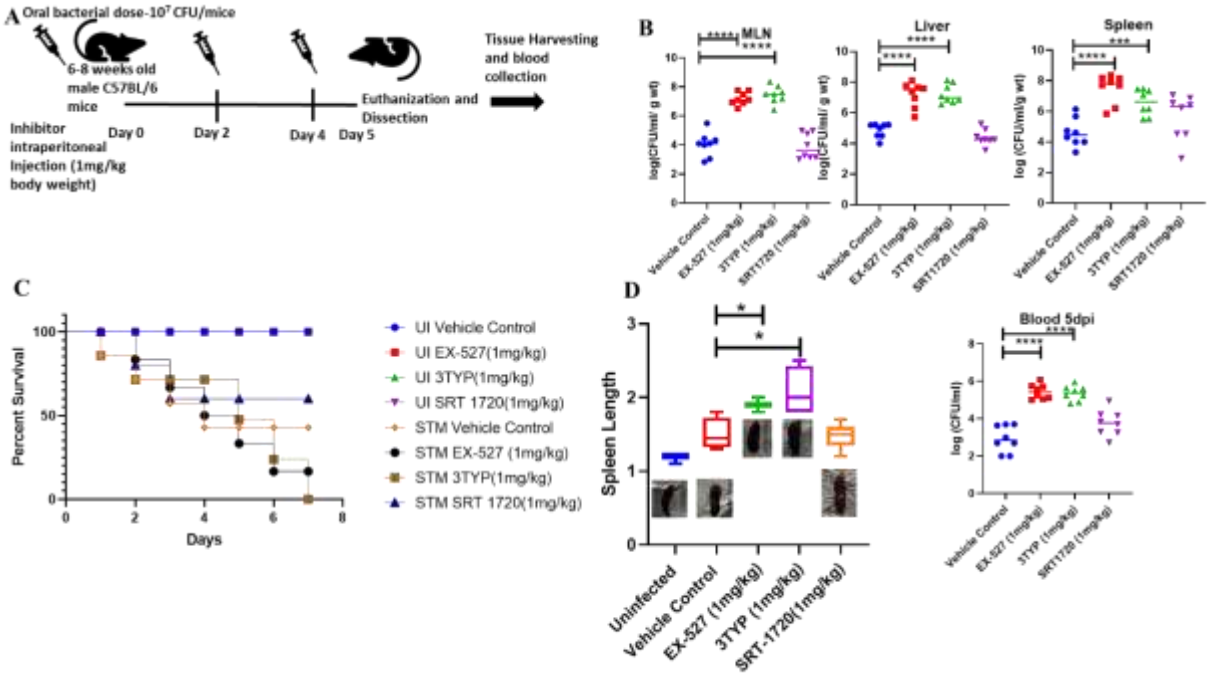

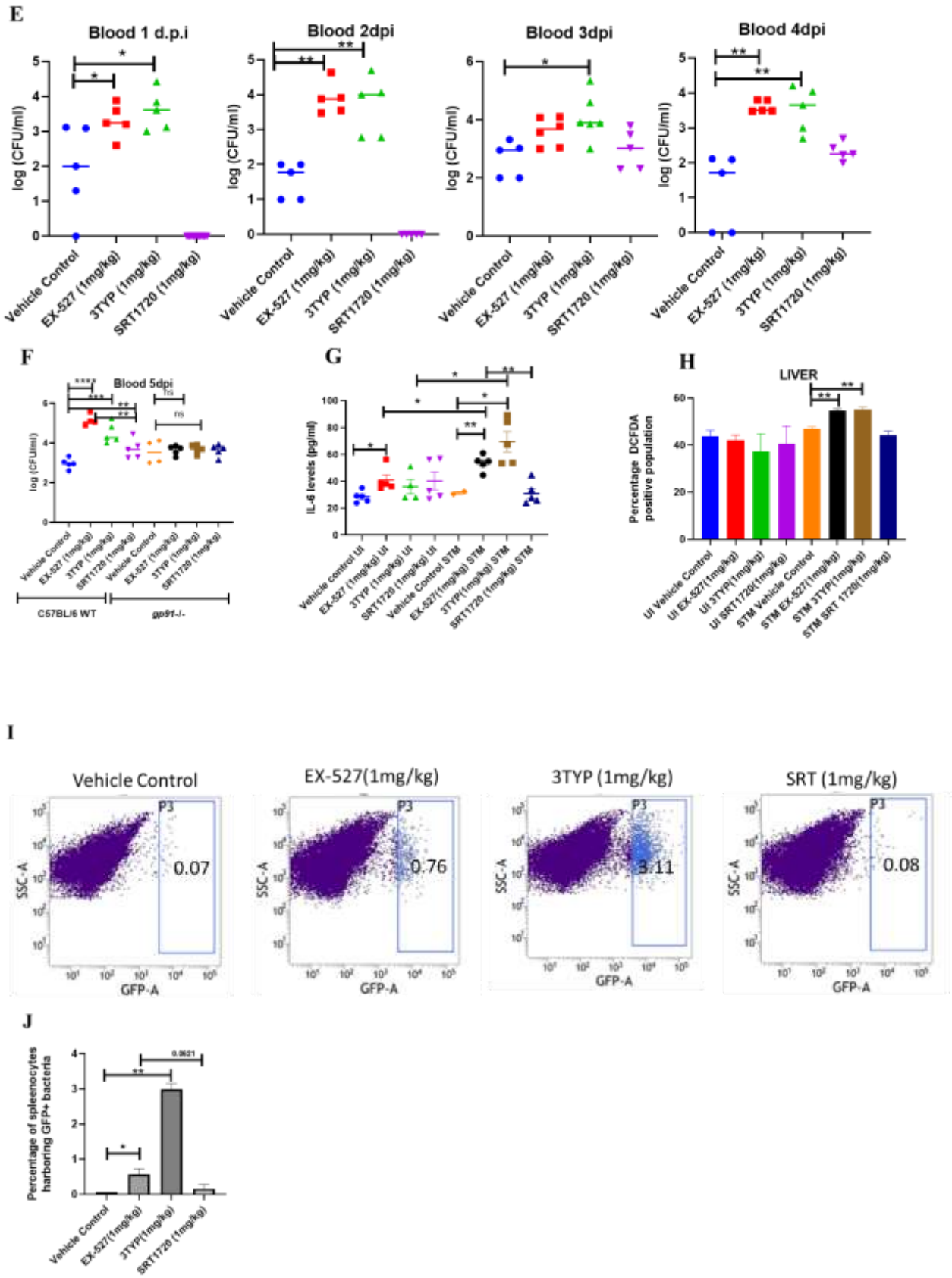
E
Blood 1 d.p.i
Blood 2dpi
Blood 3dpi
Blood 4dpi
log (CFU/ml)
Vehicle Control
EX-527 (1mg/kg)
3TYP (1mg/kg)
SRT1720 (1mg/kg)
F
Blood 5dpi
log (CFU/ml)
C57BL/6 WT
gp91-/-
G
IL-6 levels (pg/ml)
Vehicle control UI
EX-527 (1mg/kg) UI
3TYP (1mg/kg) UI
SRT1720 (1mg/kg) UI
Vehicle Control STM
EX-527(1mg/kg) STM
3TYP(1mg/kg) STM
SRT1720 (1mg/kg) STM
H
LIVER
Percentage DCFDA positive population
UI Vehicle Control
UI EX-527(1mg/kg)
UI 3TYP(1mg/kg)
UI SRT1720(1mg/kg)
STM Vehicle Control
STM EX-527(1mg/kg)
STM 3TYP(1mg/kg)
STM SRT 1720(1mg/kg)
I
Vehicle Control
EX-527(1mg/kg)
3TYP (1mg/kg)
SRT (1mg/kg)
P3
0.07
0.76
3.11
0.08
SSC-A
GFP-A
J
Percentage of spleenocytes harboring GFP+ bacteria
Vehicle Control
EX-527(1mg/kg)
3TYP(1mg/kg)
SRT1720 (1mg/kg)

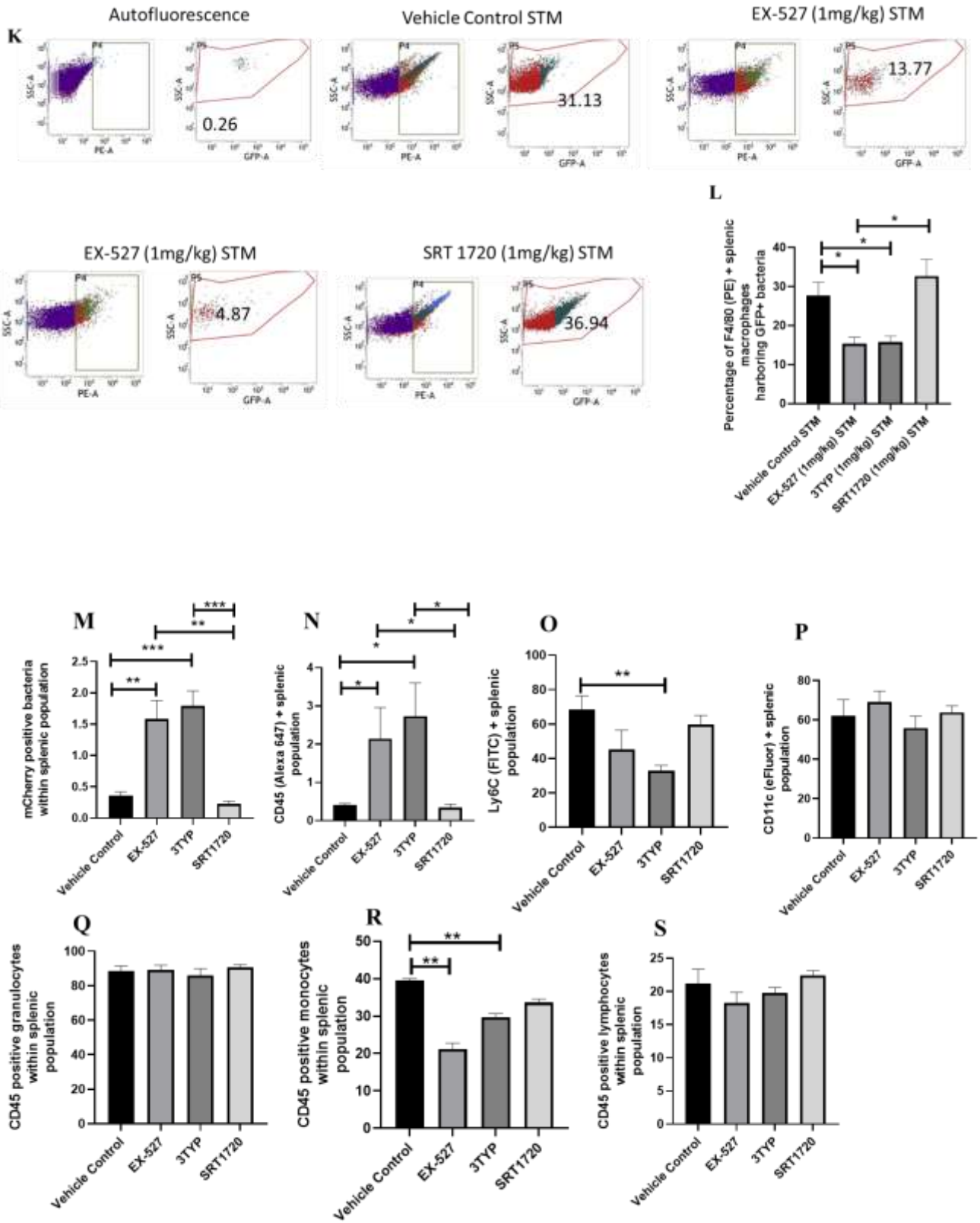
K
Autofluorescence
Vehicle Control STM
EX-527 (1mg/kg) STM
0.26
31.13
13.77
EX-527 (1mg/kg) STM
SRT 1720 (1mg/kg) STM
4.87
36.94
L
Percentage of F4/80 (PE) + splenic macrophages harboring GFP+ bacteria
Vehicle Control STM
EX-527 (1mg/kg) STM
3TYP (1mg/kg) STM
SRT1720 (1mg/kg) STM
M
mCherry positive bacteria within splenic population
N
CD45 (Alexa 647) + splenic population
O
Ly6C (FITC) + splenic population
P
CD11c (eFluor) + splenic population
Q
CD45 positive granulocytes within splenic population
R
CD45 positive monocytes within splenic population
S
CD45 positive lymphocytes within splenic population
Vehicle Control
EX-527
3TYP
SRT1720

T

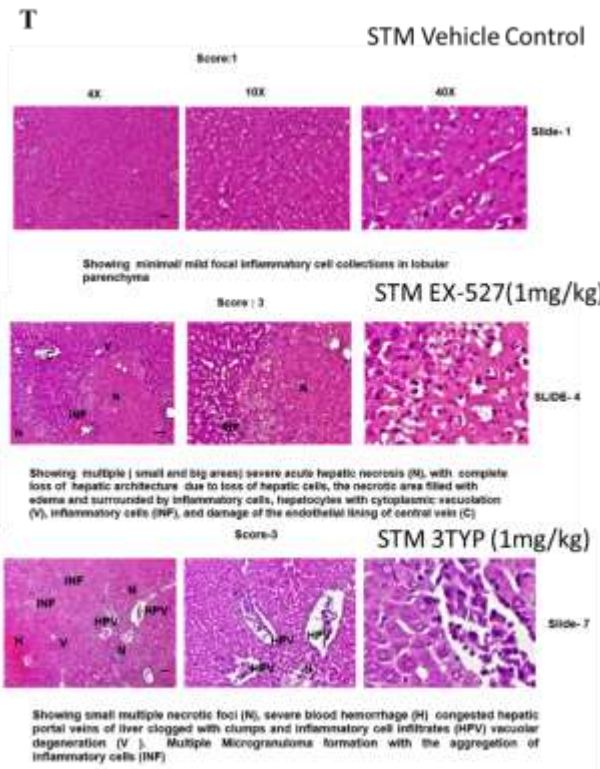
STM Vehicle Control
Score:1
4X
10X
40X
Slide- 1
Showing minimal/ mild focal inflammatory cell collections in lobular parenchyma
STM EX-527(1mg/kg)
Score : 3
SLIDE- 4
Showing multiple (small and big areas) severe acute hepatic necrosis (N), with complete loss of hepatic architecture due to loss of hepatic cells, the necrotic area filled with edema and surrounded by inflammatory cells, hepatocytes with cytoplasmic vacuolation (V), inflammatory cells (INF), and damage of the endothelial lining of central vein (C)
Score-3
STM 3TYP (1mg/kg)
Slide- 7
Showing small multiple necrotic foci (N), severe blood hemorrhage (H) congested hepatic portal veins of liver clogged with clumps and inflammatory cell infiltrates (HPV) vacuolar degeneration (V). Multiple Microgranuloma formation with the aggregation of inflammatory cells (INF)

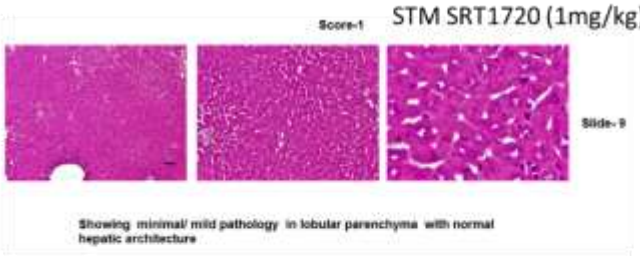
Score-1
STM SRT1720 (1mg/kg)
Slide- 9
Showing minimal/ mild pathology in lobular parenchyma with normal hepatic architecture

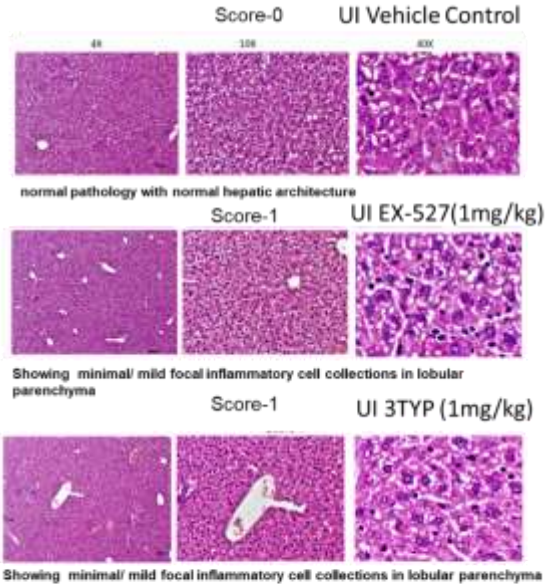
Score-0
UI Vehicle Control
normal pathology with normal hepatic architecture
Score-1
UI EX-527(1mg/kg)
Showing minimal/ mild focal inflammatory cell collections in lobular parenchyma
Score-1
UI 3TYP (1mg/kg)
Showing minimal/ mild focal inflammatory cell collections in lobular parenchyma

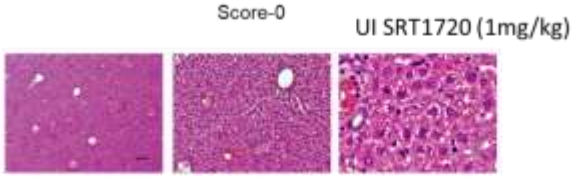
Score-0
UI SRT1720 (1mg/kg)
normal pathology with normal hepatic architecture

U

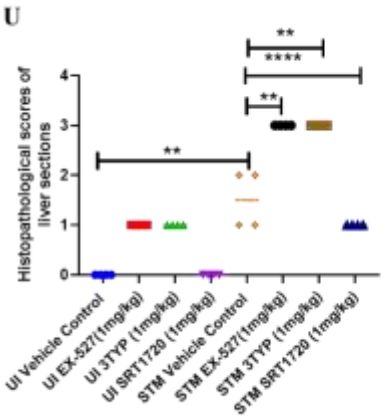
Histopathological scores of liver sections
0
1
2
3
4
**
****
**
**
UI Vehicle Control
UI EX-527(1mg/kg)
UI 3TYP (1mg/kg)
UI SRT1720 (1mg/kg)
STM Vehicle Control
STM EX-527(1mg/kg)
STM 3TYP (1mg/kg)
STM SRT1720 (1mg/kg)

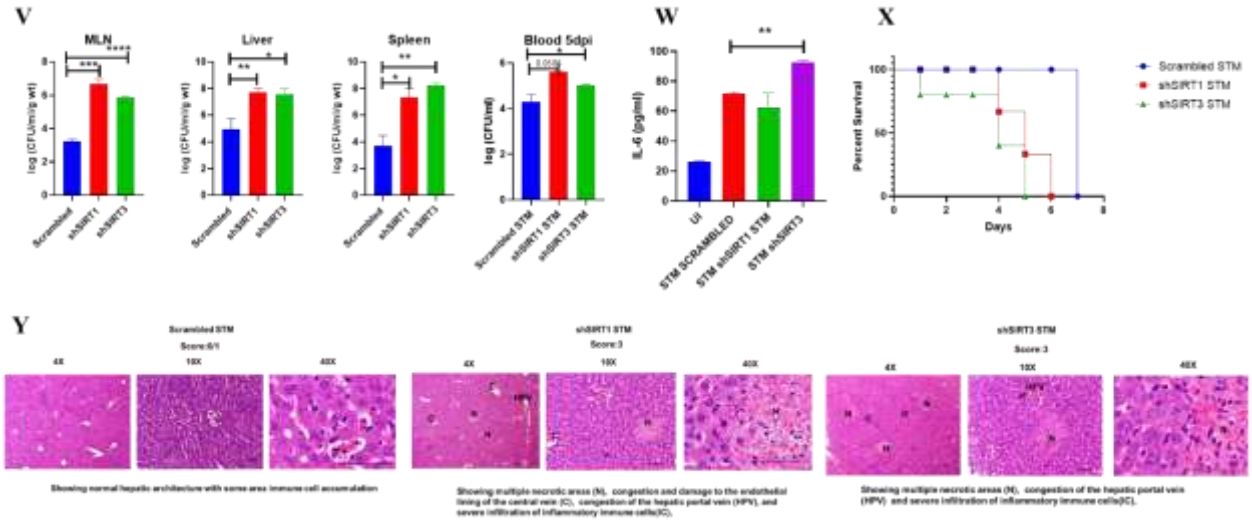

Fig.8- Effect of SIRT1 or SIRT3 inhibition on *S.* Typhimurium infected C57BL/6 mice

A**.** The schematic representation of the experimental strategy for studying the effect of SIRT1 and SIRT3 on the *in vivo* pathogenesis of STM (WT).

B. *In-vivo* organ burden of *S.* Typhimurium upon SIRT1 or SIRT3 inhibition in C57BL/6 mice at day 5 post-infection under specified dosage of inhibitor treatment. Data is representative of N=4, n=8. Mann-Whitney Test was performed to obtain the p values.(****p<0.0001, *** p < 0.001, ** p<0.01, * p<0.05).

C. Percent survival of *S.* Typhimurium infected C57BL/6 mice upon SIRT1 or SIRT3 inhibitor treatment at a specific dose of inhibitor treatment. Data is representative of N=4, n=5.

D. Representation of splenic length of *S.* Typhimurium infected spleen tissue harvested from C57BL/6 mice (males) at day 5 post-infection upon SIRT1 or SIRT3 inhibition at 1mg/kg dosage. Data is representative of N=4, n=8. (** p<0.01, * p<0.05).

E. Bacterial load in blood at different days post-infection upon SIRT1 or SIRT3 inhibition at 1mg/kg dosage in C57BL/6 mice (males). Data is representative of N=3, n>5. (** p<0.01, * p<0.05) Mann-Whitney Test was performed to obtain the p values. (** p<0.01, * p<0.05).

F. Bacterial load in blood at day 5 post-infection upon SIRT1 or SIRT3 inhibition at 1mg/kg dosage in C57BL/6 WT mice (males) and *gp91phox*-/- (males) mice. Data is representative of N=3, n>5. Mann-Whitney Test was performed to obtain the p values. (** $p<0.01$, * $p<0.05$).

G. Serum IL-6 levels of *S.* Typhimurium infected C57BL/6 WT mice (males) mice treated with SIRT1(EX-527) or SIRT3 (3TYP) inhibitors or SRT1720 (SIRT1 activator) at 1mg/kg dosage at 5th day post-infection. Data is representative of N=3, n>5. Unpaired two-tailed Student's t test was performed to obtain the p values.(** $p<0.01$, * $p<0.05$).

H. Quantitative analysis of percentage population of cells within liver showing DCFDA positive staining shown in Fig. S9, A. Data is representative of N=3, n>5. Unpaired two-tailed Student's t- test was performed to obtain the p values. (** $p < 0.01$).

I. Enumeration of GFP positive bacterial cells through flow cytometry in splenic tissues homogenate harvested from adult male 6-8 week old C57BL/6 mice (subjected to different chemical treatment-Vehicle treated or SIRT1 (EX-527) or SIRT3 (3-TYP) inhibitor or SIRT1 activator SRT1720 treated at a dose of 1mg/kg) at 5^{th} day post *S.* Typhimurium (expressing GFP) infection (10^7 CFU orally). Data is representative of N=3, n>5. Unpaired two-tailed Student's t test was performed to obtain the p values. (** $p < 0.01$).

J. Quantitative analysis of the percentage population of splenic cells harboring GFP+ bacterial cells shown in I. Unpaired two-tailed Student's t test was performed. (** $p<0.01$, * $p<0.05$).

K. Enumeration of GFP positive bacterial cells through flow cytometry within F4/80 positive splenic macrophages present within splenic tissues homogenate harvested from adult male 6-8 week old C57BL/6 mice (subjected to different chemical treatment-Vehicle treated or SIRT1 (EX-527) or SIRT3 (3-TYP) inhibitor or SIRT1 activator SRT1720 treated aa t dose of 1mg/kg) at 5^{th} day post *S.* Typhimurium infection. Data is representative of N=3, n>5.

L. Quantitative analysis of percentage population of F4/80 positive macrophage cells harboring GFP+ bacteria shown in K . Unpaired two-tailed Student's t test was performed to obtain the p values. Data is representative of N=3, n>5.(* $p < 0.05$).

M-S. Quantitative analysis of different mCherry-*S.*Typhimurium-infected splenic populations harboring mCherry+bacteria via flow cytometry depicted in Fig. S8. Unpaired two-tailed Student's t test was performed. (*** $p < 0.001$,** $p<0.01$, * $p<0.05$).

T. Representative image of haematoxylin-eosin-stained liver sections to assess the liver tissue architecture upon *Salmonella* infection at 5^{th} days post-infection in different mice cohorts. (UI-Uninfected, STM- *S.* Typhimurium infected, EX-527-SIRT1 inhibitor, 3TYP-SIRT3 inhibitor, SRT1720- SIRT1 activator, Vehicle Control-(PBS containing 0.1% DMSO). Scale bar-50µm. **Scoring system:-** according to pathological changes the tissue sections are scored as 0 for normal pathology, 1 for mild/ minor pathology, 2 for moderate pathology, and 3 for severe pathological changes.

U. Graph representing the histopathological scoring of the liver sections depicted in L. Unpaired two-tailed Student's t test was performed to obtain the p values. (* $p < 0.05$)(****$p<0.0001$, *** $p < 0.001$, ** $p<0.01$, * $p<0.05$).

V. *In-vivo* organ burden of *S.* Typhimurium upon SIRT1 or SIRT3 adenovirus-mediated *in vivo* knockdown in C57BL/6 mice at day 5 post-infection. Data is representative of N=3, n>3. Mann-Whitney Test was performed to obtain the p values. (****$p<0.0001$, *** $p < 0.001$, ** $p<0.01$, * $p<0.05$).

W. Serum IL-6 levels of *S.* Typhimurium infected C57BL/6 WT mice (males) upon *in vivo* adenovirus-mediated SIRT1 or SIRT3 knockdown. Data is representative of N=3, n>3. Unpaired two-tailed Student's t test was performed to obtain the p values. (** $p<0.01$, * $p<0.05$).

X. Percent survival of *S.* Typhimurium infected C57BL/6 mice upon *in vivo* adenovirus-mediated SIRT1 or SIRT3 knockdown. Data is representative of N=3, n>3.

Y. Representative image of haematoxylin-eosin-stained liver sections upon *Salmonella* infection at 5th days post-infection in different mice cohorts. (Scrambled STM, shSIRT1 STM, shSIRT3 STM). Scale bar-50µm. **Scoring system:-** according to pathological changes the tissue sections are scored as 0 for normal pathology, 1 for mild/ minor pathology, 2 for moderate pathology, and 3 for severe pathological changes.

SIRT3 inhibition only led to enhanced mitochondrial superoxide generation in the infected macrophages

Mitochondrial superoxide generation is an essential arsenal of host defense and an important determinant of mitochondrial health (74, 75). *Salmonella* Typhimurium strain 14028S infection triggered an increase in mitochondrial superoxide generation in RAW264.7 murine macrophages in comparison to the uninfected control in flow cytometric studies. This increment in mitochondrial superoxide was further aggravated (around 2-fold) in knockdown condition of SIRT3 in infected RAW264.7 macrophages. However, the mitochondrial ROS production within SIRT1 knocked down macrophages remained comparable to scrambled control under infection scenario (Fig. 9 A). This result was further corroborated by the findings in the *Salmonella* infected primary peritoneal macrophages (PMs) treated with SIRT1 or SIRT3 inhibitors EX-527 (76), and 3TYP (77), respectively. Treatment with only SIRT3 inhibitor resulted in heightened production of mitochondrial ROS (mtROS) in the infected PMs in comparison to the untreated control (Fig. 9B). Immunofluorescence data further showed an increased coefficient of colocalization of mitoSOX with mitochondria in SIRT3 knockdown RAW264.7 macrophages when compared to the scrambled control (Fig. 9C-D). SIRT3

knockdown triggered increased mitochondrial oxidative stress in infected RAW264.7 macrophages, prompting the hypothesis that elevated mtROS might hinder intracellular bacterial replication. To investigate this hypothesis, we performed an intracellular bacterial proliferation assay in the presence or absence of mitochondrial superoxide scavenger, mitoTEMPO in SIRT3 knockdown macrophages. The untreated macrophages depicted attenuated intracellular proliferation of *S.* Typhimurium in SIRT3 knockdown macrophages compared to the scrambled control. However, alleviating mtROS with mitoTEMPO, restored *Salmonella* intracellular proliferation in SIRT3 knockdown macrophages (Fig.9E). Therefore, the increased mitochondrial oxidative burst within SIRT3 knockdown macrophages limits *Salmonella* intracellular proliferation, a restriction reversed upon alleviating mtROS production by mitoTEMPO.

Together, these results implicate the role of SIRT3 in mitigating mitochondrial ROS generation in the *Salmonella*-infected murine macrophages and thereby facilitating bacterial proliferation.

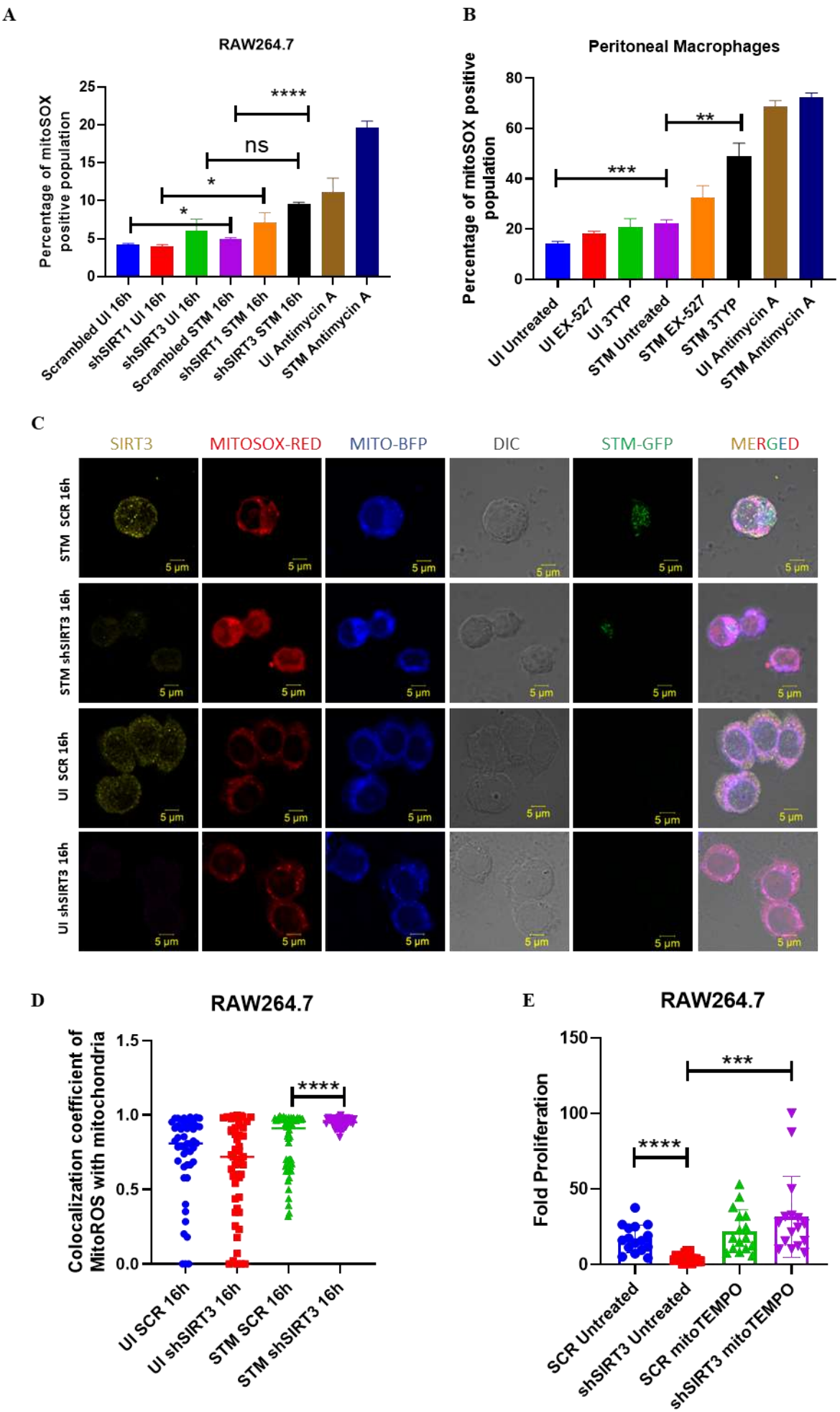
A
RAW264.7
Percentage of mitoSOX positive population
25
20
15
10
5
0
****
ns
*
*
Scrambled UI 16h
shSIRT1 UI 16h
shSIRT3 UI 16h
Scrambled STM 16h
shSIRT1 STM 16h
shSIRT3 STM 16h
UI Antimycin A
STM Antimycin A
B
Peritoneal Macrophages
Percentage of mitoSOX positive population
80
60
40
20
0
**
***
UI Untreated
UI EX-527
UI 3TYP
STM Untreated
STM EX-527
STM 3TYP
UI Antimycin A
STM Antimycin A
C
SIRT3
MITOSOX-RED
MITO-BFP
DIC
STM-GFP
MERGED
STM SCR 16h
STM shSIRT3 16h
UI SCR 16h
UI shSIRT3 16h
5 µm
D
RAW264.7
Colocalization coefficient of MitoROS with mitochondria
1.5
1.0
0.5
0.0
****
UI SCR 16h
UI shSIRT3 16h
STM SCR 16h
STM shSIRT3 16h
E
RAW264.7
Fold Proliferation
150
100
50
0
***
****
SCR Untreated
shSIRT3 Untreated
SCR mitoTEMPO
shSIRT3 mitoTEMPO

Fig.9- SIRT3 inhibition leads to enhanced mitochondrial ROS generation in infected macrophages leading to attenuated *Salmonella* replication.

A-Mitochondrial ROS estimation via flow cytometry in *S.* Typhimurium infected RAW264.7 macrophages at 16hr post infection under SIRT1 or SIRT3 knockdown condition. Data is representative of N=4, n=2. 10μM antimycin A-treated (ROS inducer) uninfected and infected cells served as positive control. Unpaired two-tailed Student's t test was performed to obtain the p values. *** $p < 0.001$, ** $p<0.01$, * $p<0.05$

B-Mitochondrial ROS estimation via flow cytometry in *S.* Typhimurium infected peritoneal macrophages (isolated post 5^{th} day of thioglycolate injection) at 16hr post infection in the presence of SIRT1 (EX-527,1μM) or SIRT3 (3TYP, 1μM) inhibitor treatment. Data is representative of N=3, n=2. Unpaired two-tailed Student's t test was performed to obtain the p values. *** $p < 0.001$, ** $p<0.01$, * $p<0.05$

C-D- Representative confocal images of SIRT3 knockdown RAW264.7 macrophages exhibiting co-localization coefficient of mitoSox Red detecting mitochondrial ROS with mitochondria (mitoBFP) upon *S.* Typhimurium infection at indicated time points post-infection. Data is representative of N=3, n>50 (microscopic field). Unpaired two-tailed Student's t test was performed to obtain the p values. *** $p < 0.001$, ** $p<0.01$, * $p<0.05$

E- Intracellular proliferation assay of *S.* Typhimurium within scrambled control or SIRT3 knockdown macrophages in presence or absence of mitoTEMPO treatment. Data is representative of N=3, n=2. Unpaired two-tailed Student's t test was performed to obtain the p values. *** $p < 0.001$, ** $p<0.01$, * $p<0.05$

SIRT1 and SIRT3 inhibition compromised the mitochondrial antioxidant defence in the *S.* Typhimurium-infected macrophages

Our prior data suggested increased mitochondrial ROS-mediated mitochondrial oxidative stress in SIRT3 knockdown RAW264.7 macrophages in *S.* Typhimurium infected macrophages. Considering the host's mitochondrial antioxidant defense mechanisms crucial in countering oxidative stress (78, 79), we conducted RT-qPCR studies of several mitochondrial antioxidant genes (*Gpx*, *Ho-1*, *Cat*, and *Sod2*) upon SIRT1 and SIRT3 knockdown in RAW264.7 macrophages and in peritoneal macrophages treated with SIRT1 (EX-527) or SIRT3 (3TYP) inhibitors. Both SIRT1 and SIRT3 knockdown, as well as inhibitor treatments, resulted in decreased transcript levels of mitochondrial antioxidant genes in both RAW264.7 and peritoneal macrophages during infection (Fig. 10A-B). Subsequently, we evaluated the status of bacterial antioxidant gene expression within SIRT1 or SIRT3 knockdown macrophages. Previous literature implicates SIRT3 deacetylating SOD2 at critical lysine residues (K53 and K89), promoting its antioxidant activity(80). To validate this interaction during *S.* Typhimurium infection condition, immunoprecipitation studies were performed. Immunoprecipitation studies revealed the interaction of SOD2 with SIRT3 upon infection. However, this interaction got dampened in SIRT3 knockdown, and inhibitor-treated infected RAW264.7 macrophages, alongside SOD2 hyperacetylation (Fig. 10C-D). Further, SOD2 activity assay demonstrated reduced active SOD2 or MnSOD2 concentration in the *S.* Typhimurium-infected RAW264.7 macrophages under both SIRT3 knockdown or inhibited conditions (Fig. 10E-F). Together, our results highlight the role of SIRT1 and more predominantly SIRT3 in rendering protection against mitochondrial oxidative stress upon *Salmonella* infection by deacetylating SOD2 and thereby promoting its antioxidant properties.

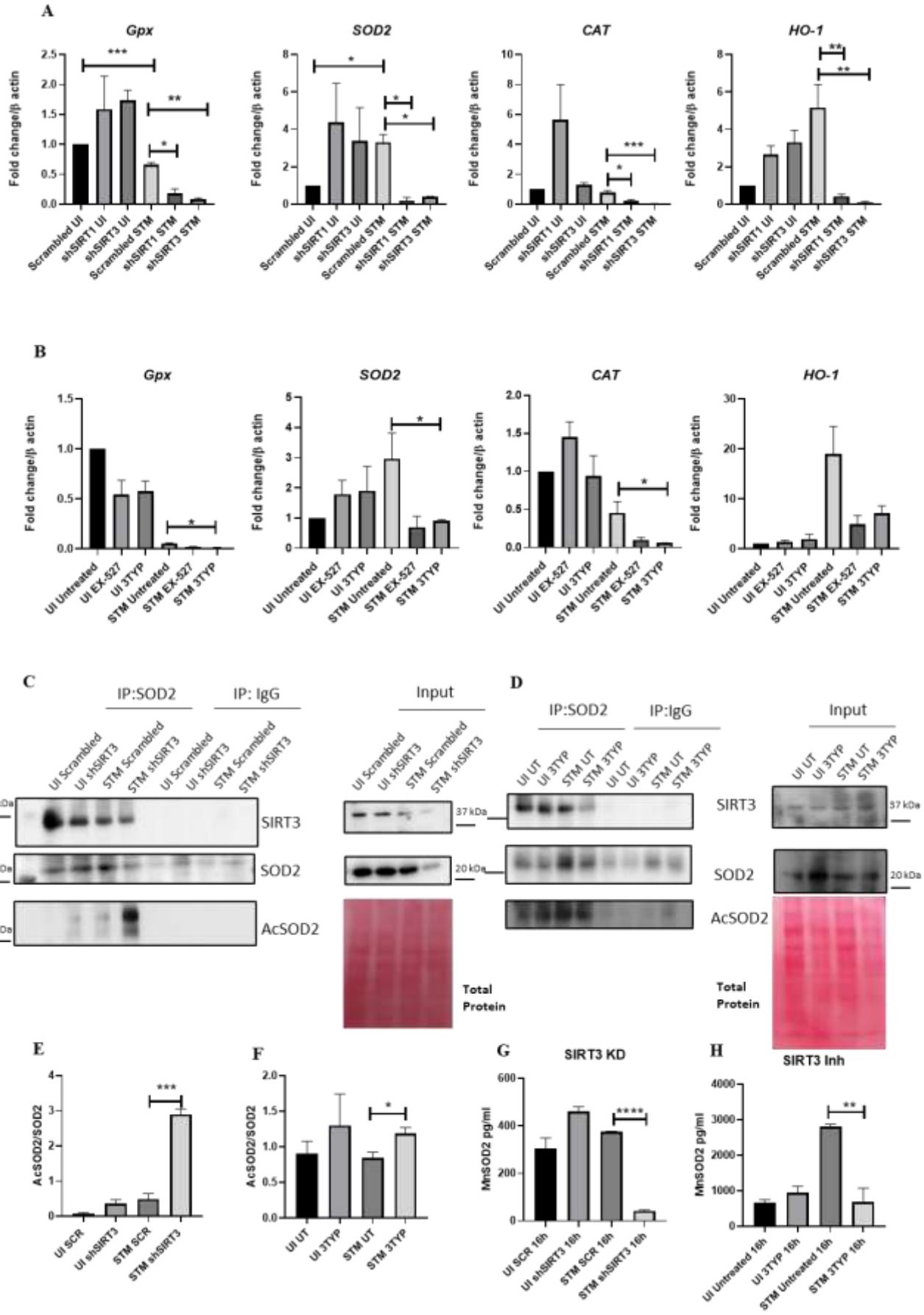
A
Gpx
SOD2
CAT
HO-1
Fold change/β actin
Scrambled UI
shSIRT1 UI
shSIRT3 UI
Scrambled STM
shSIRT1 STM
shSIRT3 STM
B
Gpx
SOD2
CAT
HO-1
Fold change/β actin
UI Untreated
UI EX-527
UI 3TYP
STM Untreated
STM EX-527
STM 3TYP
C
IP:SOD2
IP: IgG
Input
UI Scrambled
UI shSIRT3
STM Scrambled
STM shSIRT3
37 kDa
20 kDa
SIRT3
SOD2
AcSOD2
Total Protein
D
IP:SOD2
IP:IgG
Input
UI UT
UI 3TYP
STM UT
STM 3TYP
SIRT3
SOD2
AcSOD2
Total Protein
E
AcSOD2/SOD2
UI SCR
UI shSIRT3
STM SCR
STM shSIRT3
F
AcSOD2/SOD2
UI UT
UI 3TYP
STM UT
STM 3TYP
G
SIRT3 KD
MnSOD2 pg/ml
UI SCR 16h
UI shSIRT3 16h
STM SCR 16h
STM shSIRT3 16h
H
SIRT3 Inh
MnSOD2 pg/ml
UI Untreated 16h
UI 3TYP 16h
STM Untreated 16h
STM 3TYP 16h

Fig.10 Effect of SIRT1 or SIRT3 inhibition on host mitochondrial antioxidant defense in *Salmonella* Typhimurium infection scenario.

A-Quantitative gene expression studies of several host mitochondrial antioxidant genes such as *Gpx*, *Sod2*, *Cat*, and *Ho-1* in RAW264.7 macrophages upon knockdown of SIRT1 and SIRT3 in *S.* Typhimurium infection scenario. Data is representative of N=3, n=2. Unpaired two-tailed Student's t test was performed to obtain the p values. *** $p < 0.001$, ** $p<0.01$, * $p<0.05$

B-Quantitative gene expression studies of several host mitochondrial antioxidant genes such as *Gpx*, *Sod2*, *Cat*, and *Ho-1* in peritoneal macrophages (isolated from 6–8-week-old adult male mice post 5^{th} day of thioglycolate injection) after 16h of *S.* Typhimurium infection upon SIRT1 (EX-527,1μM) or SIRT3 (3TYP, 1μM) inhibitor treatment. Data is representative of N=3, n=2. Unpaired two-tailed Student's t test was performed to obtain the p values. *** $p < 0.001$, ** $p<0.01$, * $p<0.05$

C- Immunoprecipitation studies depicting SOD2 interaction with SIRT3 upon immunoprecipitation of SOD2 in uninfected (UI) or *S.* Typhimurium (STM) infected SIRT3 knockdown RAW264.7 macrophages at 16hr post-infection. Data is representative of N=2, n=1. *** $p < 0.001$, ** $p<0.01$, * $p<0.05$

D- Immunoprecipitation studies depicting SOD2 interaction with SIRT3 upon immunoprecipitation of SOD2 in uninfected (UI) or *S.* Typhimurium (STM) infected RAW264.7 macrophages at 16hr post-infection upon inhibitor treatment of SIRT3 . Data is representative of N=2, n=1. *** $p < 0.001$, ** $p<0.01$, * $p<0.05$

E- Mitochondrial SOD2 activity assay in uninfected and *S.* Typhimurium infected RAW264.7 macrophages in the knockdown condition of SIRT3. Data is representative of N=2, n=2. Unpaired two-tailed Student's t test was performed to obtain the p values. *** $p < 0.001$, ** $p<0.01$, * $p<0.05$

F- Mitochondrial SOD2 activity assay in uninfected and *S*. Typhimurium infected RAW264.7 macrophages upon SIRT3 inhibitor treatment. Data is representative of N=2, n=2. Unpaired two-tailed Student's t test was performed to obtain the p values. *** $p < 0.001$, ** $p<0.01$, * $p<0.05$

SIRT1 or SIRT3 inhibition resulted in compromised ETC function and lowered ATP generation in the infected macrophages

SIRT3, crucial for maintaining healthy mitochondrial homeostasis, is associated with ATP synthase subunit (81) and regulates basal ATP levels in vivo (46). Therefore, to explore the impact of SIRT3 inhibition or downregulation on ATP production during *Salmonella* infection, an ATP estimation assay was performed. *Salmonella*-infected SIRT1 or SIRT3 RAW264.7 macrophages exhibited decreased ATP production in the later phases of infection at 16hr post-infection compared to the infected scrambled or un-transfected control (Fig. 11A). Moreover, earlier data showed exacerbated production of mtROS upon SIRT3 knockdown or inhibition in *Salmonella*-infected murine macrophages. Given that both mtROS production and ATP synthesis are governed by mitochondrial ETC (Electron transport chain), we investigated whether SIRT1 and SIRT3 inhibition or knockdown disrupts ETC function during *Salmonella* infection. qPCR-mediated ETC Complex gene profiling in infected RAW264.7 macrophages under SIRT1 or SIRT3 knockdown conditions revealed decreased expression of Complex I subunit genes (*NDUFV1*, *NDUFS1*, *NDUFA9*), Complex II (*SDHD),* Complex III (*UQCR*), Complex IV (*COX5B*) and Complex V genes (*ATP5B*) (Fig. 11B). Similar findings were obtained from infected peritoneal macrophages treated with SIRT1 or SIRT3 catalytic inhibitors (Fig. 11C). Consequently, SIRT1 or SIRT3 knockdown or inhibition triggers

mitochondrial ETC dysfunction in infected macrophages, potentially leading to enhanced mitochondrial ROS generation and reduced ATP production.

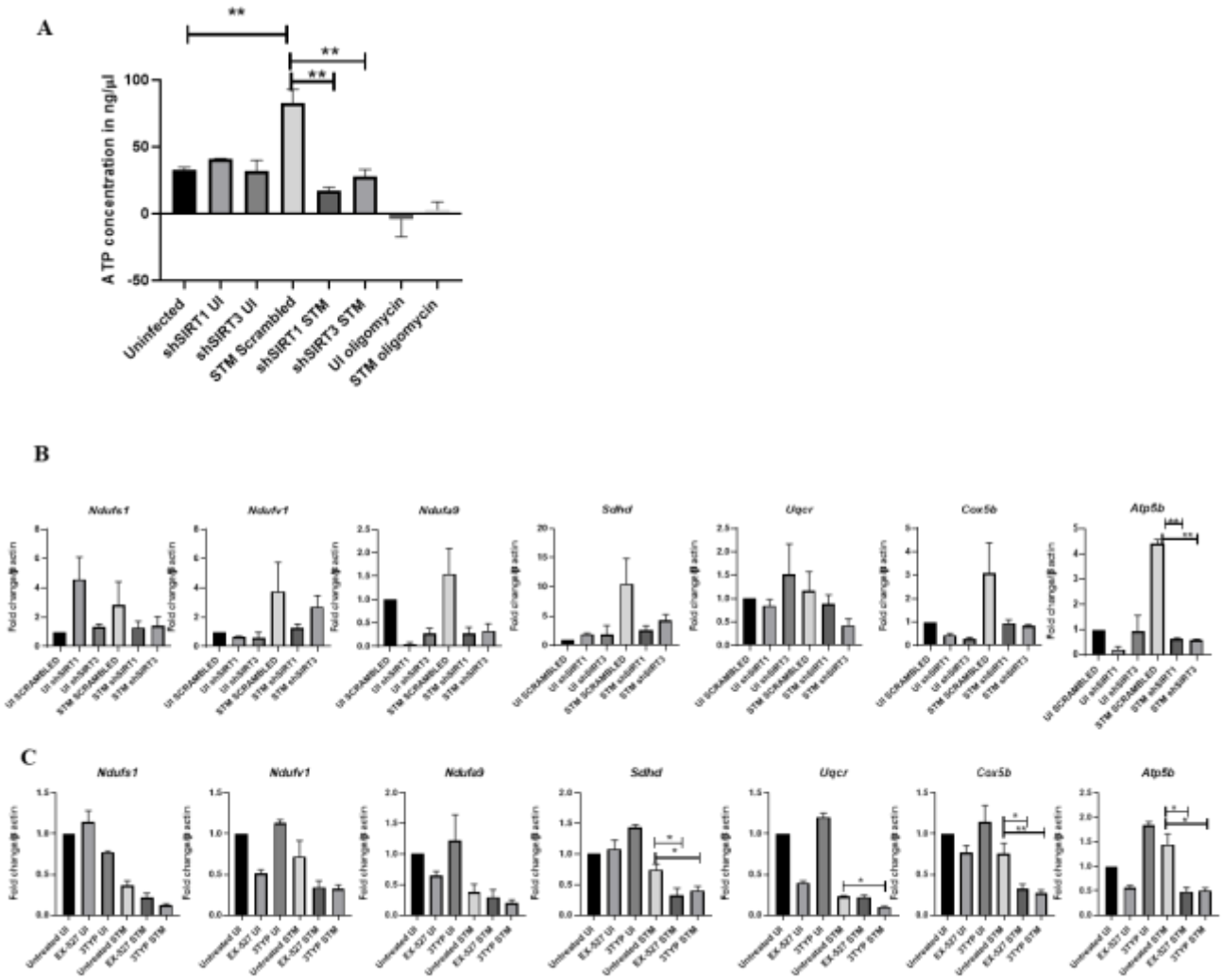

Fig.11 Inhibition of SIRT1 or SIRT3 leads to disruption of mitochondrial bioenergetics in *S.* Typhimurium-infected macrophages.

A-ATP estimation assay in SIRT1 or SIRT3 knockdown RAW264.7 macrophages in the presence or absence of *S.* Typhimurium infection at specified time points post-infection. Data is representative of N=3, n=2. 10µM oligomycin-treated (ATP synthase inhibitor) uninfected

and infected cells served as negative control. Unpaired two-tailed Student's t test was performed to obtain the p values. *** $p < 0.001$, ** $p<0.01$, * $p<0.05$

B-qRTPCR mediated expression analysis of several Complex I, Complex II, Complex III, Complex IV, and Complex V genes of the Electron Transport Chain in *S.* Typhimurium infected RAW264.7 macrophages at 16hr post infection under the knockdown condition of either SIRT1 or SIRT3. Data is representative of N=3, n=2. Unpaired two-tailed Student's t test was performed to obtain the p values. *** $p < 0.001$, ** $p<0.01$, * $p<0.05$

C-qRTPCR mediated expression analysis of several Complex I, Complex II, Complex III, Complex IV, and Complex V genes of the Electron Transport Chain in *S.* Typhimurium infected peritoneal macrophages at 16hr post-infection in the presence or absence of SIRT1 (EX-527) or SIRT3 (3TYP) inhibitor treatment at a concentration of 1μM. Data is representative of N=3, n=2. Unpaired two-tailed Student's t test was performed to obtain the p values. *** $p < 0.001$, ** $p<0.01$, * $p<0.05$

SIRT3 modulated the mitochondrial membrane potential of the infected macrophages

Mitochondrial function, ATP production and mtROS generation rely on mitochondrial membrane potential. To investigate alteration in the mitochondrial membrane potential during *S.* Typhimurium infection, we undertook TMRM staining of the infected macrophages in SIRT1 or SIRT3 knockdown condition through flow cytometry. TMRM (Tetramethylrhodamine Methyl Ester, Perchlorate) is a cell-permeant fluorescent dye assessing mitochondrial membrane potential (82). TMRM staining of the infected RAW 264.7 macrophages revealed enhanced membrane potential under the knockdown condition of SIRT3 only at 16hr post-infection compared to the scrambled control (Fig. 12). SIRT1 knockdown alone did not exert significant alterations in mitochondrial membrane potential within infected

macrophages. Mitochondrial hyperpolarization has been shown to be caused by Complex I inhibition which subsequently triggers reduced activity of Complex II, III, and IV and reduced forward action of Complex V(83). Our data of mitochondrial hyperpolarization in *Salmonella*-infected RAW264.7 macrophages coincides with decreased expression of Complex I, II, III, IV and V (as shown earlier).

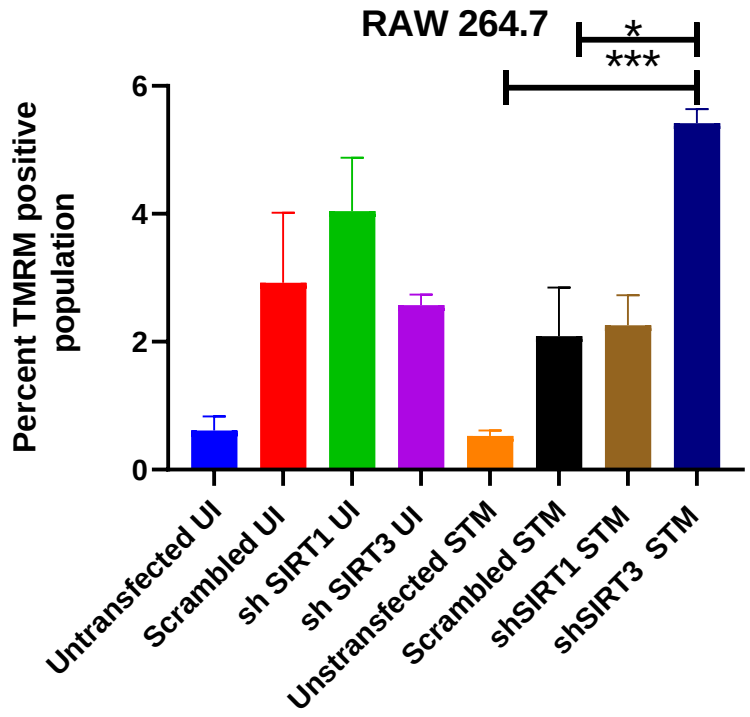

Fig.12- SIRT3 inhibition mediates mitochondrial membrane hyperpolarization

Mitochondrial membrane potential determination using TMRM dye via flow cytometry in RAW264.7 macrophages under knockdown condition of SIRT1 or SIRT3 at 16hr post infection. Data is representative of N=3, n=2. Unpaired two-tailed Student's t test was performed to obtain the p values. *** $p < 0.001$, ** $p<0.01$, * $p<0.05$

SIRT1 and SIRT3 inhibition led to altered mitochondrial respiration in *S.* Typhimurium infected macrophages

Upon observing reduced ATP production following SIRT1 or SIRT3 inhibition, we determined mitochondrial bioenergetics in infected peritoneal macrophages under SIRT1 and SIRT3 inhibitor treatment. Using a modified Seahorse Mito stress test (63), we assessed the mitochondrial oxygen consumption rates (OCR) post 6hr of infection and inhibitor treatment in peritoneal macrophages over a 60 min interval (Fig. 13A). The baseline OCR provided basal respiration by eliminating the non-mitochondrial respiration. Oligomycin addition allowed computation of ATP-linked OCR and proton leakage, while Antimycin A and rotenone revealed the rate of non-mitochondrial respiration. Simultaneously, the extracellular acidification rate (ECAR), which is proportional to the lactate efflux, was measured and interpreted as an indicator of glycolytic flux in the macrophages. Results revealed increased basal respiration, non-mitochondrial respiration, proton leakage, and mitochondrial ATP-linked respiration (Fig. 13B) and an increase in ECAR in the infected peritoneal macrophages under both SIRT1 (EX-527) and SIRT3 (3TYP) catalytic inhibitor treatment compared to the infected untreated control (Fig. 13C). This underscores the function of SIRT1 and SIRT3 in regulating mitochondrial bioenergetics during *Salmonella* infection (Fig. 13). The overall increase in mitochondrial respiratory flux and proton leakage may contribute to increased mitochondrial ROS production and mitochondrial hyperpolarization (84) (as depicted earlier). Previous reports suggest enhanced respiration alongside decreased ATP production may involve compensation through increased glycolysis (85) or non-mitochondrial respiration (86). Additionally, heightened respiration leading to increased superoxide generation can result in proton leakage across the inner mitochondrial membrane and decreased ATP synthesis (84, 87).

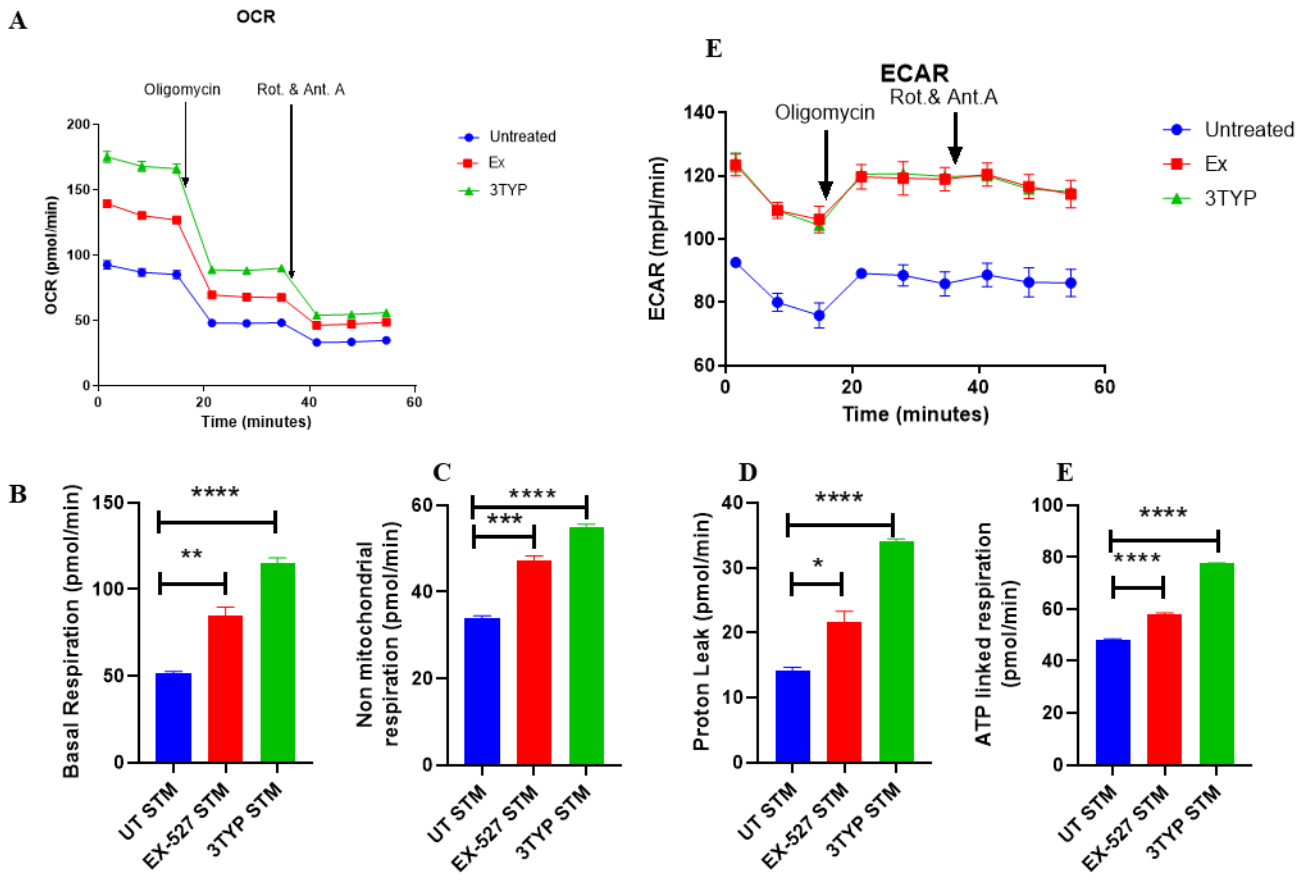

Fig.13 – Mito stress test of *S.* Typhimurium infected peritoneal macrophages under SIRT3 inhibitor treatment

A-Mitochondrial Oxygen Consumption Rate (OCR) curve of infected peritoneal macrophages isolated from 6-8 week old adult male mice post 5th day of thioglycolate injection in the presence or absence of SIRT1 (EX-527) or SIRT3 inhibitor (3TYP,1µM) treatment. Data is representative of N=3, n=2. Unpaired two-tailed Student's t test was performed to obtain the p values. *** $p < 0.001$, ** $p<0.01$, * $p<0.05$

B- Basal mitochondrial respiration of infected peritoneal macrophages isolated from 6–8-week-old adult male mice post 5th day of thioglycolate injection in the presence or absence of SIRT3 inhibitor (3TYP,1µM) treatment as calculated from A. Data is representative of N=3,

n=2. Unpaired two-tailed Student's t test was performed to obtain the p values. *** $p < 0.001$, ** $p<0.01$, * $p<0.05$

C- Non-mitochondrial respiration of infected peritoneal macrophages upon SIRT1 and SIRT3 inhibitor treatment post 6h of *S.* Typhimurium infection as shown in A. Data is representative of N=3, n=2. Unpaired two-tailed Student's t test was performed to obtain the p values. *** $p < 0.001$, ** $p<0.01$, * $p<0.05$

D-Proton leak of infected peritoneal macrophages upon SIRT1 and SIRT3 inhibitor treatment post 6h of *S.* Typhimurium infection as obtained from A. Data is representative of N=3, n=2. Unpaired two-tailed Student's t test was performed to obtain the p values. *** $p < 0.001$, ** $p<0.01$, * $p<0.05$

E-ATP-linked respiration infected peritoneal macrophages upon SIRT1 and SIRT3 inhibitor treatment post 6h of *S.* Typhimurium infection as obtained from A. Data is representative of N=3, n=2. Unpaired two-tailed Student's t test was performed to obtain the p values. *** $p < 0.001$, ** $p<0.01$, * $p<0.05$

F-Extracellular Acidification Rate (ECAR) profile of infected peritoneal macrophages upon SIRT1 and SIRT3 inhibitor treatment post 6h of *S.* Typhimurium infection. Data is representative of N=3, n=2. Unpaired two-tailed Student's t test was performed to obtain the p values. *** $p < 0.001$, ** $p<0.01$, * $p<0.05$

pH homoeostasis within *S.* Typhimurium infected macrophages is mediated by SIRT3

Our previous findings showed defects in mitochondrial bioenergetics, ETC function loss, increased mtROS generation, mitochondrial membrane hyperpolarization and lowered ATP production in STM-infected macrophages upon SIRT3 or SIRT1 inhibition. Considering the

potential impact of mitochondrial membrane potential alterations on cytosolic pH(88, 89), we examined the cytosolic pH of STM-infected RAW264.7 macrophages under the knockdown condition of SIRT1 and SIRT3 by BCECF-AM staining. Host cytosolic pH sensing is crucial for *Salmonella* intravacuolar life, governing effector translocation (90). BCECF-AM, a cell-permeant dye, measures pH-dependent emission intensity ratios at 535nm with dual excitation at 488nm and 405nm. Knockdown of SIRT3, not SIRT1, within *S.* Typhimurium-infected RAW264.7 macrophages intensified the cytosolic acidity of the macrophages (pH~4.8) (Fig.13A-B). Similar observations were obtained from the peritoneal macrophages wherein SIRT3 enzymatic inhibitor treatment resulted in decreased fluorometric ratio of BCECF-AM, indicative of lowered intracellular pH (pH~4.43) (Fig.13C-D). Altogether, our findings suggest the role of SIRT3 in maintaining cytosolic pH through regulation of mitochondrial membrane potential and bioenergetics.

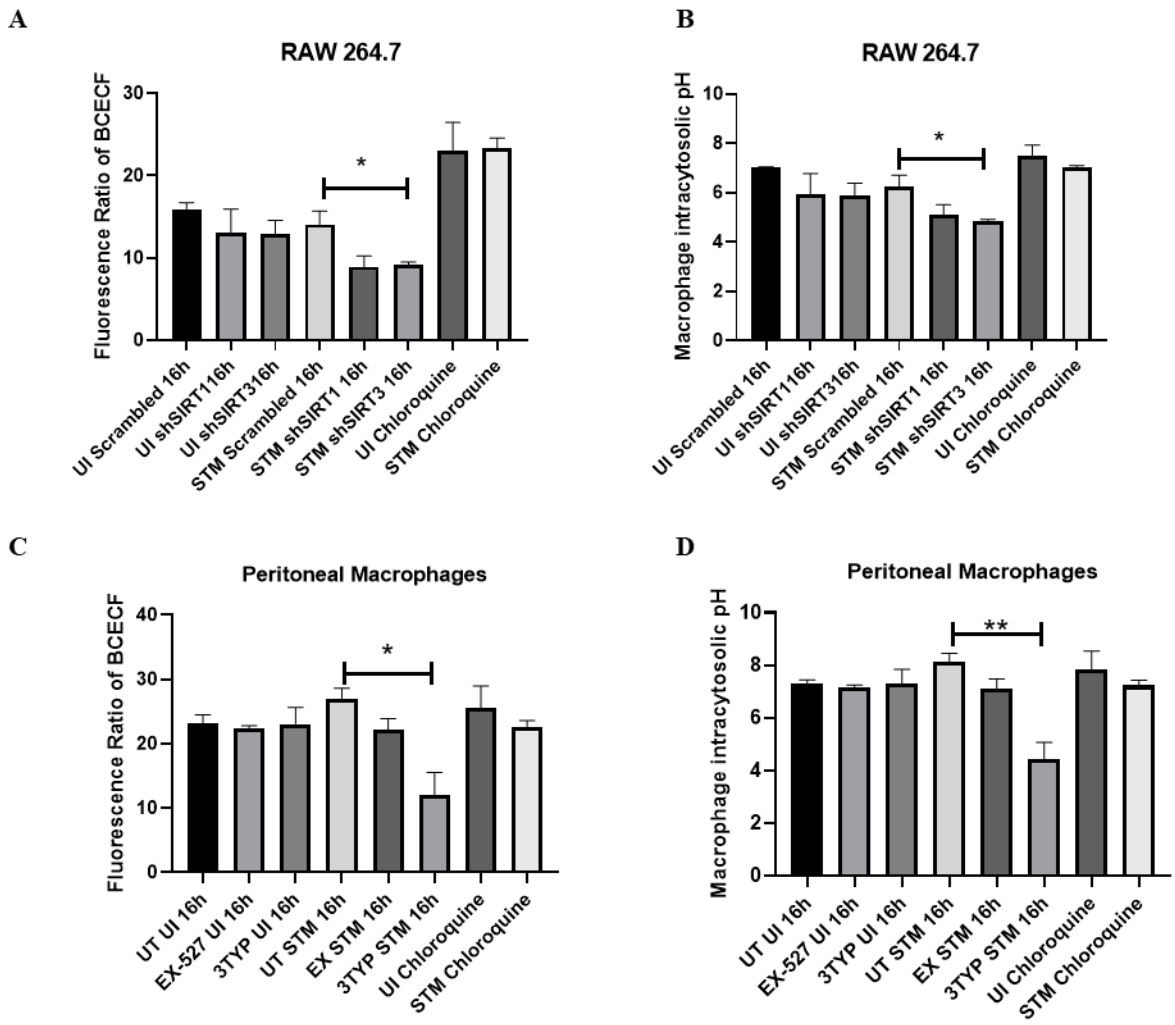

Fig.13 – SIRT3 knockdown causes alteration in the intracellular cytosolic pH of the infected macrophages.

A-B-Flow cytometric analysis of cytosolic pH of *S.* Typhimurium infected RAW264.7 macrophages using BCECF-AM dye under knockdown conditions of SIRT1 and SIRT3 or 50µg/ml of chloroquine treatment. Data is representative of N=4, n=3. Unpaired two-tailed Student's t test was performed to obtain the p values. *** $p < 0.001$, ** $p<0.01$, * $p<0.05$

C-D-Flow cytometric analysis of cytosolic pH of *S.* Typhimurium infected peritoneal macrophages using BCECF-AM dye under inhibitor treatment of SIRT1 (EX-527) and SIRT3 (3TYP) inhibitor at the concentration of 1µM or 50µg/ml of chloroquine treatment. Data is

representative of N=4, n=3. Unpaired two-tailed Student's t test was performed to obtain the p values. *** $p < 0.001$, ** $p<0.01$, * $p<0.05$

SIRT3 triggered host cytosolic pH alterations influenced both intra-phagosomal and intra-*Salmonella* pH and its T3SS mediated virulence protein secretion

Previous reports suggested the prerequisite for host cytosol sensing by *Salmonella* to facilitate *Salmonella* Pathogenicity Island 2 (SPI-2) (91) encoded complex dissociation, degradation, and effector secretion(90). In light of this, we hypothesized that alterations in host cytosolic pH alteration due to SIRT1 or SIRT3 knockdown or inhibition might influence intra-phagosomal and intra-bacterial pH, subsequently impacting SPI-2 effector secretion. Examination of SCV pH within the pH rhodo-labelled STM-infected SIRT1 or SIRT3 RAW264.7 macrophages revealed an increase in intra-vacuolar pH (pH~7.0) when compared to the scrambled control (pH~5.7 to 6.0) (Fig. 14A). Similarly, SIRT1 or SIRT3 inhibitor-treated RAW264.7 macrophages exhibited a loss in intra-phagosomal acidification (pH~7.0) relative to the untreated control (pH~4.5 to 5.8) (Fig. 14B). Subsequently, intra-bacterial pH within the SIRT1 and SIRT3 knockdown macrophages were evaluated by infecting RAW264.7 macrophages with *S.* Typhimurium 14028S expressing pBAD-pHuji (65) (a plasmid encoding pH-sensitive red fluorescent protein). The intra-*Salmonella* pH in SIRT1 or SIRT3 knockdown macrophages exhibited a loss in acidic pH, approaching neutrality (pH~7.2 to 7.6) compared to the scrambled control (pH~5.4) (Fig.14C). Similar results were obtained in inhibitor-treated peritoneal macrophages, wherein both SIRT1 and SIRT3 inhibitor treatment resulted in a loss of acidification in the intra-bacterial pH (Fig.14D). In addition to host cytosolic pH, SPI-2 effector secretion is influenced by the acidic pH of the bacterial cytosol, activating OmpR, a regulator of SPI-2(92). Inside the macrophages, the cadaverine operon *cadC/B* was repressed

by OmpR and the *Salmonella* cytoplasm remained acidified. In *ompR* deficient *Salmonella,* the intracellular pH is returned to a near neutral in a CadC/BA-dependent manner. This activation of EnvZ/OmpR by acid stress stimulates the production of the SsrA/B, another two-component system, and subsequently, expression of SPI-2-secreted effectors(92-94). This phenomenon holds true in bacteria residing inside the SIRT1 and SIRT3 knockdown macrophages wherein the *S*. Typhimurium within the knockdown or inhibitor treated macrophages exhibit increased pH like that of *ompR* deficient *S*. Typhimurium strain and consequently exhibit increased expression of *cadA*, *cadB* and *cadC* together amounting to decreased SPI-2 gene expression such as *pipB2*, and *steE* (Fig.14E-I).

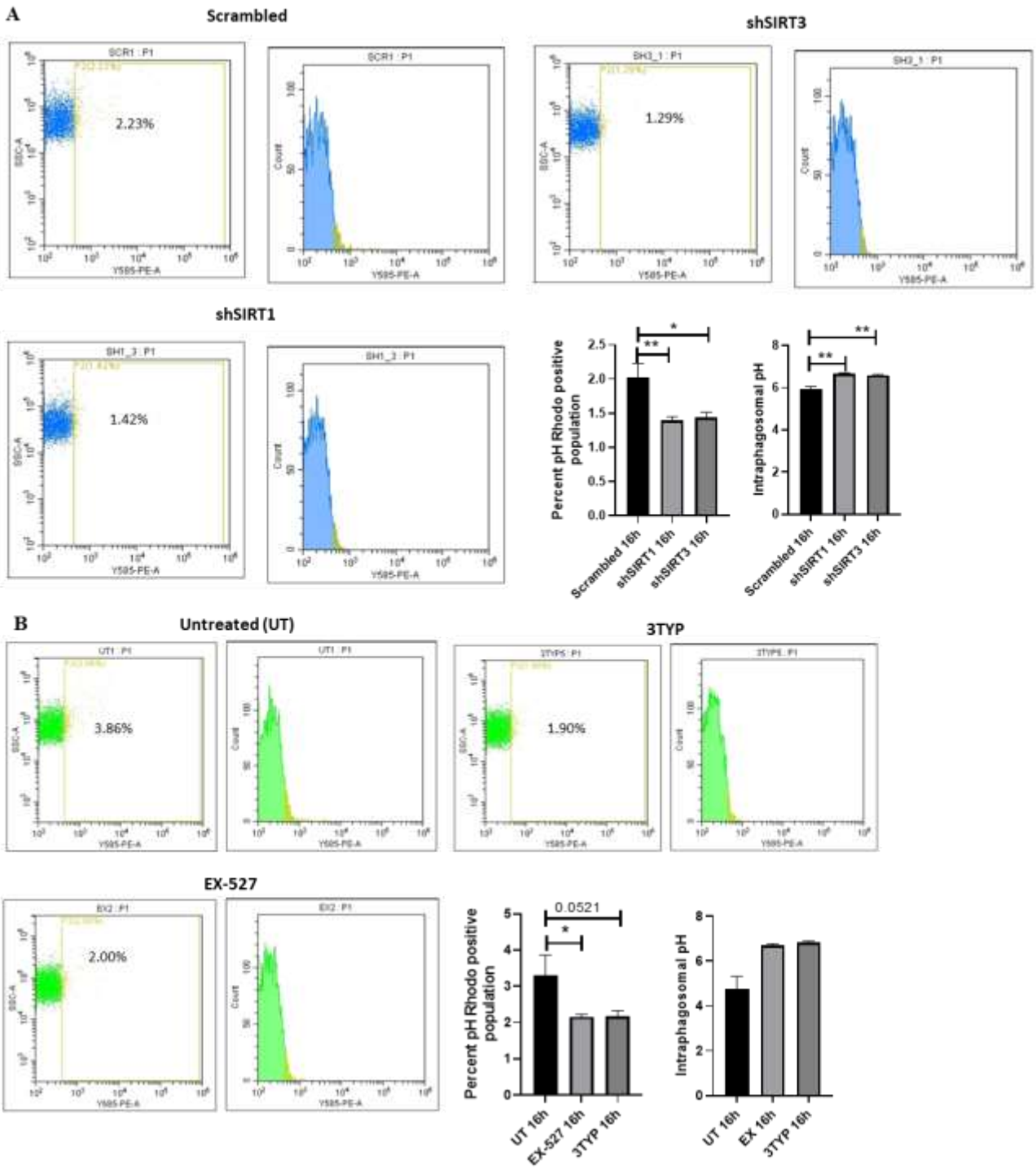
A
Scrambled
2.23%
shSIRT3
1.29%
shSIRT1
1.42%
Percent pH Rhodo positive population
Intraphagosomal pH
Scrambled 16h
shSIRT1 16h
shSIRT3 16h
B
Untreated (UT)
3.86%
3TYP
1.90%
EX-527
2.00%
0.0521
UT 16h
EX-527 16h
3TYP 16h
EX 16h

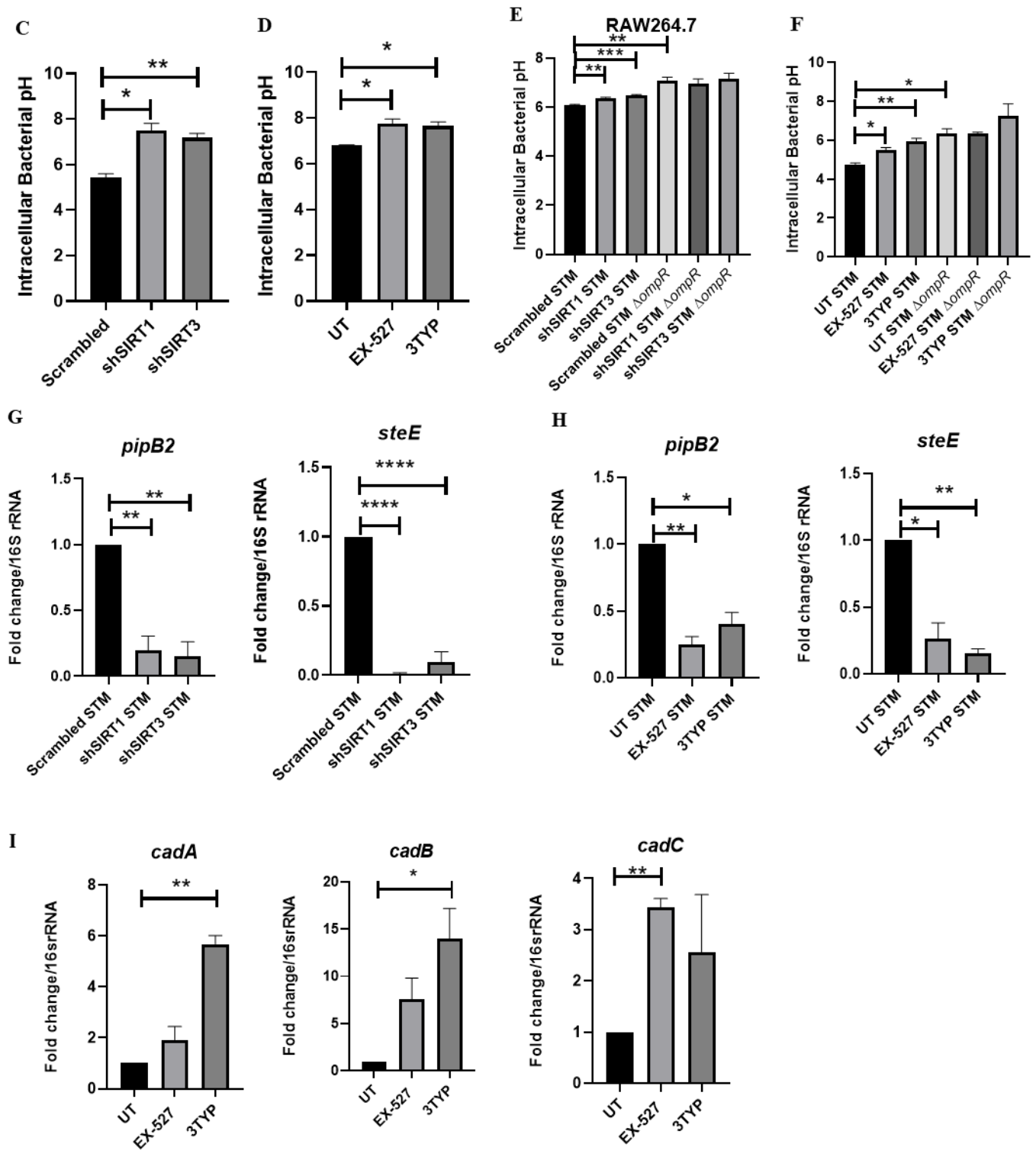

Fig.14 – SIRT1 and SIRT3 knockdown or inhibition trigger loss in acidification of bacterial pH and subsequently its SPI-2 secretion within infected macrophages

A- Flow cytometric analysis of SCV pH of infected RAW264.7 macrophages under knockdown condition of SIRT1 or SIRT3 at 16h post-infection. Data is representative of N=2,n=3. Unpaired two-tailed Student's t-test was performed to obtain the p-values. *** $p < 0.001$, ** $p<0.01$, * $p<0.05$

B- Flow cytometric analysis of SCV pH of infected RAW264.7 macrophages under inhibitor treatment of SIRT1 or SIRT3 at 16h post-infection. Data is representative of N=2,n=3. Unpaired two-tailed Student's t-test was performed to obtain the p-values. *** $p < 0.001$, ** $p<0.01$, * $p<0.05$

C-Intra-bacterial pH of *S.* Typhimurium expressing pH-sensitive plasmid pHUji was measured from infected RAW264.7 macrophages using flow cytometry under knockdown conditions of SIRT1 and SIRT3. Data is representative of N=3, n=4. Unpaired two-tailed Student's t-test was performed to obtain the p values. *** $p < 0.001$, ** $p<0.01$, * $p<0.05$

D-Intra-bacterial pH of *S.* Typhimurium expressing pH-sensitive plasmid pHUji was measured from infected peritoneal macrophages using flow cytometry under inhibitor treatment of SIRT1 (EX-527) and SIRT3 (3TYP) inhibitor at the concentration of 1μM. Data is representative of N=3, n=2. Unpaired two-tailed Student's t-test was performed to obtain the p values. *** $p < 0.001$, ** $p<0.01$, * $p<0.05$

E-Intra-bacterial pH of *S.* Typhimurium WT (STM WT) and STMΔ*ompR* expressing pH-sensitive plasmid pHUji was measured from infected RAW264.7 macrophages using flow cytometry under knockdown conditions of SIRT1 and SIRT3. Data is representative of N=3, n=4. Unpaired two-tailed Student's t-test was performed to obtain the p values. *** $p < 0.001$, ** $p<0.01$, * $p<0.05$

F-Intra-bacterial pH of *S.* Typhimurium WT (STM WT) and STMΔ*ompR* expressing pH-sensitive plasmid pHUji was measured from infected RAW264.7 macrophages using flow

cytometry under inhibitor treatment of SIRT1 (EX-527) and SIRT3 (3TYP) inhibitor at the concentration of 1μM. Data is representative of N=3, n=4. Unpaired two-tailed Student's t-test was performed to obtain the p values. *** $p < 0.001$, ** $p<0.01$, * $p<0.05$

G- Quantitative PCR-mediated expression studies of SPI-2 genes within infected RAW264.7 macrophages under the knockdown condition of SIRT1 and SIRT3. Data is representative of N=3, n=4. Unpaired two-tailed Student's t-test was performed to obtain the p values. *** $p < 0.001$, ** $p<0.01$, * $p<0.05$

H- Quantitative PCR-mediated expression studies of SPI-2 genes within infected peritoneal macrophages under the inhibitor treatment of SIRT1 (EX-527) and SIRT3 (3TYP) inhibitors. Data is representative of N=3, n=4. Unpaired two-tailed Student's t-test was performed to obtain the p values. *** $p < 0.001$, ** $p<0.01$, * $p<0.05$

I- Quantitative PCR-mediated expression studies of *cadA*, *cadB,* and *cadC* genes within infected peritoneal macrophages under the inhibitor treatment of SIRT1 (EX-527) and SIRT3 (3TYP) inhibitors. Data is representative of N=3, n=4. Unpaired two-tailed Student's t-test was performed to obtain the p values. *** $p < 0.001$, ** $p<0.01$, * $p<0.05$

Inhibition of SIRT3 triggered mitophagy in the S. Typhimurium-infected macrophages by altering mitochondrial fusion-fission dynamics

Our previous data suggested disruption in mitochondrial bioenergetics in murine macrophages during *S.* Typhimurium infection under SIRT1 and SIRT3 knockdown conditions. To examine whether SIRT1 or SIRT3 knockdown alters mitochondrial dynamics upon *S.* Typhimurium infection, we assessed mitophagy occurrence through immunoblotting and immunofluorescence studies. Using a mito-eGFP-mCherry traffic light construct we observed increased mitophagy induction in SIRT1 and SIRT3 inhibitor-treated infected macrophages at

16hr post-infection (Fig.15A-B). Immunoblotting studies revealed increased mitophagy initiation in the SIRT3 knockdown infected RAW264.7 macrophages as early as 2hr post-infection, with reduced levels of mitochondrial outer membrane protein TOM20 and elevated LC3B II protein levels (Fig. 15C-D). Altogether, our data depicts increased mitophagy influx upon knockdown of SIRT3 in the *Salmonella* infected murine macrophages.

Since we observed an increased mitophagy induction upon SIRT3 knockdown condition in infected murine macrophages, we hypothesized whether increased mitophagy coincides with increased incidences of mitochondrial fission. Therefore, we assessed the mitochondrial fission and fusion genes via qPCR in infected SIRT1 or SIRT3 knockdown RAW264.7 macrophages or peritoneal macrophages under the chemical inhibitor treatment of either SIRT1 (EX-527) or SIRT3 (3TYP). qPCR analysis revealed increased transcript level expression of mitochondrial fission genes (*Drp1*, *Fis1*, *Mid49* and *Mid51)* and decreased expression of mitochondrial fusion genes (*Mff*, *Mfn2*, and *Opa1)* in infected macrophages under SIRT1 or SIRT3 knockdown (Fig. 15 E-F) or inhibitor-treated conditions (Fig.S6) with SIRT3 inhibition showing more prominent effect. Evaluation of mitochondrial dynamics in infected macrophages under inhibitor treatment via immunofluorescence studies revealed an increased percentage of cells exhibiting mitochondrial fusion in *S.* Typhimurium-infected macrophages at 6hr post-infection. However, SIRT1 and SIRT3 inhibitor treatment enhanced mitochondrial fission with around 60% and 80% of cells depicting fragmented morphology, respectively (Fig. 15G) along with reduced mitochondrial tubular length (Fig. 15G). Previous studies have shown the role of SIRT3 in deacetylating OPA-1 and thereby causing activation of OPA-1 in cardiac tissues (95). In line with this observation, we evaluated the interaction of SIRT3 with OPA-1 in infected RAW 264.7 macrophages and observed an enhanced interaction in the infected macrophages compared to the uninfected control (Fig. 15H). However, SIRT3 knockdown or treatment with catalytic inhibitor 3TYP, led to a decline in OPA-1 protein interaction with SIRT3,

accompanied by increased OPA-1 acetylation at 16hr post-infection (Fig.15 I-K). These results reveal the role of SIRT3 in controlling the mitochondrial fusion dynamics in *Salmonella*-infected macrophages.

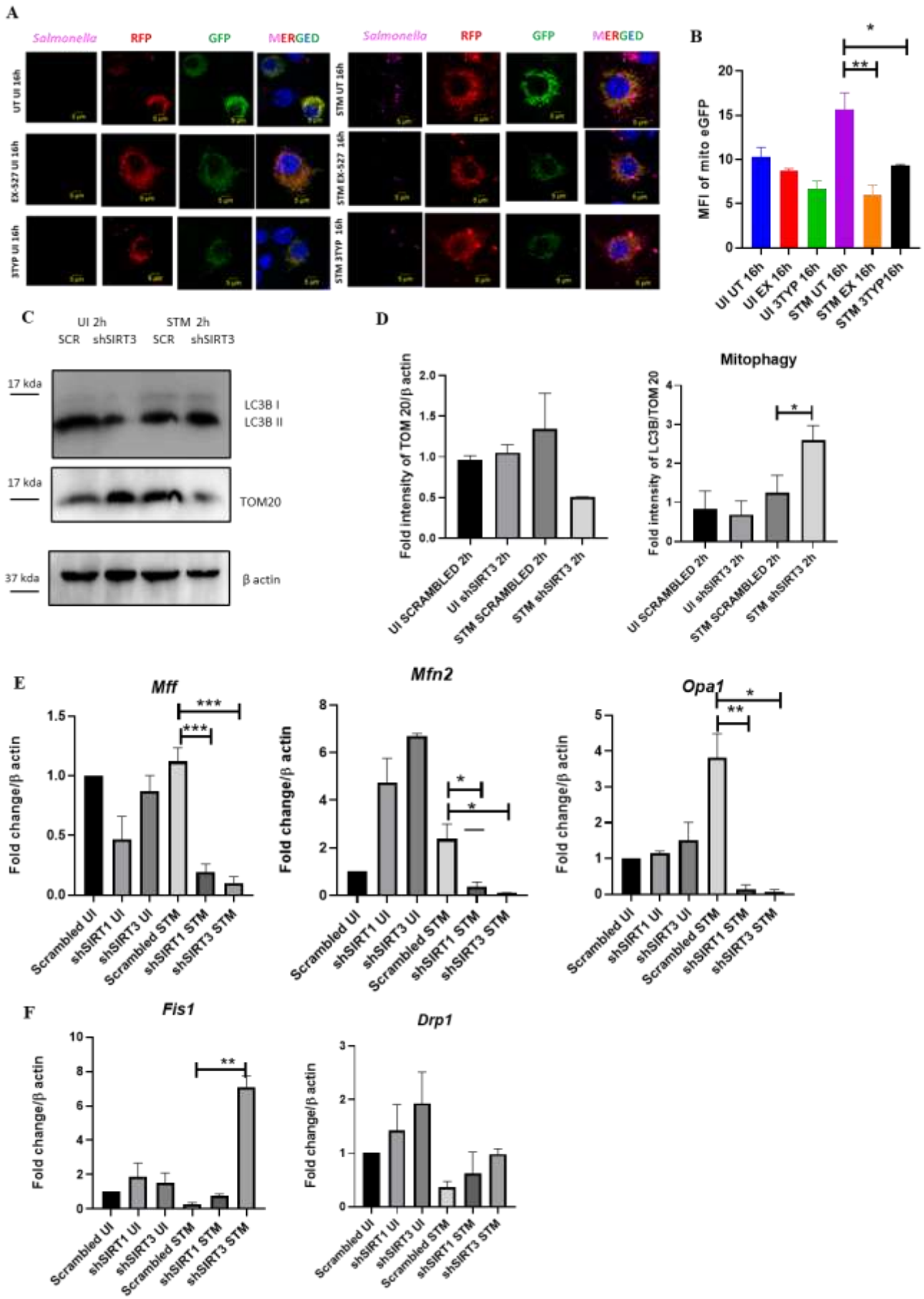
A
Salmonella
RFP
GFP
MERGED
UT UI 16h
EX-527 UI 16h
3TYP UI 16h
STM UT 16h
STM EX-527 16h
STM 3TYP 16h
B
MFI of mito eGFP
UI UT 16h
UI EX 16h
UI 3TYP 16h
STM UT 16h
STM EX 16h
STM 3TYP16h
C
UI 2h
STM 2h
SCR
shSIRT3
17 kda
LC3B I
LC3B II
TOM20
37 kda
β actin
D
Fold intensity of TOM 20/β actin
Mitophagy
Fold intensity of LC3B/TOM 20
UI SCRAMBLED 2h
UI shSIRT3 2h
STM SCRAMBLED 2h
STM shSIRT3 2h
E
Mff
Mfn2
Opa1
Fold change/β actin
Scrambled UI
shSIRT1 UI
shSIRT3 UI
Scrambled STM
shSIRT1 STM
shSIRT3 STM
F
Fis1
Drp1

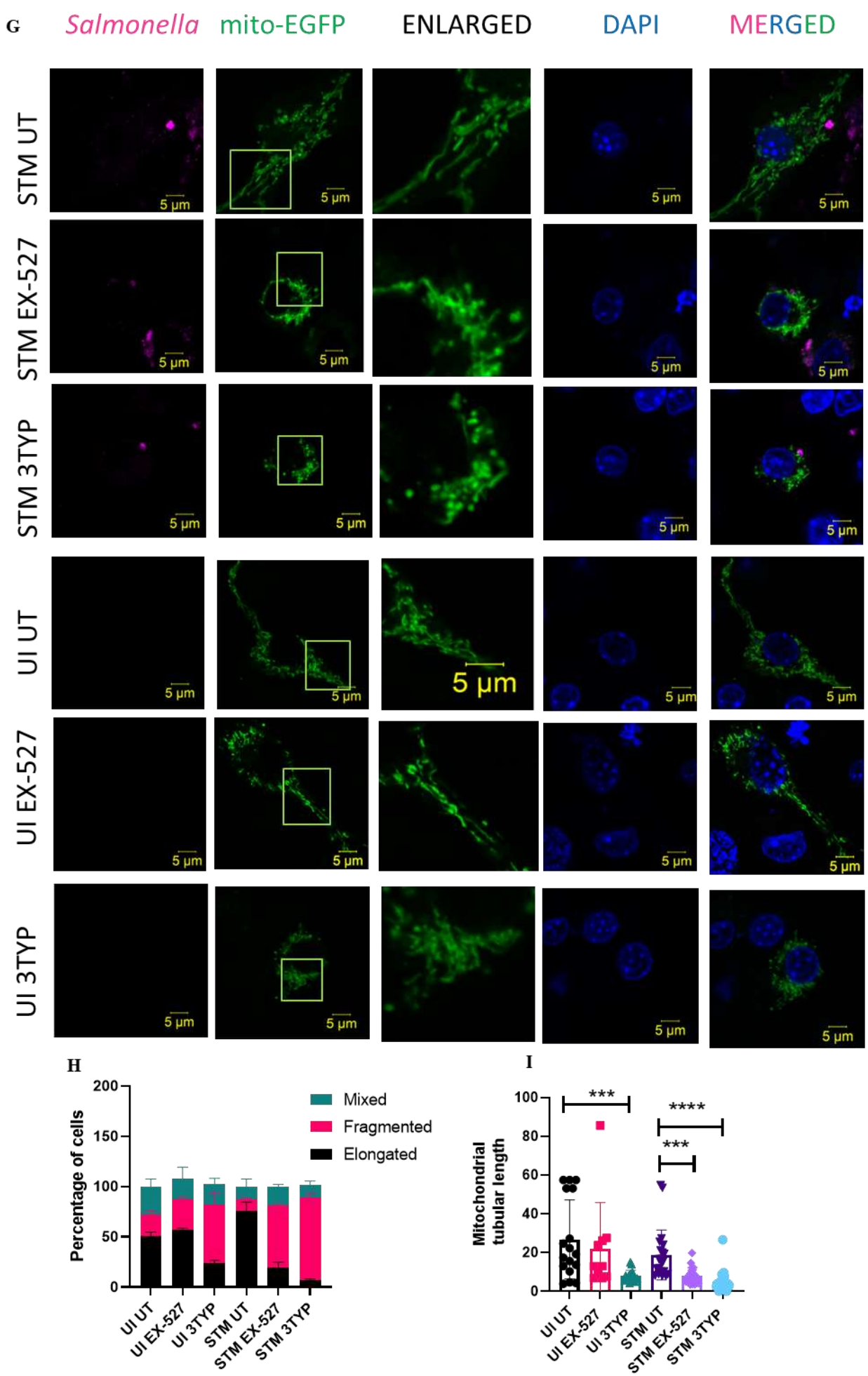
G
Salmonella
mito-EGFP
ENLARGED
DAPI
MERGED
STM UT
STM EX-527
STM 3TYP
UI UT
UI EX-527
UI 3TYP
5 µm
H
Percentage of cells
200
150
100
50
0
Mixed
Fragmented
Elongated
UI UT
UI EX-527
UI 3TYP
STM UT
STM EX-527
STM 3TYP
I
Mitochondrial tubular length
100
80
60
40
20
0
***
****
***
UI UT
UI EX-527
UI 3TYP
STM UT
STM EX-527
STM 3TYP

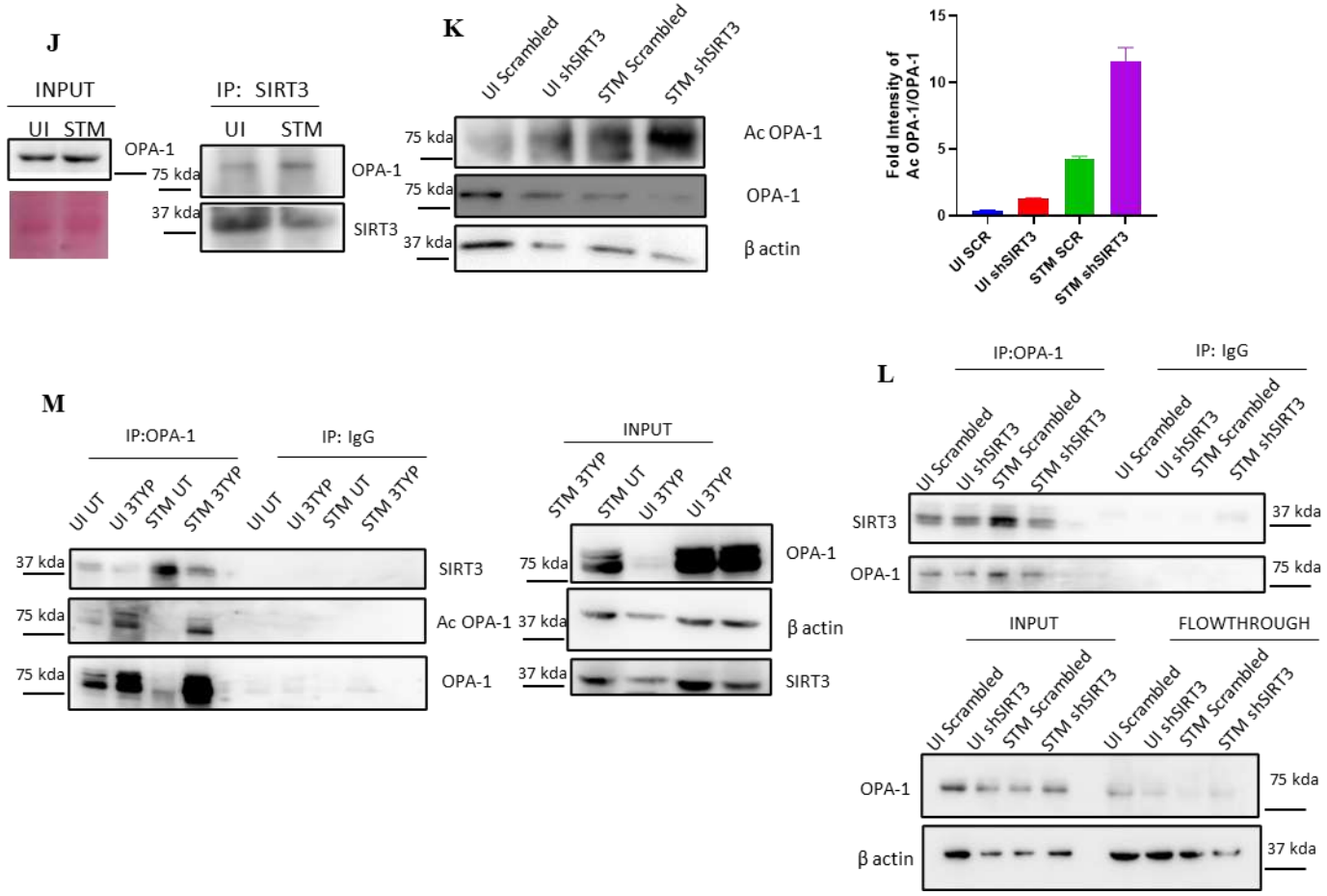

Fig. 15- SIRT1 and SIRT3 inhibition triggers mitophagy in the *S.* Typhimurium-infected macrophages by regulating fusion-fission dynamics

A-Representative confocal images of RAW264.7 macrophages (transfected with mito-eGFP-mCherry) exhibiting mitophagy flux upon *S.* Typhimurium infection at 16h points post-infection. Data is representative of N=2, n>50 (microscopic field).

B- Quantitative representation of the MFI of mitochondrial eGFP as shown in the confocal images (A). Unpaired two-tailed Student's t-test was performed to obtain the p values. *** $p < 0.001$, ** $p<0.01$, * $p<0.05$

C- Immunoblotting of LC3B and TOM20 in uninfected and infected RAW264.7 macrophages under knockdown condition of SIRT3 at 2hr post-infection. UI-Uninfected, STM-*S.* Typhimurium infected, Scrambled shRNA control

D-Densitometric analysis of TOM20 with respect to βactin LC3BII with respect to TOM20 and of the immunoblot A to detect mitophagy.

E-F- qRTPCR mediated expression analysis of mitochondrial fusion (E) and fission (F) genes in *S.* Typhimurium infected RAW264.7 macrophages at 16hr post infection under knockdown of SIRT1 or SIRT3.

G- Representative confocal images of RAW264.7 macrophages demonstrating mitochondrial fusion-fission dynamics upon *S.* Typhimurium infection at 6h post-infection upon SIRT1 or SIRT3 inhibitor treatment. Data is representative of N=2, n>100.

H-Quantitative representation of the percentage of cells depicted in (G) exhibiting elongated, fragmented, and mixed population mitochondrial morphologies.

I-Quantitative representation of the mitochondrial tubular length of infected (STM) and uninfected (UI) RAW264.7 macrophages as shown in (G). Unpaired two-tailed Student's t-test was performed to obtain the p values. *** $p < 0.001$, ** $p<0.01$, * $p<0.05$

J- Immunoprecipitation of SIRT3 in uninfected or *S.* Typhimurium infected RAW264.7 macrophages at 16hr post infection to detect interaction of SIRT3 with OPA-1.

K- Immunoblotting of SIRT3 knockdown RAW 264.7 cells in *S.* Typhimurium infected and uninfected upon immunoprecipitation of OPA-1 to check the acetylation status of OPA-1.

L- Immunoprecipitation of OPA-1 in uninfected or *S.* Typhimurium infected RAW264.7 macrophages at 16hr post infection under the knockdown condition of SIRT3 to assess the interaction of OPA-1 with SIRT3 in knockdown condition.

M- Immunoprecipitation of OPA-1 in uninfected or *S.* Typhimurium infected RAW264.7 macrophages at 16hr post infection under the catalytic inhibitor treatment of SIRT3.

DISCUSSION

Several studies have confirmed the propensity of *Salmonella* to skew the polarization state of the infected macrophages toward an immunosuppressive anti-inflammatory state(96-98). We have validated such findings and further elaborated them by depicting the role of SIRT1 and SIRT3 in the modulation of host immune responses as well as host-bacterial metabolism. *Salmonella* Typhimurium infection modulates the expression profile of both SIRT1 and SIRT3 in the infected macrophages at both mRNA and protein level via its SPI-2 effectors, SsaV and SteE. Downregulation of SIRT1 and SIRT3 through shRNA mediated knockdown resulted in heightened pro-inflammatory immune responses with increased production of IL-6 cytokine and decreased surface expression of anti-inflammatory CD206. SIRT1 and SIRT3 downregulation also increased intracellular ROS production in the infected macrophages. SIRT1 and SIRT3 knockdown macrophages not only show altered host immune status but also depicted shift in the metabolic state with increased glycolytic shift. This altered host metabolism upon SIRT1 and SIRT3 knockdown condition influences the infection outcome by regulating the intracellular bacterial metabolism which show reduced bacterial glycolysis and increased fatty acid oxidation. All these outcomes account for attenuated intracellular bacterial proliferation in the SIRT1 and SIRT3 knockdown macrophages. However, in murine model of infection, SIRT1 or SIRT3 inhibitor treatment led to increased organ burden and triggered bacterial dissemination (Fig. 2.13). Overall, our study highlights the crucial role of SIRT1 and SIRT3 in governing the host immune-metabolic shift during *Salmonella* infection which in turn is vital for maintaining *Salmonella* metabolism.

Previous reports have elucidated the role of SIRT1 and SIRT2 pertaining to *Salmonella* infection. Ganesan *et al*., have depicted the role of SIRT1 in autophagy in *Salmonella* infection scenario(99). Gogoi *et al*., have demonstrated SIRT2 mediated modulation of immune responses in dendritic cells(100). Till date, there is no report highlighting the role of SIRT3 governing the *Salmonella* pathogenesis. The function of SIRT3 in infection scenario has been explored quite recently. In *Mycobacterium tuberculosis* infection condition, SIRT3 control mitochondrial function and autophagy(35). SIRT3 downregulation in *Mycobacterium tuberculosis* infected macrophages is associated with dysregulated mitochondrial metabolism and increased cell death (56). In this study we have explored the role of SIRT1 and SIRT3 in mediating host immune-metabolic switch in *Salmonella* Typhimurium infected macrophages which further govern intracellular bacterial metabolism and pathogenesis.

Our findings suggest the role of SIRT1 and SIRT3 in mediating polarization of the *Salmonella* infected macrophages toward an anti-inflammatory state. Upon knockdown of SIRT1 and SIRT3 in the infected macrophages we detect robust pro-inflammatory response and oxidative burst. This is in line with the findings by S. Elsela *et al*., wherein SIRT1 knockout RSV(Respiratory Syncytial Virus) - infected BMDCs showed significant increase in *Il1β*, *Il6* and *Il23* expression and ROS generation in comparison to the wild type RSV-infected BMDCs(32). Also, Kim *et al*., showed presence of aggravated inflammatory responses in *Mycobacterium tuberculosis* infected SIRT3-/- BMDMs(35). This heightened pro-inflammatory cytokine and oxidative burst restrict the intracellular survival of the pathogen as detected by the lower intracellular bacterial burden in the SIRT1 and SIRT3 knockdown murine macrophages. *Salmonella* showed enhanced proliferation in the M2 macrophages owing to the reduced arsenals in terms of pro-inflammatory cytokines and ROS production. Moreover, the M2 macrophages are fuelled by increased fatty acid oxidation and reduced glycolysis(101). This might facilitate enhanced bacterial proliferation as the host un-utilized intracellular

glucose can be readily up taken by the pathogen and used to support its own glycolysis. Similarly, M1 or pro-inflammatory macrophages resort to glycolysis to meet their energy demands (102) thereby limiting the glucose availability for the intracellular pathogen (102, 103). In such condition, bacteria show enhanced fatty acid metabolism to sustain their energy demand(104). In our study, we found that wild type *S.* Typhimurium infection drive host metabolism toward increased fatty acid oxidation via its SPI-2 effector protein with concomitant increase in the bacterial glycolysis. SIRT1 and SIRT3 inhibition abrogates the metabolic switch and triggers increase in host glycolysis which in turn skew the bacterial metabolism from increased glycolysis to enhanced fatty acid oxidation and reduced glycolysis. Together, these findings implicate the role of SIRT1 and SIRT3 in reprograming the host metabolism which in turn affect the intracellular nutrient niche of the pathogen thereby influencing intracellular *Salmonella* proliferation. However, our *in vivo* findings in the murine model of infection show increased bacterial burden upon SIRT1 or SIRT3 inhibition. This increased burden could be attributed to increased dissemination from the macrophages into the bloodstream owing to the increased level of serum IL-6 levels. This is in concert with previous findings in *Klebsiella pneumoniae* infection in mice wherein increased inflammatory response upon HIF-1α activation induces bacterial dissemination(105). Further correlation analysis of immune responses to *Salmonella* infection revealed that increased innate immune "cassette" opposes the adaptive immune arm leading to increased bacterial load (106). Future studies might explore the host and bacterial interacting partners of SIRT1 and SIRT3 through mass spectrometry analyses in *Salmonella* infected macrophages which might hint at the underlying mechanisms and their regulation. Together, this study highlights the complex and multifaceted nature of host-pathogen interactions, and the need for further research to fully unravel the role of SIRT1 and SIRT3 in the context of *Salmonella* infection.

Mitochondrial health emerges as a vital determinant in infection outcomes (107). For instance, pathogens like *L. monocytogenes* and *S. flexneri* induce mitochondrial fragmentation to gain a survival advantage(37, 39) while the intracellular pathogen *Legionella pneumophila* triggers fragmentation via its type IV secretion system effector, MitF, leading to decreased ATP production (40). In contrast, *Chlamydia trachomatis* preserves the mitochondrial framework to maintain the mitochondrial ATP production capacity by preventing Drp-1 mediated mitochondrial fission(41) while *C. pneumoniae* causes mitochondrial dysfunction by inducing mitochondrial hyperpolarization, increased ROS production and induction of host metabolic shift to glycolysis(108).

Our study investigates how *Salmonella* Typhumurium infection in murine macrophages modulates mitochondrial dynamics and bioenergetics through SIRT1 and SIRT3, influencing infection progression. SIRT3 inhibition increases mitochondrial superoxide generation coinciding with mitochondrial membrane hyperpolarization, proton leakage and decreased ATP production. However, mitochondrial ROS production and membrane hyperpolarization remained unperturbed by inhibition of SIRT1, implicating SIRT3's predominant role in mitochondrial energy homeostasis and oxidative stress (46, 47). This aligns with the recent publication on *Mycobacterium tuberculosis* infection wherein SIRT3 deficiency led to increased accumulation of dysfunctional mitochondria with heightened oxidative stress (35). While both SIRT1 and SIRT3 deficiencies reduced antioxidant host gene transcript expression, possibly due to their overlapping role in activating the antioxidant defense Nrf2 pathway (109-111), mitostress profile showed increased respiration parameters upon both SIRT1 and SIRT3 inhibition. The increased respiratory flux and proton leak gets dissipated in the production of mitochondrial ROS generation leading to decreased ATP content and increased ECAR upon SIRT1 and SIRT3 inhibitor treatment in *S.* Typhimurium infected macrophages. Proton leak and electron slip are the two critical mechanisms contributing to incomplete coupling of ATP

generation and substrate oxygen resulting in disproportionate increase in oxygen consumption rate at high protonmotive force and mitochondrial membrane potential with lower ATP yield (112-114).

An important underlying question is how these alterations in the mitochondrial energetics impact the intracellular life of the *Salmonella* within the infected macrophages. Our data indicates that the mitochondrial bioenergetic alteration triggers increased acidification of the macrophage cytosolic pH. SIRT1 or SIRT3 loss or inhibition skews intra-phagosomal and intra-bacterial pH, resulting in decreased SPI-2 gene expression and attenuated intracellular replication.

Numerous evidence suggest how different pathogen assaults lead to remodeling of the mitochondria that eventually dictates the fate of the war between the host and the pathogen (115-119). Our work reveals increased mitochondrial fusion dynamics upon *S*. Typhimurium infection via SIRT3-mediated deacetylation of OPA-1. This aligns with *Chlamydia trachomatis* infection studies wherein the infection induces mitochondrial elongation at the early stages and the abrogation of the fusion dynamics led to attenuated chlamydial proliferation(42). In our study, the *S.* Typhimurium-infected macrophages depicted altered mitochondrial dynamics with increased mitophagy and decreased mitochondrial fusion dynamics under SIRT3 silenced or inhibited condition. The role of mitophagy in host defense varies dictating the infection outcome. During *Pseudomonas aeruginosa* (120), *Vibrio splendidus* (121) or *Mycobacterium tuberculosis* (122) infection, host promotes mitophagy for pathogen clearance, while *Listeria monocytogenes* (123), *Yersinia pestis* (124), *Brucella abortus* (125) and *Helicobacter pylori* (38) (126) induce mitophagy for survival or dissemination.

In summary, our results highlight the role of SIRT1 and predominantly, SIRT3 in governing *Salmonella'*s intracellular niche through regulation of mitochondrial energetics, fusion-fission

remodeling and host-bacterial intracellular pH balance during *S.* Typhimurium infection. This work contributes to our understanding of host-pathogen crosstalk, offering insights for future avenues in *Salmonella* infection control.

Mitochondrial health emerges as a vital determinant in infection outcomes (107). For instance, pathogens like *L. monocytogenes* and *S. flexneri* induce mitochondrial fragmentation to gain a survival advantage(37, 39) while the intracellular pathogen *Legionella pneumophila* triggers fragmentation via its type IV secretion system effector, MitF, leading to decreased ATP production (40). In contrast, *Chlamydia trachomatis* preserves the mitochondrial framework to maintain the mitochondrial ATP production capacity by preventing Drp-1 mediated mitochondrial fission(41) while *C. pneumoniae* causes mitochondrial dysfunction by inducing mitochondrial hyperpolarization, increased ROS production and induction of host metabolic shift to glycolysis(108).

Our study investigates how *Salmonella* Typhumurium infection in murine macrophages modulates mitochondrial dynamics and bioenergetics through SIRT1 and SIRT3, influencing infection progression. SIRT3 inhibition increases mitochondrial superoxide generation coinciding with mitochondrial membrane hyperpolarization, proton leakage and decreased ATP production. However, mitochondrial ROS production and membrane hyperpolarization remained unperturbed by inhibition of SIRT1, implicating SIRT3's predominant role in mitochondrial energy homeostasis and oxidative stress (46, 47). This aligns with the recent publication on *Mycobacterium tuberculosis* infection wherein SIRT3 deficiency led to increased accumulation of dysfunctional mitochondria with heightened oxidative stress (35). While both SIRT1 and SIRT3 deficiencies reduced antioxidant host gene transcript expression,

possibly due to their overlapping role in activating the antioxidant defense Nrf2 pathway (109-111), mitostress profile showed increased respiration parameters upon both SIRT1 and SIRT3 inhibition. The increased respiratory flux and proton leak gets dissipated in the production of mitochondrial ROS generation leading to decreased ATP content and increased ECAR upon SIRT1 and SIRT3 inhibitor treatment in *S.* Typhimurium infected macrophages. Proton leak and electron slip are the two critical mechanisms contributing to incomplete coupling of ATP generation and substrate oxygen resulting in disproportionate increase in oxygen consumption rate at high protonmotive force and mitochondrial membrane potential with lower ATP yield (112-114).

An important underlying question is how these alterations in the mitochondrial energetics impact the intracellular life of the *Salmonella* within the infected macrophages. Our data indicates that the mitochondrial bioenergetic alteration triggers increased acidification of the macrophage cytosolic pH. SIRT1 or SIRT3 loss or inhibition skews intra-phagosomal and intra-bacterial pH, resulting in decreased SPI-2 gene expression and attenuated intracellular replication.

Numerous evidence suggest how different pathogen assaults lead to remodeling of the mitochondria that eventually dictates the fate of the war between the host and the pathogen (115-119). Our work reveals increased mitochondrial fusion dynamics upon *S*. Typhimurium infection via SIRT3-mediated deacetylation of OPA-1. This aligns with *Chlamydia trachomatis* infection studies wherein the infection induces mitochondrial elongation at the early stages and the abrogation of the fusion dynamics led to attenuated chlamydial proliferation(42). In our study, the *S.* Typhimurium-infected macrophages depicted altered mitochondrial dynamics with increased mitophagy and decreased mitochondrial fusion dynamics under SIRT3 silenced or inhibited condition. The role of mitophagy in host defense varies dictating the infection outcome. During *Pseudomonas aeruginosa* (120), *Vibrio splendidus* (121) or *Mycobacterium*

tuberculosis (122) infection, host promotes mitophagy for pathogen clearance, while *Listeria monocytogenes* (123), *Yersinia pestis* (124), *Brucella abortus* (125) and *Helicobacter pylori* (38) (126) induce mitophagy for survival or dissemination.

In summary, our results highlight the role of SIRT1 and predominantly, SIRT3 in governing *Salmonella'*s intracellular niche through regulation of mitochondrial energetics, fusion-fission remodeling and host-bacterial intracellular pH balance during *S.* Typhimurium infection. This work contributes to our understanding of host-pathogen crosstalk, offering insights for future avenues in *Salmonella* infection control.

SUMMARY

Salmonella have adopted several strategies to combat the host immune responses and establish a suitable intracellular survival niche within their hosts. In this study, we explored the role of two critical sirtuins, namely SIRT1 and SIRT3, in mediating a metabolic switch in both *Salmonella* and their infected host. Our investigation revealed that live *Salmonella* Typhimurium can actively regulate the levels of SIRT1 and SIRT3, thereby sustaining a high glycolytic metabolism and low fatty acid oxidative metabolism in the bacteria. Upon SIRT1 or SIRT3 knockdown or inhibition, the intracellular *Salmonella* underwent a metabolic shift, favouring high acid oxidation and low glycolysis, consequently leading to reduced proliferation within macrophages. Furthermore, we observed that elevated levels of SIRT1 and SIRT3 induced by *Salmonella* triggered a polarization of macrophages from a pro-inflammatory M1 state to an immunosuppressive M2 state, creating a conducive environment for *Salmonella*'s intracellular survival. In addition to their immunological functions via modulation of p65 NF-κB acetylation, SIRT1 and SIRT3 influenced the host's metabolic switch during *Salmonella* infection by regulating the acetylation status of HIF-1α and PDHA1. Although SIRT1 or SIRT3 knockdown resulted in decreased *Salmonella* proliferation in macrophages, interestingly,

knockdown or inhibition of these sirtuins in an *in vivo* mouse model of infection led to higher organ burden and increased dissemination. This phenomenon was associated with elevated ROS and IL-6 production. Therefore, our findings indicate that *Salmonella* strategically modulates the levels of SIRT1 and SIRT3 to maintain its own metabolism, contributing to successful intracellular pathogenesis.

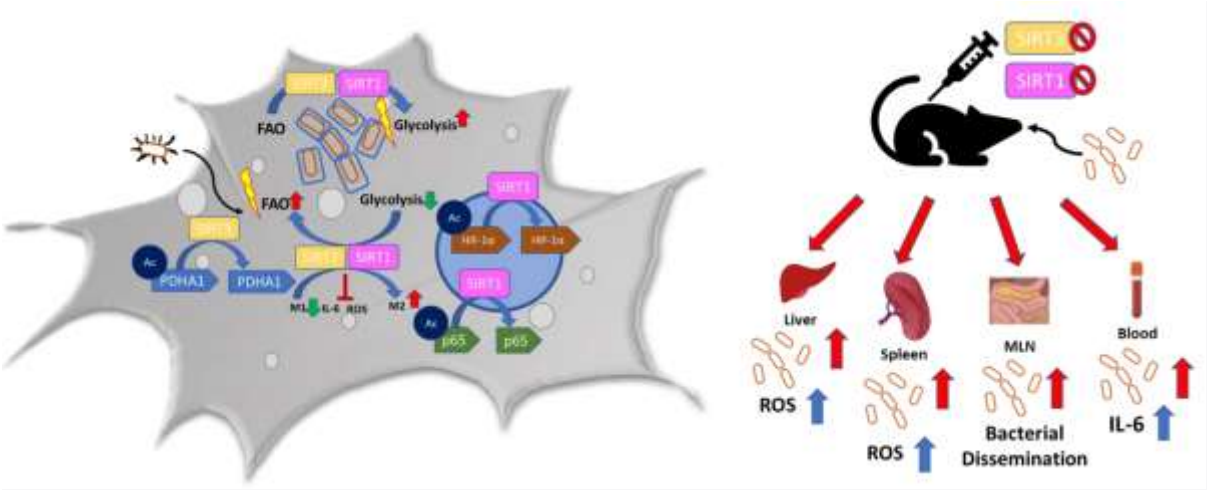

Fig. 16 Schematic Diagram-In murine macrophages, *Salmonella* infection drives an immuno-metabolic shift toward an immunosuppressive state with an increase in host fatty acid oxidation rate by modulating SIRT1 and SIRT3. SIRT1 and SIRT3 regulate the acetylation status of NFκB p65 subunit, HIF-1α, PDHA1 thereby influencing host metabolism which in turn impacts the intracellular *Salmonella* metabolism. Inhibition or knockdown of SIRT1 or SIRT3 triggers increased ROS, pro-inflammatory cytokine burst with a concomitant decline in host fatty acid oxidation and a corresponding increase in bacterial fatty acid oxidation together amounting to decreased intracellular bacterial replication. Contrastingly, in *in vivo* mice model of infection, SIRT1 and SIRT3 cause increased bacterial dissemination owing to increased ROS and IL-6 production.

Mitochondria play a vital role in regulating energy balance within the host. Mitochondrial health and their dynamics significantly impact the outcomes of various bacterial infections. Among the mitochondrial sirtuins, SIRT3 and SIRT1 are crucial in governing essential mitochondrial functions. Our study reveals that the loss of SIRT1 and SIRT3 function, achieved through shRNA-mediated knockdown or inhibitor treatment, leads to increased mitochondrial dysfunction in *Salmonella*-infected macrophages. This dysfunction manifests as alterations in mitochondrial bioenergetics, as well as an upsurge in mitochondrial superoxide generation. Moreover, the presence of dysfunctional mitochondria triggers mitophagy and affects the balance of mitochondrial fusion-fission dynamics in the infected macrophages. Furthermore, the perturbation in mitochondrial bioenergetics contributes to an acidification of the cytosolic pH in infected macrophages, which, in turn, skews the pH within the intracellular *Salmonella*. This altered pH environment ultimately results in decreased expression of the SPI-2 genes. Overall, our findings highlight a novel role for SIRT1 and SIRT3 in maintaining the intracellular niche for *Salmonella* by preserving mitochondrial bioenergetics and dynamics in infected macrophages. This sheds new light on the intricate interplay between mitochondrial regulation and bacterial infection, offering potential avenues for further research and therapeutic interventions.

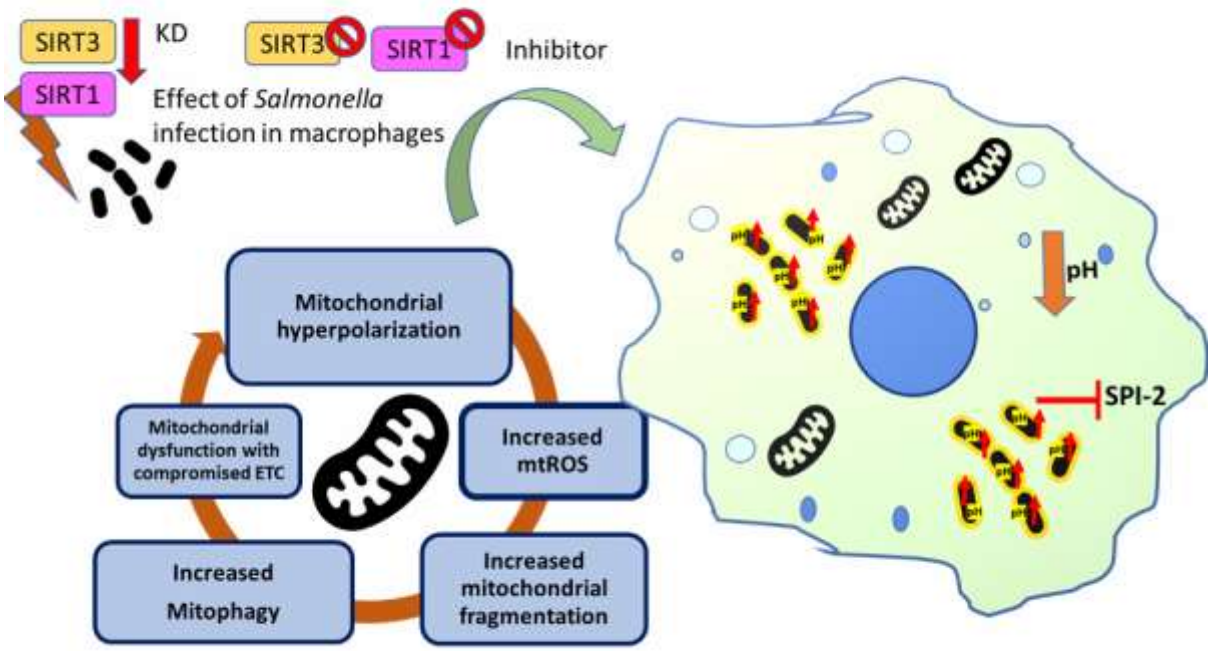

Fig. 17. Schematic diagram depicting the perturbations in mitochondrial dynamics, bioenergetics, and function in *Salmonella* infected macrophages upon knockdown or inhibition of SIRT1 and SIRT3 leading to acidified macrophage cytosolic pH which, in turn, skews the intra-phagosomal *Salmonella* pH and SPI-2 secretion.

IMPACT OF RESEARCH IN THE ADVANCEMENT OF KNOWLEDGE AND BENEFIT TO MANKIND

Salmonella enterica is a facultative, anaerobic, flagellated, intracellular pathogen causing food- and water borne enteric typhoid fever and gastroenteritis worldwide. *Salmonella* Typhimurium causes localized gastroenteritis however in certain instances it contributes to systemic invasive infections in immunocompromised individuals(127). The emergence of several multi-drug resistant *Salmonella* strains continues to be a major healthcare concern calling for a comprehensive understanding of the mechanism underlying *Salmonella* pathogenesis and its interaction with its host. Here we have demonstrated how *Salmonella* strategically modulates

the levels of SIRT1 and SIRT3 to maintain its own metabolism, contributing to successful intracellular pathogenesis. Moreover, SIRT1 and SIRT3 are crucial in maintaining the intracellular niche for *Salmonella* by preserving host mitochondrial bioenergetics and dynamics in infected macrophages and thereby modulating both host and bacterial pH dynamics, important for *Salmonella* virulence effector secretion. Although SIRT1 or SIRT3 knockdown resulted in decreased *Salmonella* proliferation in macrophages, interestingly, knockdown or inhibition of these sirtuins in an *in vivo* mouse model of infection led to higher organ burden and increased dissemination owing to enhanced inflammation and tissue damage.

Our current study aims to understand the complex and multifaceted intricacies of host-*Salmonella* dynamics aiming to develop host-targeted therapeutics to thwart *Salmonella* burden.

LITERATURE REFERENCE

1. Landry J, Sutton A, Tafrov ST, Heller RC, Stebbins J, Pillus L, et al. The silencing protein SIR2 and its homologs are NAD-dependent protein deacetylases. Proceedings of the National Academy of Sciences of the United States of America. 2000;97(11):5807-11.
2. Sauve AA, Celic I, Avalos J, Deng H, Boeke JD, Schramm VL. Chemistry of gene silencing: the mechanism of NAD+-dependent deacetylation reactions. Biochemistry. 2001;40(51):15456-63.
3. Bitterman KJ, Anderson RM, Cohen HY, Latorre-Esteves M, Sinclair DA. Inhibition of silencing and accelerated aging by nicotinamide, a putative negative regulator of yeast sir2 and human SIRT1. The Journal of biological chemistry. 2002;277(47):45099-107.
4. Sanders BD, Jackson B, Marmorstein R. Structural basis for sirtuin function: what we know and what we don't. Biochimica et biophysica acta. 2010;1804(8):1604-16.
5. Lin Z, Fang D. The Roles of SIRT1 in Cancer. Genes & cancer. 2013;4(3-4):97-104.
6. Guarente L. Sirtuins in aging and disease. Cold Spring Harbor symposia on quantitative biology. 2007;72:483-8.
7. Martínez-Redondo P, Vaquero A. The diversity of histone versus nonhistone sirtuin substrates. Genes & cancer. 2013;4(3-4):148-63.
8. Liu TF, Yoza BK, El Gazzar M, Vachharajani VT, McCall CE. NAD+-dependent SIRT1 deacetylase participates in epigenetic reprogramming during endotoxin tolerance. The Journal of biological chemistry. 2011;286(11):9856-64.
9. El Gazzar M, Yoza BK, Hu JY, Cousart SL, McCall CE. Epigenetic silencing of tumor necrosis factor alpha during endotoxin tolerance. The Journal of biological chemistry. 2007;282(37):26857-64.
10. Liu TF, Vachharajani V, Millet P, Bharadwaj MS, Molina AJ, McCall CE. Sequential actions of SIRT1-RELB-SIRT3 coordinate nuclear-mitochondrial communication during

immunometabolic adaptation to acute inflammation and sepsis. The Journal of biological chemistry. 2015;290(1):396-408.
11. Kong X, Wang R, Xue Y, Liu X, Zhang H, Chen Y, et al. Sirtuin 3, a new target of PGC-1alpha, plays an important role in the suppression of ROS and mitochondrial biogenesis. PloS one. 2010;5(7):e11707.
12. Scarpulla RC. Transcriptional activators and coactivators in the nuclear control of mitochondrial function in mammalian cells. Gene. 2002;286(1):81-9.
13. van de Ven RAH, Santos D, Haigis MC. Mitochondrial Sirtuins and Molecular Mechanisms of Aging. Trends Mol Med. 2017;23(4):320-31.
14. Agbaje M, Begum RH, Oyekunle MA, Ojo OE, Adenubi OT. Evolution of Salmonella nomenclature: a critical note. Folia Microbiologica. 2011;56(6):497-503.
15. Galán JE. Salmonella interactions with host cells: type III secretion at work. Annual review of cell and developmental biology. 2001;17:53-86.
16. Garcia-del Portillo F, Foster JW, Finlay BB. Role of acid tolerance response genes in Salmonella typhimurium virulence. Infection and immunity. 1993;61(10):4489-92.
17. Haraga A, Ohlson MB, Miller SI. Salmonellae interplay with host cells. Nature reviews Microbiology. 2008;6(1):53-66.
18. Lawrence T, Natoli G. Transcriptional regulation of macrophage polarization: enabling diversity with identity. Nature reviews Immunology. 2011;11(11):750-61.
19. Martinez FO, Helming L, Gordon S. Alternative activation of macrophages: an immunologic functional perspective. Annual review of immunology. 2009;27:451-83.
20. Namgaladze D, Brüne B. Fatty acid oxidation is dispensable for human macrophage IL-4-induced polarization. Biochimica et biophysica acta. 2014;1841(9):1329-35.
21. Hui X, Zhang M, Gu P, Li K, Gao Y, Wu D, et al. Adipocyte SIRT1 controls systemic insulin sensitivity by modulating macrophages in adipose tissue. EMBO reports. 2017;18(4):645-57.
22. Jia Y, Han S, Li J, Wang H, Liu J, Li N, et al. IRF8 is the target of SIRT1 for the inflammation response in macrophages. Innate immunity. 2017;23(2):188-95.
23. Kratz M, Coats BR, Hisert KB, Hagman D, Mutskov V, Peris E, et al. Metabolic dysfunction drives a mechanistically distinct proinflammatory phenotype in adipose tissue macrophages. Cell Metab. 2014;20(4):614-25.
24. Cimen H, Han MJ, Yang Y, Tong Q, Koc H, Koc EC. Regulation of succinate dehydrogenase activity by SIRT3 in mammalian mitochondria. Biochemistry. 2010;49(2):304-11.
25. Vazquez-Torres A, Xu Y, Jones-Carson J, Holden DW, Lucia SM, Dinauer MC, et al. Salmonella pathogenicity island 2-dependent evasion of the phagocyte NADPH oxidase. Science (New York, NY). 2000;287(5458):1655-8.
26. Miller BH, Fratti RA, Poschet JF, Timmins GS, Master SS, Burgos M, et al. Mycobacteria inhibit nitric oxide synthase recruitment to phagosomes during macrophage infection. Infection and immunity. 2004;72(5):2872-8.
27. Das P, Lahiri A, Lahiri A, Chakravortty D. Novel role of the nitrite transporter NirC in Salmonella pathogenesis: SPI2-dependent suppression of inducible nitric oxide synthase in activated macrophages. Microbiology (Reading, England). 2009;155(Pt 8):2476-89.
28. Bost KL, Clements JD. Intracellular Salmonella dublin induces substantial secretion of the 40-kilodalton subunit of interleukin-12 (IL-12) but minimal secretion of IL-12 as a 70-kilodalton protein in murine macrophages. Infection and immunity. 1997;65(8):3186-92.
29. Pathak SK, Basu S, Basu KK, Banerjee A, Pathak S, Bhattacharyya A, et al. Direct extracellular interaction between the early secreted antigen ESAT-6 of Mycobacterium tuberculosis and TLR2 inhibits TLR signaling in macrophages. Nature immunology. 2007;8(6):610-8.
30. Tumitan AR, Monnazzi LG, Ghiraldi FR, Cilli EM, Machado de Medeiros BM. Pattern of macrophage activation in yersinia-resistant and yersinia-susceptible strains of mice. Microbiology and immunology. 2007;51(10):1021-8.

31. Brubaker RR. Interleukin-10 and inhibition of innate immunity to Yersiniae: roles of Yops and LcrV (V antigen). Infection and immunity. 2003;71(7):3673-81.
32. Elesela S, Morris SB, Narayanan S, Kumar S, Lombard DB, Lukacs NW. Sirtuin 1 regulates mitochondrial function and immune homeostasis in respiratory syncytial virus infected dendritic cells. PLoS pathogens. 2020;16(2):e1008319.
33. Liu G, Bi Y, Xue L, Zhang Y, Yang H, Chen X, et al. Dendritic cell SIRT1-HIF1α axis programs the differentiation of CD4+ T cells through IL-12 and TGF-β1. Proc Natl Acad Sci U S A. 2015;112(9):E957-65.
34. Yang H, Hu J, Chen YJ, Ge B. Role of Sirt1 in innate immune mechanisms against Mycobacterium tuberculosis via the inhibition of TAK1 activation. Archives of biochemistry and biophysics. 2019;667:49-58.
35. Kim TS, Jin YB, Kim YS, Kim S, Kim JK, Lee HM, et al. SIRT3 promotes antimycobacterial defenses by coordinating mitochondrial and autophagic functions. Autophagy. 2019;15(8):1356-75.
36. Tiku V, Tan MW, Dikic I. Mitochondrial Functions in Infection and Immunity. Trends in cell biology. 2020;30(4):263-75.
37. Stavru F, Bouillaud F, Sartori A, Ricquier D, Cossart P. Listeria monocytogenes transiently alters mitochondrial dynamics during infection. Proc Natl Acad Sci U S A. 2011;108(9):3612-7.
38. Jain P, Luo ZQ, Blanke SR. Helicobacter pylori vacuolating cytotoxin A (VacA) engages the mitochondrial fission machinery to induce host cell death. Proceedings of the National Academy of Sciences of the United States of America. 2011;108(38):16032-7.
39. Lum M, Morona R. Dynamin-related protein Drp1 and mitochondria are important for Shigella flexneri infection. Int J Med Microbiol. 2014;304(5-6):530-41.
40. Escoll P, Song OR, Viana F, Steiner B, Lagache T, Olivo-Marin JC, et al. Legionella pneumophila Modulates Mitochondrial Dynamics to Trigger Metabolic Repurposing of Infected Macrophages. Cell host & microbe. 2017;22(3):302-16.e7.
41. Chowdhury SR, Reimer A, Sharan M, Kozjak-Pavlovic V, Eulalio A, Prusty BK, et al. Chlamydia preserves the mitochondrial network necessary for replication via microRNA-dependent inhibition of fission. J Cell Biol. 2017;216(4):1071-89.
42. Kurihara Y, Itoh R, Shimizu A, Walenna NF, Chou B, Ishii K, et al. Chlamydia trachomatis targets mitochondrial dynamics to promote intracellular survival and proliferation. Cellular microbiology. 2019;21(1):e12962.
43. Shi L, Salamon H, Eugenin EA, Pine R, Cooper A, Gennaro ML. Infection with Mycobacterium tuberculosis induces the Warburg effect in mouse lungs. Sci Rep. 2015;5:18176.
44. Czyż DM, Willett JW, Crosson S. Brucella abortus Induces a Warburg Shift in Host Metabolism That Is Linked to Enhanced Intracellular Survival of the Pathogen. J Bacteriol. 2017;199(15).
45. Siegl C, Prusty BK, Karunakaran K, Wischhusen J, Rudel T. Tumor suppressor p53 alters host cell metabolism to limit Chlamydia trachomatis infection. Cell reports. 2014;9(3):918-29.
46. Ahn BH, Kim HS, Song S, Lee IH, Liu J, Vassilopoulos A, et al. A role for the mitochondrial deacetylase Sirt3 in regulating energy homeostasis. Proceedings of the National Academy of Sciences of the United States of America. 2008;105(38):14447-52.
47. Jing E, Emanuelli B, Hirschey MD, Boucher J, Lee KY, Lombard D, et al. Sirtuin-3 (Sirt3) regulates skeletal muscle metabolism and insulin signaling via altered mitochondrial oxidation and reactive oxygen species production. Proceedings of the National Academy of Sciences of the United States of America. 2011;108(35):14608-13.
48. Hallows WC, Yu W, Smith BC, Devries MK, Ellinger JJ, Someya S, et al. Sirt3 promotes the urea cycle and fatty acid oxidation during dietary restriction. Molecular cell. 2011;41(2):139-49.
49. Hirschey MD, Shimazu T, Goetzman E, Jing E, Schwer B, Lombard DB, et al. SIRT3 regulates mitochondrial fatty-acid oxidation by reversible enzyme deacetylation. Nature. 2010;464(7285):121-5.

50. Sundaresan NR, Gupta M, Kim G, Rajamohan SB, Isbatan A, Gupta MP. Sirt3 blocks the cardiac hypertrophic response by augmenting Foxo3a-dependent antioxidant defense mechanisms in mice. The Journal of clinical investigation. 2009;119(9):2758-71.
51. Li P, Meng X, Bian H, Burns N, Zhao KS, Song R. Activation of sirtuin 1/3 improves vascular hyporeactivity in severe hemorrhagic shock by alleviation of mitochondrial damage. Oncotarget. 2015;6(35):36998-7011.
52. Powell RD, Swet JH, Kennedy KL, Huynh TT, McKillop IH, Evans SL. Resveratrol attenuates hypoxic injury in a primary hepatocyte model of hemorrhagic shock and resuscitation. The journal of trauma and acute care surgery. 2014;76(2):409-17.
53. Menzies KJ, Hood DA. The role of SirT1 in muscle mitochondrial turnover. Mitochondrion. 2012;12(1):5-13.
54. Nemoto S, Fergusson MM, Finkel T. SIRT1 Functionally Interacts with the Metabolic Regulator and Transcriptional Coactivator PGC-1α*. Journal of Biological Chemistry. 2005;280(16):16456-60.
55. Wu Z, Puigserver P, Andersson U, Zhang C, Adelmant G, Mootha V, et al. Mechanisms Controlling Mitochondrial Biogenesis and Respiration through the Thermogenic Coactivator PGC-1. Cell. 1999;98(1):115-24.
56. Smulan LJ, Martinez N, Kiritsy MC, Kativhu C, Cavallo K, Sassetti CM, et al. Sirtuin 3 Downregulation in Mycobacterium tuberculosis-Infected Macrophages Reprograms Mitochondrial Metabolism and Promotes Cell Death. mBio. 2021;12(1).
57. Han YH, Kim SH, Kim SZ, Park WH. Antimycin A as a mitochondrial electron transport inhibitor prevents the growth of human lung cancer A549 cells. Oncology reports. 2008;20(3):689-93.
58. Park WH, Han YW, Kim SH, Kim SZ. An ROS generator, antimycin A, inhibits the growth of HeLa cells via apoptosis. Journal of cellular biochemistry. 2007;102(1):98-109.
59. Roy Chowdhury A, Sah S, Varshney U, Chakravortty D. Salmonella Typhimurium outer membrane protein A (OmpA) renders protection from nitrosative stress of macrophages by maintaining the stability of bacterial outer membrane. PLoS pathogens. 2022;18(8):e1010708.
60. Di Trani L, Savarino A, Campitelli L, Norelli S, Puzelli S, D'Ostilio D, et al. Different pH requirements are associated with divergent inhibitory effects of chloroquine on human and avian influenza A viruses. Virology journal. 2007;4:39.
61. Zhou W, Faraldo-Gómez JD. Membrane plasticity facilitates recognition of the inhibitor oligomycin by the mitochondrial ATP synthase rotor. Biochimica et biophysica acta Bioenergetics. 2018;1859(9):789-96.
62. Shchepina LA, Pletjushkina OY, Avetisyan AV, Bakeeva LE, Fetisova EK, Izyumov DS, et al. Oligomycin, inhibitor of the F0 part of H+-ATP-synthase, suppresses the TNF-induced apoptosis. Oncogene. 2002;21(53):8149-57.
63. Cumming BM, Addicott KW, Adamson JH, Steyn AJC. Mycobacterium tuberculosis induces decelerated bioenergetic metabolism in human macrophages. eLife. 2018;7:e39169.
64. Gogoi M, Ravikumar V, Dixit NM, Chakravortty D. Salmonella escapes antigen presentation through K63 ubiquitination mediated endosomal proteolysis of MHC II via modulation of endosomal acidification in dendritic cells. Pathogens and disease. 2018;76(2).
65. Shen Y, Rosendale M, Campbell RE, Perrais D. pHuji, a pH-sensitive red fluorescent protein for imaging of exo- and endocytosis. The Journal of cell biology. 2014;207(3):419-32.
66. Yeung F, Hoberg JE, Ramsey CS, Keller MD, Jones DR, Frye RA, et al. Modulation of NF-kappaB-dependent transcription and cell survival by the SIRT1 deacetylase. Embo j. 2004;23(12):2369-80.
67. Yang H, Zhang W, Pan H, Feldser HG, Lainez E, Miller C, et al. SIRT1 activators suppress inflammatory responses through promotion of p65 deacetylation and inhibition of NF-κB activity. PLoS One. 2012;7(9):e46364.

68. De Santa F, Vitiello L, Torcinaro A, Ferraro E. The Role of Metabolic Remodeling in Macrophage Polarization and Its Effect on Skeletal Muscle Regeneration. Antioxidants & redox signaling. 2019;30(12):1553-98.
69. Galván-Peña S, O'Neill LA. Metabolic reprograming in macrophage polarization. Frontiers in immunology. 2014;5:420.
70. Taylor SJ, Winter SE. Salmonella finds a way: Metabolic versatility of Salmonella enterica serovar Typhimurium in diverse host environments. PLoS pathogens. 2020;16(6):e1008540.
71. Kierans SJ, Taylor CT. Regulation of glycolysis by the hypoxia-inducible factor (HIF): implications for cellular physiology. The Journal of physiology. 2021;599(1):23-37.
72. Lim JH, Lee YM, Chun YS, Chen J, Kim JE, Park JW. Sirtuin 1 modulates cellular responses to hypoxia by deacetylating hypoxia-inducible factor 1alpha. Molecular cell. 2010;38(6):864-78.
73. Wang Y, Bi Y, Chen X, Li C, Li Y, Zhang Z, et al. Histone Deacetylase SIRT1 Negatively Regulates the Differentiation of Interleukin-9-Producing CD4(+) T Cells. Immunity. 2016;44(6):1337-49.
74. West AP, Brodsky IE, Rahner C, Woo DK, Erdjument-Bromage H, Tempst P, et al. TLR signalling augments macrophage bactericidal activity through mitochondrial ROS. Nature. 2011;472(7344):476-80.
75. Suomalainen A, Nunnari J. Mitochondria at the crossroads of health and disease. Cell. 2024;187(11):2601-27.
76. Morató L, Astori S, Zalachoras I, Rodrigues J, Ghosal S, Huang W, et al. eNAMPT actions through nucleus accumbens NAD(+)/SIRT1 link increased adiposity with sociability deficits programmed by peripuberty stress. Science advances. 2022;8(9):eabj9109.
77. Hu B, Wang P, Zhang S, Liu W, Lv X, Shi D, et al. HSP70 attenuates compression-induced apoptosis of nucleus pulposus cells by suppressing mitochondrial fission via upregulating the expression of SIRT3. Experimental & molecular medicine. 2022;54(3):309-23.
78. Forman HJ, Zhang H. Targeting oxidative stress in disease: promise and limitations of antioxidant therapy. Nature Reviews Drug Discovery. 2021;20(9):689-709.
79. Chen Y, Zhou Z, Min W. Mitochondria, Oxidative Stress and Innate Immunity. Frontiers in physiology. 2018;9:1487.
80. Qiu X, Brown K, Hirschey MD, Verdin E, Chen D. Calorie Restriction Reduces Oxidative Stress by SIRT3-Mediated SOD2 Activation. Cell Metabolism. 2010;12(6):662-7.
81. Yang W, Nagasawa K, Münch C, Xu Y, Satterstrom K, Jeong S, et al. Mitochondrial Sirtuin Network Reveals Dynamic SIRT3-Dependent Deacetylation in Response to Membrane Depolarization. Cell. 2016;167(4):985-1000.e21.
82. Chen Y, Cai J, Murphy TJ, Jones DP. Overexpressed human mitochondrial thioredoxin confers resistance to oxidant-induced apoptosis in human osteosarcoma cells. The Journal of biological chemistry. 2002;277(36):33242-8.
83. Forkink M, Manjeri GR, Liemburg-Apers DC, Nibbeling E, Blanchard M, Wojtala A, et al. Mitochondrial hyperpolarization during chronic complex I inhibition is sustained by low activity of complex II, III, IV and V. Biochimica et Biophysica Acta (BBA) - Bioenergetics. 2014;1837(8):1247-56.
84. Amorim JA, Coppotelli G, Rolo AP, Palmeira CM, Ross JM, Sinclair DA. Mitochondrial and metabolic dysfunction in ageing and age-related diseases. Nature Reviews Endocrinology. 2022;18(4):243-58.
85. Hajra D, Rajmani RS, Chakravortty D. SIRT1 and SIRT3 mediated immuno-metabolic switch govern Salmonella survival within infected macrophages both in vitro and <em>in vivo</em&gt. bioRxiv. 2022:2022.11.21.517246.
86. Yang M, Darwish T, Larraufie P, Rimmington D, Cimino I, Goldspink DA, et al. Inhibition of mitochondrial function by metformin increases glucose uptake, glycolysis and GDF-15 release from intestinal cells. Scientific Reports. 2021;11(1):2529.

87. BUTLER A, JANSON J, BONNER-WEIR S, RITZEL R, RIZZA R, BUTLER P. β-Cell deficit and increased β-cell apoptosis in humans with type 2 diabetes.(ON LINE) Diabetes 52: 102-110. 2003.
88. Bonora M, Giorgi C, Pinton P. Molecular mechanisms and consequences of mitochondrial permeability transition. Nature reviews Molecular cell biology. 2022;23(4):266-85.
89. Poburko D, Santo-Domingo J, Demaurex N. Dynamic regulation of the mitochondrial proton gradient during cytosolic calcium elevations. The Journal of biological chemistry. 2011;286(13):11672-84.
90. Yu XJ, McGourty K, Liu M, Unsworth KE, Holden DW. pH sensing by intracellular Salmonella induces effector translocation. Science (New York, NY). 2010;328(5981):1040-3.
91. Chakravortty D, Rohde M, Jäger L, Deiwick J, Hensel M. Formation of a novel surface structure encoded by Salmonella Pathogenicity Island 2. The EMBO journal. 2005;24(11):2043-52.
92. Chakraborty S, Mizusaki H, Kenney LJ. A FRET-based DNA biosensor tracks OmpR-dependent acidification of Salmonella during macrophage infection. PLoS biology. 2015;13(4):e1002116.
93. Garmendia J, Beuzón CR, Ruiz-Albert J, Holden DW. The roles of SsrA-SsrB and OmpR-EnvZ in the regulation of genes encoding the Salmonella typhimurium SPI-2 type III secretion system. Microbiology (Reading, England). 2003;149(Pt 9):2385-96.
94. Wang LC, Morgan LK, Godakumbura P, Kenney LJ, Anand GS. The inner membrane histidine kinase EnvZ senses osmolality via helix-coil transitions in the cytoplasm. The EMBO journal. 2012;31(11):2648-59.
95. Samant SA, Zhang HJ, Hong Z, Pillai VB, Sundaresan NR, Wolfgeher D, et al. SIRT3 deacetylates and activates OPA1 to regulate mitochondrial dynamics during stress. Molecular and cellular biology. 2014;34(5):807-19.
96. Panagi I, Jennings E, Zeng J, Günster RA, Stones CD, Mak H, et al. Salmonella Effector SteE Converts the Mammalian Serine/Threonine Kinase GSK3 into a Tyrosine Kinase to Direct Macrophage Polarization. Cell host & microbe. 2020;27(1):41-53.e6.
97. Stapels DAC, Hill PWS, Westermann AJ, Fisher RA, Thurston TL, Saliba AE, et al. Salmonella persisters undermine host immune defenses during antibiotic treatment. Science (New York, NY). 2018;362(6419):1156-60.
98. Pham THM, Brewer SM, Thurston T, Massis LM, Honeycutt J, Lugo K, et al. Salmonella-Driven Polarization of Granuloma Macrophages Antagonizes TNF-Mediated Pathogen Restriction during Persistent Infection. Cell host & microbe. 2020;27(1):54-67.e5.
99. Ganesan R, Hos NJ, Gutierrez S, Fischer J, Stepek JM, Daglidu E, et al. Salmonella Typhimurium disrupts Sirt1/AMPK checkpoint control of mTOR to impair autophagy. PLoS pathogens. 2017;13(2):e1006227.
100. Gogoi M, Chandra K, Sarikhani M, Ramani R, Sundaresan NR, Chakravortty D. Salmonella escapes adaptive immune response via SIRT2 mediated modulation of innate immune response in dendritic cells. PLoS pathogens. 2018;14(11):e1007437.
101. Eisele NA, Ruby T, Jacobson A, Manzanillo PS, Cox JS, Lam L, et al. Salmonella require the fatty acid regulator PPARδ for the establishment of a metabolic environment essential for long-term persistence. Cell host & microbe. 2013;14(2):171-82.
102. Cramer T, Yamanishi Y, Clausen BE, Förster I, Pawlinski R, Mackman N, et al. HIF-1alpha is essential for myeloid cell-mediated inflammation. Cell. 2003;112(5):645-57.
103. Merrill GF, Kurth EJ, Hardie DG, Winder WW. AICA riboside increases AMP-activated protein kinase, fatty acid oxidation, and glucose uptake in rat muscle. The American journal of physiology. 1997;273(6):E1107-12.
104. Reens AL, Nagy TA, Detweiler CS. Salmonella enterica Requires Lipid Metabolism Genes To Replicate in Proinflammatory Macrophages and Mice. Infection and immunity. 2019;88(1).

105. Holden VI, Breen P, Houle S, Dozois CM, Bachman MA. Klebsiella pneumoniae Siderophores Induce Inflammation, Bacterial Dissemination, and HIF-1α Stabilization during Pneumonia. mBio. 2016;7(5).
106. Hotson AN, Gopinath S, Nicolau M, Khasanova A, Finck R, Monack D, et al. Coordinate actions of innate immune responses oppose those of the adaptive immune system during Salmonella infection of mice. Science signaling. 2016;9(410):ra4.
107. Ramond E, Jamet A, Coureuil M, Charbit A. Pivotal Role of Mitochondria in Macrophage Response to Bacterial Pathogens. Frontiers in immunology. 2019;10.
108. Käding N, Kaufhold I, Müller C, Szaszák M, Shima K, Weinmaier T, et al. Growth of Chlamydia pneumoniae Is Enhanced in Cells with Impaired Mitochondrial Function. Front Cell Infect Microbiol. 2017;7:499.
109. Yao Y, Chen T, Wu H, Yang N, Xu S. Melatonin attenuates bisphenol A-induced colon injury by dual targeting mitochondrial dynamics and Nrf2 antioxidant system via activation of SIRT1/PGC-1α signaling pathway. Free radical biology & medicine. 2023;195:13-22.
110. Yang R, Song C, Chen J, Zhou L, Jiang X, Cao X, et al. Limonin ameliorates acetaminophen-induced hepatotoxicity by activating Nrf2 antioxidative pathway and inhibiting NF-κB inflammatory response via upregulating Sirt1. Phytomedicine : international journal of phytotherapy and phytopharmacology. 2020;69:153211.
111. Kim A, Koo JH, Lee JM, Joo MS, Kim TH, Kim H, et al. NRF2-mediated SIRT3 induction protects hepatocytes from ER stress-induced liver injury. FASEB journal : official publication of the Federation of American Societies for Experimental Biology. 2022;36(3):e22170.
112. Cheng J, Nanayakkara G, Shao Y, Cueto R, Wang L, Yang WY, et al. Mitochondrial Proton Leak Plays a Critical Role in Pathogenesis of Cardiovascular Diseases. Advances in experimental medicine and biology. 2017;982:359-70.
113. Kadenbach B. Intrinsic and extrinsic uncoupling of oxidative phosphorylation. Biochimica et biophysica acta. 2003;1604(2):77-94.
114. Murphy MP. Slip and leak in mitochondrial oxidative phosphorylation. Biochimica et biophysica acta. 1989;977(2):123-41.
115. Cervantes-Silva MP, Cox SL, Curtis AM. Alterations in mitochondrial morphology as a key driver of immunity and host defence. EMBO reports. 2021;22(9):e53086.
116. Carvalho F, Spier A, Chaze T, Matondo M, Cossart P, Stavru F. Listeria monocytogenes Exploits Mitochondrial Contact Site and Cristae Organizing System Complex Subunit Mic10 To Promote Mitochondrial Fragmentation and Cellular Infection. mBio. 2020;11(1).
117. Shi L, Jiang Q, Bushkin Y, Subbian S, Tyagi S. Biphasic Dynamics of Macrophage Immunometabolism during Mycobacterium tuberculosis Infection. mBio. 2019;10(2).
118. Chen LT, Lin CT, Lin LY, Hsu JM, Wu YC, Pan CL. Neuronal mitochondrial dynamics coordinate systemic mitochondrial morphology and stress response to confer pathogen resistance in C. elegans. Developmental cell. 2021;56(12):1770-85.e12.
119. Suzuki M, Danilchanka O, Mekalanos JJ. Vibrio cholerae T3SS effector VopE modulates mitochondrial dynamics and innate immune signaling by targeting Miro GTPases. Cell host & microbe. 2014;16(5):581-91.
120. Kirienko NV, Ausubel FM, Ruvkun G. Mitophagy confers resistance to siderophore-mediated killing by Pseudomonas aeruginosa. Proceedings of the National Academy of Sciences of the United States of America. 2015;112(6):1821-6.
121. Sun LL, Shao YN, You MX, Li CH. ROS-mediated BNIP3-dependent mitophagy promotes coelomocyte survival in Apostichopus japonicus in response to Vibrio splendidus infection. Zoological research. 2022;43(2):285-300.
122. Lee HJ, Kang SJ, Woo Y, Hahn TW, Ko HJ, Jung YJ. TLR7 Stimulation With Imiquimod Induces Selective Autophagy and Controls Mycobacterium tuberculosis Growth in Mouse Macrophages. Frontiers in microbiology. 2020;11:1684.

123. Zhang Y, Yao Y, Qiu X, Wang G, Hu Z, Chen S, et al. Listeria hijacks host mitophagy through a novel mitophagy receptor to evade killing. Nature immunology. 2019;20(4):433-46.
124. Jiao Y, Cao S, Zhang Y, Tan Y, Zhou Y, Wang T, et al. Yersinia pestis-Induced Mitophagy That Balances Mitochondrial Homeostasis and mROS-Mediated Bactericidal Activity. Microbiology spectrum. 2022;10(3):e0071822.
125. Verbeke J, Fayt Y, Martin L, Yilmaz O, Sedzicki J, Reboul A, et al. Host cell egress of Brucella abortus requires BNIP3L-mediated mitophagy. The EMBO journal. 2023;42(14):e112817.
126. Verbeke J, De Bolle X, Arnould T. To eat or not to eat mitochondria? How do host cells cope with mitophagy upon bacterial infection? PLoS pathogens. 2023;19(7):e1011471.
127. Knodler LA, Elfenbein JR. Salmonella enterica. Trends in microbiology. 2019;27(11):964-5.